Photonic Time Division Multiple Access Systems for Fiber-Optic Radio Access Networks

by

YOZO SHOJI

OSAKA UNIVERSITY

OSAKA 565-0871, JAPAN

JANUARY, 1999

Acknowledgement

This research has been carried out by the author during his Ph.D. course at the Department of Communications Engineering, Graduate School of Engineering, Osaka University.

The author would like to express his deepest appreciation to Professor Shozo Komaki for his supervision, continuing encouragement, valuable discussions, academic advices, and various supports throughout this research.

The author also gives his deep appreciation to Professor Hiromasa Ikeda, and Assistant Professor Hiroyuki Toda of the Department of Communications Engineering, Faculty of Engineering, Osaka University, for their reading and valuable criticism on the whole contents of this thesis.

Likewise thanks go to Professors of Osaka University, Norihiko Morinaga and Hajime Maeda of the Department of Communications Engineering, Hiroshi Motoda of the Institute of Scientific and Industrial Research, and Yuji Kodama and Toshiyuki Shiozawa of the Department of Communications Engineering, for their creative comments for this research.

The author wishes to thank Associate Professors of Osaka University, Seiichi Sampei, Masayuki Matsumoto, Yoji Iiguni, and Miki Yamamoto of the Department of Communications Engineering, Takashi Washio of the Institute of Scientific and Industrial Research, and Shinsuke Hara of the Department of Electronics and Information Systems Engineering, for their valuable comments for this research.

The author appreciates Emeritus Professor Sadao Kurazono of Osaka University, Professor Akira Hasegawa of Kochi University of Technology, and Professor Tadahiro Kitahashi and Associate Professor Noboru Babaguchi of the Institute of Scientific and Industrial Research of Osaka University, for their valuable comments in the course of development of this research.

The author appreciates all members of Komaki Laboratory for their valuable advice for this research, especially Mr. Sangjo Park and Mr. Masahiro Nishi for their helpful discussions, Shigeyuki Fujii for his willing cooperation in the experiments, and Takahiro Hida for his valuable discussions.

The author appreciates Dr. Hiroshi Harada of Communications Research Laboratory, Ministry of Posts and Telecommunications, and Mr. Satoshi Kajiya of Mitsubishi Electric Corporation for their valuable discussions in the course of development of this research.

The author thanks to Japan Society for the Promotion of Science (JSPS) for its financial support on the experimental works.

The author wishes to thank Dr. Bokuji Komiyama, Dr. Yoshihiko Mizuguchi, and Mr. Keizo Inagaki of Advanced Telecommunications Research Institute International (ATR) for their offers of the experimental environment and their helpful instructions in the experimental works.

The author gives thanks to Research Associate Minoru Okada for his valuable comments and discussions throughout this research.

Finally, the author would like to express his much deep appreciation to Associate Professor Katsutoshi Tsukamoto for his helpful discussions, various academic comments, untiring efforts in guidance, and continuing encouragement from the beginning to the end of this research.

Abstract

This thesis describes the author's researches about photonic time division multiple access systems for fiber-optic radio access networks, which were conducted during his Ph.D. course at the Department of Communications Engineering, Graduate School of Engineering, Osaka University, Japan. This thesis consists of eight chapters as follows:

Chapter 1 presents a review of previous and recent works on the problems discussed in this thesis, and clarifies the background of this study.

Chapter 2 introduces some candidates for network configuration and photonic multiplexing scheme in fiber-optic radio access networks, and discusses their suitabilities from the viewpoint of the future demands on radio access networks. In addition, this chapter specifically presents the principle of photonic natural bandpass sampling method for radio-fiber transmission system, and the basic configuration of time division multiplexing system applying the photonic sampling technique treated in this thesis. The final part of this chapter describes the topics to study in this thesis, the difficulty of time synchronization control for time division multiplexing of radio signals and the realization of photonic routing of radio signals in the network.

Chapter 3 proposes self-synchronous time division multiplexing bus link system. It reduces the difficulty of time synchronization that is necessary for time division multiplexing of radio signals among whole radio base stations, and also realizes the sharing of a light source among radio base stations. Carrier-to-noise power ratio (CNR) of signals detected at a control station is theoretically analyzed, and the CNR improvement obtained by the use of an optical pre-amplifier is theoretically investigated.

Chapter 4 proposes asynchronous time division multiple access bus link system. It requires no time synchronization function, and allows the asynchronous access of radio signals to the fiber-optic bus link. However some of radio bursts is lost due to collision on the bus link transmission. The system performance is investigated by the theoretical analyses of burst loss probability and carrier-to-noise power ratio of signals detected at the control station.

Chapter 5 proposes the chirp multiplexing transform (CMT) fiber-optic radio access system, in which the different frequency signals are converted to the different time signals. The aim of this proposal is the universal use of radio base stations by the various radio service carrier, and the system can route the different radio frequency signal to the different destination, even if the signals are in the base station. The system performance is investigated and discussed by the theoretical analyses of power ratio of desired signal to the sum of noises, such as interchannel interference, intersymbol interference, 3rd order intermodulation distortion, and the noises inherent to the optical transmission.

Chapter 6 proposes the asynchronous time division multiple access bus link system using chirp multiplexing transform. It is the combination of the asynchronous access

bus link system described in Chapter 4 and the chirp multiplexing transform systems described in Chapter 5. The proposed system converts the different frequency signal into TDMA format signal by use of chirp multiplexing transformer. System performance is investigated under the condition of the non-uniform traffic distribution in service area, and is theoretically analyzed the probability that transmitted TDMA pulse is lost due to the asynchronous access of radio signals.

Chapter 7 describes the results of fundamental experiments on fiber-optic radio transmission system using photonic natural bandpass sampling. The carrier-to-noise power ratio and the carrier-to-distortion power ratio are measured, and the measured performances are compared with the results of conventional SCM transmission system. In addition, the performance degradation caused by increasing the number of transmitted radio carriers, or fiber-optic length are estimated using the experimental results.

Chapter 8 summarizes all the conclusions obtained in this thesis, and clarifies the significance of this study and proposed systems.

Contents

Acknowledgement i

Abstract iii

List of Figures vii

List of Tables ix

1 Introduction 1

2 Fiber-optic Radio Access Networks and Photonic TDM Systems 7
- 2.1 Introduction . . . 7
- 2.2 Photonic Link Configurations and Photonic Multiplexing Schemes . . . 8
- 2.3 Principle of Photonic Natural Bandpass Sampling . . . 10
- 2.4 Photonic TDM Bus Link Systems . . . 12
- 2.5 Concluding Remarks . . . 14

3 Photonic Self-synchronous Time Division Multiplexing Bus Link System 17
- 3.1 Introduction . . . 17
- 3.2 Self-synchronous TDM Bus Link System . . . 17
- 3.3 Theoretical analysis of Received CNR . . . 20
- 3.4 Numerical results of the CNR Performance . . . 22
- 3.5 Concluding Remarks . . . 26

4 Photonic Asynchronous Time Division Multiple Access Bus Link System 27
- 4.1 Introduction . . . 27
- 4.2 Asynchronous TDMA Bus Link System . . . 28
- 4.3 Radio Burst Collision . . . 29
- 4.4 Theoretical Analysis of Burst Loss Probability . . . 31
  - 4.4.1 Analysis in case of no control . . . 32
  - 4.4.2 Analysis in case of carrier sense control . . . 33
  - 4.4.3 Analysis in case of carrier-sense / collision avoidance control . . . 33
- 4.5 Theoretical Analysis of Received CNR . . . 34
- 4.6 Performance Evaluations . . . 35
  - 4.6.1 Performance in case of no control . . . 35

4.6.2 Performance improvement due to CS, CS/CA, and variable pulse width controls . . . 37
4.7 Concluding Remarks . . . 40

5 Chirp Multiplexing Transform Fiber-Optic Radio Access System 41
5.1 Introduction . . . 41
5.2 Principle of Chirp Multiplexing Transform . . . 42
5.3 CMT/IM/DD System for FDM-PSK Radio Signals . . . 46
5.4 Theoretical ICI and ISI Performance Analyses . . . 48
5.5 Double CMT System . . . 51
5.6 Theoretical Analyses of SNR and Overall Performances . . . 53
5.7 Concluding Remarks . . . 57

6 Asynchronous Time Division Multiple Access Bus Link System using Chirp Multiplexing Transform 59
6.1 Introduction . . . 59
6.2 Asynchronous TDMA Bus Link System using Chirp Multiplexing Transform 60
6.3 Theoretical Analyses of Pulse Loss and Call Blocking Probabilities . . . 62
6.4 Numerical Results of Pulse Loss and Call Blocking Probabilities . . . 65
6.5 Concluding Remarks . . . 70

7 Fundamental Experiments on Fiber-Optic Radio Transmission System using Photonic Natural Bandpass Sampling 71
7.1 Introduction . . . 71
7.2 Experimental Setup . . . 71
7.3 Measured Received CNR and CDR Performances . . . 76
7.4 System Parameters Estimation from Measured Data . . . 81
7.5 Estimation of the system capacity . . . 82
7.6 Concluding Remarks . . . 84

8 Conclusions 85

Appendix A 89

References 91

Related Publications 97

List of Figures

2.1 Concept of fiber-optic radio access networks. 7
2.2 Network configurations. 8
2.3 Principle of photonic natural bandpass sampling. 11
2.4 Configuration of photonic TDM bus link system. 13
2.5 Configuration of SCM bus link system. 14

3.1 System configuration of self-synchronous TDM bus link. 18
3.2 Required fiber delay length versus sampling frequency. 19
3.3 Received CNR versus the number of connected RBSs in case of no pre-amplification. 24
3.4 Received CNR versus pre-amplifier gain. 24
3.5 Connectable number of RBSs versus pre-amplifier gain. 25
3.6 Received CNR versus pulse duty. 25

4.1 Configuration of Asynchronous TDMA bus link system. 28
4.2 Mechanism of collision among PAM/IM bursts. 29
4.3 Collision among bursts. 32
4.4 Burst loss probability versus pulse width. 36
4.5 Required pulse width and received CNR as a function of average traffic per RBS. 37
4.6 Burst loss probability and received CNR versus the RBS number. 37
4.7 Burst loss probability and received CNR versus the RBS number with variable pulse width and control. 38
4.8 Maximum number of connectable RBSs versus pulse width in the network with CS or with no control. 39

5.1 Network configuration of CMT fiber-optic radio access system. 42
5.2 Configuration of CMT. 43
5.3 Input and output signals of the chirp filter. 46
5.4 Performance analysis models of CMT/IM/DD system and SCM system. . . 46
5.5 Radio signal and CMT signal. 48
5.6 Normalized symbol energy versus symbol number. 49
5.7 Configuration of suboptimal correlation receiver. 50
5.8 S/ICI versus chirping dispersion time. 50
5.9 S/ISI versus chirping dispersion time. 51
5.10 Configuration of double CMT. 52
5.11 Configuration of the receiver for double CMT system. 52
5.12 SNR versus the number of radio channels. 55

5.13 S/(N+I) versus the number of radio channels. 56

6.1 Asynchronous TDMA bus link systems using CMT. 60
6.2 Configuration of CMT. 61
6.3 Traffic density distribution. 63
6.4 Traffic versus the RBS number. 64
6.5 Mechanism of PAM/IM pulse loss. 65
6.6 Pulse loss probability versus the RBS number. 66
6.7 Pulse loss probability versus the RBS number. 67
6.8 Pulse loss probability and call blocking probability versus the number of connected RBSs. 68
6.9 Accommodated total traffic versus required pulse loss probability. 68
6.10 Required number of RBSs versus normalized standard deviation of traffic distribution. 69

7.1 Experimental setup. 71
7.2 Inside view of transmitter. 72
7.3 Inside view of receiver. 72
7.4 Output optical power versus driving voltage on LN modulator. 74
7.5 Output optical power of transmitter. 74
7.6 Waveform of a receiver output signal. 75
7.7 Spectrum of a receiver output signal. 75
7.8 CNR performance versus optical transmission loss. 76
7.9 SFDR degradation due to received optical power degradation. 77
7.10 Spectrum of a receiver output in the CDR measurement. 78
7.11 CDR performance versus RF input power. 79
7.12 CNDR performance versus RF input power. 80
7.13 CNR performance versus pulse duty. 80
7.14 CNDR performance versus number of radio carriers. 83
7.15 CNDR performance versus optical transmission loss. 83

List of Tables

2.1 Performance comparison of advantages and disadvantages of various multiplexing schemes. 10

3.1 Default parameters used in calculations. 22

4.1 Parameters used in calculations 36

5.1 Parameters used in calculations 55

7.1 Specifications of devices used in experiment. 73

Chapter 1

Introduction

The number of the cellular subscribers is dramatically increasing all over the world. In Japan, the current increasing number per month of the personal digital cellular (PDC) is about 0.8 million. The total number of PDC and personal handy phone systems (PHS) subscribers at the end of October, 1998 has reached approximately 43.5 million. This number corresponds to 34% penetration ratio. This trend forces us to face frequency spectrum shortage. In order to meet such spectrum shortage, it seems that two types of study are extensively made. One is the efficient use of current frequency resources, such as micro-cellular or pico-cellular constructions, and/or the compression of informations, and the other is to extend the available frequency into higher frequency band, such as SHF band, or millimeter wave band. In such higher frequency environment, the use of micro- or pico-cellular construction becomes also inevitable in order to reduce the consumption power of handset rather than to efficiently use frequency.

The requirement of such micro- or pico-cellular system forces us to construct lots of radio base stations, and it requires a large investment of cost and time. Such requirements and problems lead us again to powerfully study the analog fiber-optic link as one of hopeful candidates for radio access link in microcellular environment, though digital fiber-optic link has been focused in modern research and development. Several concepts for the analog fiber-optic radio access networks were proposed in [1]-[7], where the analog fiber-optic link enables us to transfer radio signal generated or received at radio station into another remote radio station without baseband demodulation of radio. In other words, fiber-optic links can be used as virtual free space for radio transmission. Therefore, the fiber-optic radio access networks bring us many following attractive benefits:

- It is capable to transfer radio signals with much low transmission loss of about 0.2 dB/km, being kept from the disturbance of external electromagnetic interferences.

- Equipments in radio base stations can be much reduced because modulation and demodulation functions, and the control functions for channel allocations are concentrated in a remote control station. Thereby it is possible to construct much cost-effective radio access networks.

- The equipments for radio base stations and fiber-optic links can be independent of radio signal format. Thus, they are flexible to the modification of radio format, or the opening of a new radio service.

- Macro diversity effect can be easily obtained because the signals from several radio base stations are demodulated at a single radio control station[8].
- The system can easily support the very fast vehicle, because the hand over process is executed only at the central station, in spite of microcell stations.

Modulation of an optical carrier for the analog fiber-optic link can be basically performed by varying amplitude, intensity, frequency, phase, or polarization. In such modulation parameters, intensity is the most simple and easy to detect because a single photodiode (PD) directly converts optical energy into photocurrent. The fiber-optic link using intensity modulation is referred to as Intensity Modulation / Direct Detection (IM/DD) link. Because of its simplicity, the IM/DD type fiber-optic radio access link have been powerfully studied in [9]-[11]. It is generally known that the performance of IM/DD fiber-optic link is limited by the noises inherent to the optical link and the non-linearity of intensity modulator. In particular, the non-linearity causes the distortion referred to as 3rd order intermodulation distortion (IM3), and severely limits the number of transferred radio carriers[9] or the dynamic range allowed for radio signals received at radio station[11].

On the other hand, in order to detect other modulation parameters except for intensity, an optical coherent detection, that is, homodyne or heterodyne detection, is indispensable[12]. Such coherent type of analog fiber-optic link is also being studied and surely brings various advantages, such as, wide spurious free dynamic range[13][14], high receiver sensitivity[15], high tolerance for fiber dispersion due to the availability of single-side-band (SSB) modulation[16][17], high density optical channel allocation[18], and so on. However from our viewpoints, such coherent type of analog fiber-optic link seems still too expensive or complicated to apply for radio access networks, because a lot of fiber-optic links are required in the radio access networks.

In spite of any type of optical modulation, fiber-optic system is still generally expensive. In order to efficiently use fiber-optic link, we have to study the schemes to multiplex signals for several radio base stations into a fiber-optic link, that is, photonic multiplexing schemes. There are several candidates for photonic multiplexing schemes, such as, subcarrier multiplexing[19]-[22], time division multiplexing[23]-[25], frequency division multiplexing[18][26], code division multiplexing[27]-[30], and so on. However the available photonic multiplexing schemes so far are not independent of modulation types. Therefore we should carefully select the modulation type and the photonic multiplexing scheme when we construct fiber-optic radio access networks.

The objects of this study is to pursue the most effective fiber-optic radio access system from the various viewpoints of future demands and trends, feasibility, cost-efficiency, flexibility, universality, and so on.

Chapter 2 is devoted to review and discuss the suitability of various network configurations and photonic multiplexing schemes in fiber-optic radio access networks, and it will conclude that the photonic time division multiplexing (TDM) bus link system with IM/DD type of fiber-optic link proposed in [23]-[25] has the priority in cost-efficiency, simplicity, flexibility, and the possibility to universally use the fiber-optic links among various radio services. The use of photonic time division multiplexing can generally bring the following advantages:

- It can be realized by simple IM/DD fiber-optic link.

- The signal quality is not deteriorated due to the optical beat noise generated by the mixing of several optical carriers.

- Photonic TDM requires no complex equipment, and requires only photonic switch that is advanced in recent development for optical digital transmission.

From the reason mentioned above, this thesis consistently aims at the realization of photonic time division multiple access (TDMA) bus link systems and the theoretical and experimental analysis of the TDMA systems.

It has already been clarified that the TDMA bus link system has the priority in the carrier-to-noise performance in comparison with the conventional subcarrier multiplexing (SCM) bus link system because the detected signal performance is not deteriorated by the optical beat noise[25]. However the TDM of whole base stations requires the difficult time synchronization. Such difficulty comes from the fact that the signals to be multiplexed are generated at the different radio base stations, separately located in the fiber-optic radio access networks. Therefore the first important problem in this thesis is to solve the difficulty of time synchronization. Chapters 3 and 4 describe the solutions for this question.

In order to reduce the difficulty of time synchronization control among radio base stations, this thesis newly proposes self-synchronous time division multiplexing bus link system in Chapter 3, where several radio base stations connected to a fiber-optic bus link share a single optical pulse source provided from the end of the bus link, and the TDM of signals are automatically performed by a fiber delay line equipped at each radio base station. When we evaluate the performance of a fiber-optic radio access link, quality of the radio signal detected at a control station is an important subject, because it suffers from the noises inherent to the fiber-optic transmission and the signal power degradation due to the insertion of passive optical devices. Therefore we estimate the performance of the proposed system by theoretical analysis of carrier-to-noise power ratio (CNR) of signals detected at a control station. Furthermore the application of an optical pre-amplifier to the fiber-optic link is proposed and the improvement effect on the CNR performance is theoretically investigated.

Another approach to solve the difficulty of time synchronization control is the construction of asynchronous access systems. Chapter 4 proposes asynchronous time division multiple access bus link system, where the time synchronization control necessary for TDM of signals are perfectly removed and radio bursts generated at a radio base station asynchronously access to the fiber-optic bus link. However such asynchronous access system with TDMA signal format, causes the new problem that the radio burst may be lost in the middle of transmission due to collision with other radio burst. Thus, it is necessary to convert radio bursts into narrow optical pulse format signals in order to sufficiently reduce the probability of collision, though the narrower optical pulse format causes the lower detected power of radio signals. This chapter theoretically analyzes the CNR performance and the radio burst loss probability performance, and clarifies the condition to satisfy the required performances. Furthermore in order to reduce the burst loss probability without the degradation of detected signal power, this chapter proposes some applications of access control, such as carrier-sense control, carrier-sense / collision avoidance control, and variable pulse width control, and theoretically investigates their efficiencies.

By the way, radio service carriers are now planning to establish the 3rd generation wireless networks. However they have different perspective on the nature of the next generation of radio networks, such as service kind, access format, type of air-interface, and so on. Thus it is expected that radio service will be more diversified than the current systems in near future. The second aim of this study is to unify the many diversified radio services existing today (including paging, cordless, cellular, etc.) and future radio services into a unified seamless radio access network capable of offering a wide range of services. It is envisioned that such a unified flexible radio access network will allow the radio carriers to greatly improve operating efficiencies.

In general radio environment, different type of radio services is operated under different radio frequency band. In other words, radio services are multiplexed with frequency division multiplexing (FDM) format. In the ordinary IM/DD fiber-optic link, such multiple radio services with FDM format can be easily transfered via a unified fiber-optic link with subcarrier multiplexing (SCM) format. However different radio service unfortunately needs to be delivered to different radio control station in most cases. Therefore in order to provide a unified flexible fiber-optic radio access network available among different radio services, the network must include a routing node (RN) which has the functions of distinguishing and switching radio service. If multiple radio services are transfered with the SCM format, the RN has to execute a series of processes of photodetection, filtering and switching of radio service in electrical stage, and conversion into optical signal to again transfer via fiber-optic link. Thus the complexity of RN configuration much increases. Therefore it is necessary to study the realization method of photonic routing of radio service, that is, distinguishing and switching of radio service in the optical stage.

From the perspective on the feasibility of photonic routing of radio service, the transmission of multiple radio services with TDM format seems most desirable if possible, because the time switching seems to be most simply realizable way to route signal in the optical stage and it can be benefited by the recent advanced high-speed switching technique in digital optical communication systems or self-routing technique in optical Asynchronous Transfer Mode (ATM) transmissions[31]-[33]. Therefore this thesis studies the scheme to transfer multiple radio services with TDM format in a fiber-optic link.

Chapter 5 proposes chirp multiplexing transform (CMT) fiber-optic radio access system. The CMT is the analog Fourier transformer, and can convert signals with FDM format into ones with TDM format. In the proposed system, multiple radio services are transfered via a unified fiber-optic link after the conversion into signals with TDM format by the use of the CMT. Thus the RN composed of simple photonic time switch can execute the photonic routing of radio service. Such realization of photonic routing can provide the universal use of radio base stations and optical networks among different radio services. However it will be clarified in the chapter that the transformation using the CMT causes inter-channel interference, inter-symbol interference, and distortion into the obtained signals, and they deteriorate the quality of radio signals detected at a control station. Therefore this chapter theoretically analyzes power ratios of signal-to-inter-channel interference, signal-to-inter-symbol interference, and signal-to-noise plus distortion, and compares them with the conventional IM/DD link without the CMT.

Furthermore if the CMT fiber-optic radio access system can be combined with the asynchronous TDMA bus link system, we can construct much flexible radio access networks with the ability of photonic routing of radio service. Thus, Chapter 6 proposes asyn-

chronous time division multiple access bus link system using chirp multiplexing transform, in which the advantages of the asynchronous TDMA bus link system described in Chapter 4 and the CMT system described in Chapter 5 are combined. In the proposed system, the CMT executes two functions of the transformation of radio signals with FDMA format into the signals with TDMA format, and the conversion of them into narrow pulse format that can allow the asynchronous access, at the same time. The optical pulse loss occurs due to the asynchronous access by the similar manner to the system proposed in Chapter 4, and the theoretical results of burst loss probability performance obtained in Chapter 4 can be translated into the pulse loss probability performance in this asynchronous access system using CMT. On the other hand, the initial call blocking occurs independently to the pulse loss in the microcellular systems, and both of the call blocking probability and the pulse loss probability are related to the condition of traffic covered by a fiber-optic bus link. Therefore this chapter theoretically investigates the relationship between the call blocking probability and the pulse loss probability considering the non-uniform traffic distribution in service area, and discusses allowable number of radio base stations and total traffic accommodated in a fiber-optic bus link.

Final topic treated in this thesis is to confirm the principle of the fiber-optic radio transmission using photonic natural bandpass sampling and to investigate its signal performance on experiment. The signal performance of photonic time division multiplexing systems using photonic natural bandpass sampling have theoretically been investigated in several papers [23]-[25], and also in this thesis. However the investigation on experiment have never been performed yet. Chapter 7 reports and discusses the results of the fundamental experiments on fiber-optic radio transmission system using photonic natural bandpass sampling. The carrier-to-noise power ratio and carrier-to-distortion power ratio are measured and compared to that of the conventional IM/DD transmission system without the photonic sampling. In addition, the performance degradation caused by increasing the number of transmitted radio carriers or fiber-optic transmission length is estimated by the use of experimental results.

Chapter 8 summarizes all the conclusions obtained in this thesis.

Chapter 2

Fiber-optic Radio Access Networks and Photonic TDM Systems

2.1 Introduction

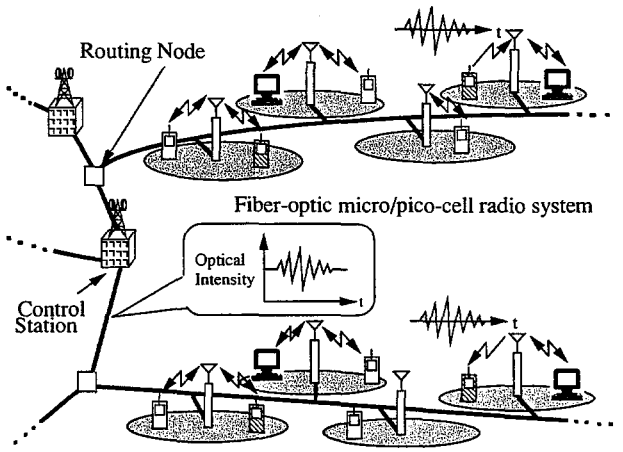

Figure 2.1: Concept of fiber-optic radio access networks.

Fiber-optic radio access networks are optical backbone networks for radio access systems, where fiber-optic links have the function to transfer radio signals into remote stations without destroying their radio format, such as radio frequency, modulation format, and so on. For that purpose, the transmission format in the fiber-optic networks is typically based on analog optical modulation techniques.

The concept of fiber-optic radio access networks is illustrated in Fig.2.1. The radio zone architecture may follow that of conventional micro-cellular or pico-cellular radio systems. However the interface receiving or radiating radio signals in each radio zone, named Radio Base Station (RBS), equips only the converter between radio signals and optical signals, and RBS requires neither modulation functions nor demodulation functions of radio. The radio signals converted into optical signals are transfered via fiber-optic link with the benefit of its low transmission loss. Therefore the architecture of fiber-optic radio access links can be independent of radio signal format and can provide much universal radio

access links that are available to any type of radio signal. This means that such radio access links are very flexible to the modification of radio signal formats or the opening of new radio services.

A remote control station, named Radio Control Station (RBS), executes the functions of modulation and demodulation of radio, and other controls such as channel allocations. Such concentrated executions of the troublesome functions provide much simplified and cost-effective constructions of radio access networks, and promise easy realization of recent advanced demodulation techniques, such as, a macro-diversity[8] and hand-over controls.

Consequently, the fiber-optic radio access networks are considered as a hopeful candidate for various future cellular radio access networks, such as future public wireless communication systems (IMT 2000)[34], wireless local area networks (wireless LAN), roadside-to-vehicle radio access link in Intelligent Transport Systems (ITS)[35], or distribution systems of cable television signals (CATV)[36].

However there exist several kinds of subjects to be studied in order to realize fiber-optic radio access networks. Basic subject is which photonic link configuration and multiplexing scheme is suitable in the construction of fiber-optic radio access networks. This subject is treated in Sect.2.2 in detail. The section introduces various types of link configuration and photonic multiplexing scheme, and clarifies the reasons that this thesis aims at the realization of bus link configuration and time division multiple access (TDMA) systems. Section 2.3 introduces the principle of photonic natural bandpass sampling technique that realizes the conversion of radio signal into photonic TDM signal format. Section 2.4 introduces the basic configuration of photonic TDM bus link system, and specifies the subjects to study in order to realize the TDM bus link systems and advance the function of it.

2.2 Photonic Link Configurations and Photonic Multiplexing Schemes

There are three candidates for link configuration in constructing networks, that is, star configuration, ring configuration, and bus configuration. Figure 2.2 illustrates their configurations. The star configuration is the most popular one in constructing networks because

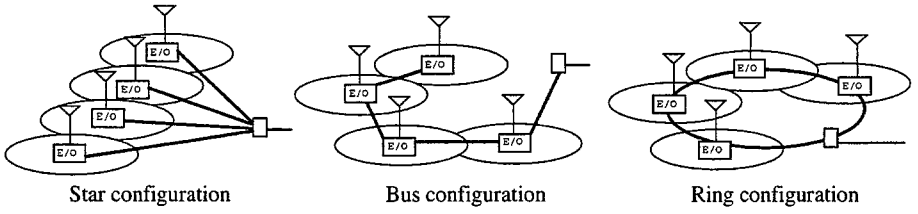

Figure 2.2: Network configurations.

of its easy maintenance, high reliability, and simple constructions. However it is difficult to construct or extend networks cost-effectively and/or quickly because fiber-counts as many as the number of RBSs are required. On the other hand, the bus configuration or the ring configuration can much reduce the fiber-counts, thus they have the capability of

cost-effective and quick construction of networks and also easy extension of RBSs. These capabilities are much important in constructing fiber-optic radio access networks because the density of RBSs becomes very high in recent micro-cellular requirements. Therefore we should study the fiber-optic link that allows the bus configuration or the ring configuration. The two configurations have much similarity except for the difference whether the network is terminated at a certain RBS or at the RCS. Then, this paper mainly concentrates the discussion on the realization of bus configuration.

Now the study on the photonic multiplexing scheme is the most important subject to construct bus link system. The candidates for multiplexing schemes are Subcarrier Multiplexing (SCM), Time Division Multiplexing (TDM), Frequency Division Multiplexing (FDM), Code Division Multiplexing (CDM) and Wave length Division Multiplexing (WDM). The features of each scheme are also summarized in Table 2.1.

In discussing which photonic multiplexing scheme is suitable for radio access networks, we should make much of the cost-efficiency, the easiness, and the simplicity of network constructions because they are most important benefits the fiber-optic radio access networks should offer. The optical communication systems are generally classified into direct detection systems and coherent detection systems[12], and the former has much advantages in the simplicity of system while the latter increases the complexity of system in general. On the other hand, the capability of de-multiplexing of signals in optical stage brings an important benefit to the fiber-optic radio access networks. The fiber-optic radio access networks have the potential to be universally used among different radio services or those operated by different providers, because the configuration of RBSs and fiber-optic networks can be independent of the radio signal format. Such advanced purpose requires further subjects to be studied. It is expected that the different types of radio services, or those operated by different provider need to be delivered to different RCS in different location in most cases. It means that the networks must include the routing node (RN) that executes routing of radio signals, that is, distinguishing and switching of radio signals. Therefore in selecting photonic multiplexing scheme it is also important to make much of the feasibility for the routing of radio signals, and it is desirable that the routing process can be executed in optical stage. The author refers to such routing of radio signals in optical stage, as photonic routing of radio signals.

Attractive features of the TDM scheme are that the IM/DD link can be applied and simple photonic switch can easily realize de-multiplexing of signals in optical stage. The SCM scheme can also apply IM/DD link, however it is impossible to de-multiplex signals in optical stage because signals are multiplexed in frequency of electrical stage. More detailed comparison between photonic TDM bus link system and SCM bus link system is described in Sect.2.4.

The FDM scheme, in particular the scheme by the use of optical Single Side Band (SSB) modulation technique has been powerfully investigated because of its effective optical frequency utilization and the robustness to optical fiber dispersions[16][18]. However such FDM scheme requires high stabilized coherent Laser Diode (LD) and very narrow optical filters to be de-multiplexed in optical stage. So it still includes many problems to be applied into fiber-optic radio access networks from the viewpoint of cost-effective and easy construction of networks. The several CDM schemes such as frequency spread code division multiplexing[28] and time spread code division multiplexing[29][30] have also been investigated because of their easy applicability to random access networks. However

they have the difficulty of high-speed code synchronization between a transmitter and a receiver on optical stage. In addition, the possibility of photonic routing of signals have never been known. The WDM scheme is a promising scheme in recent very high bit rate digital transmission systems. However it is not suitable for the multiplexing of radio signals because it is unreasonable to prepare wavelengths as many as the number of RBSs. Instead it seems to be suitable to be used for other purposes such as the duplex of uplink and downlink in fiber-optic radio access networks.

From the above perspective on the cost-efficiency and the feasibility for photonic routing of signals, the TDM bus link systems are considered as the best choice to construct fiber-optic radio access networks, and it is powerfully studied in this thesis.

Table 2.1: Performance comparison of advantages and disadvantages of various multiplexing schemes.

Multiplexing scheme	Advantages	Disadvantages
Time Division Multiplexing (TDM)	· IM/DD link configuration is allowed · easy photonic routing by photonic time switching · no generation of optical beat noise	· requirement of fast photonic switch operation · requirement of time synchronization control among radio base stations
Subcarrier Multiplexing (SCM)	· IM/DD link configuration is allowed	· the occurrence of optical beat noise · radio signals must be frequency division multiplexing format · photonic routing is impossible
Optical Frequency Division Multiplexing (FDM)	· effective utilization of optical frequency · robustness to fiber dispersion if SSB modulation is used · high receiver sensitivity dùe to coherent detection	· requirement of coherent detection · requirement of very narrow optical filters and frequency shifter for photonic routing
Code Division Multiplexing (CDM)	· easy realization of random access	· requirement of fast code synchronization · requirement of much fast operation of photonic device for coding · feasibility of photonic routing is unknown
Wavelength Division Multiplexing (WDMA)	· IM/DD link configuration is allowed	· requirement of many wavelengths · requirement of wavelength filters and wavelength converter for photonic routing

2.3 Principle of Photonic Natural Bandpass Sampling

Pulse Amplitude Modulation (PAM) systems are promising systems to realize Time Division Multiplexing systems, where multiplexing of several signals is achieved by interleaving the samples of the individual signals. According to the Nyquist sampling theorem, the signal whose highest frequency spectrum component is f_M is determined at regular intervals separated by times $T_s \leq 1/2f_M$, that is, the signal has to be periodically sampled every T_s seconds. T_s, and $f_s = 1/T_s$ are referred to as sampling interval and sampling frequency, respectively. If this theory is applied to the sampling of radio signals whose

highest frequency spectrum component is a few or dozens Giga Hertz, ultra-high-speed sampling frequency is required. However the radio signals are fortunately bandlimited in general. Let the bandwidth of radio signal be B_{RF} and you can find that the required condition about sampling interval can be reduced to,

$$T_s < 1/2B_{RF} \tag{2.1}$$

Such a sampling technique to reduce sampling frequency is referred to as bandpass sampling[37].

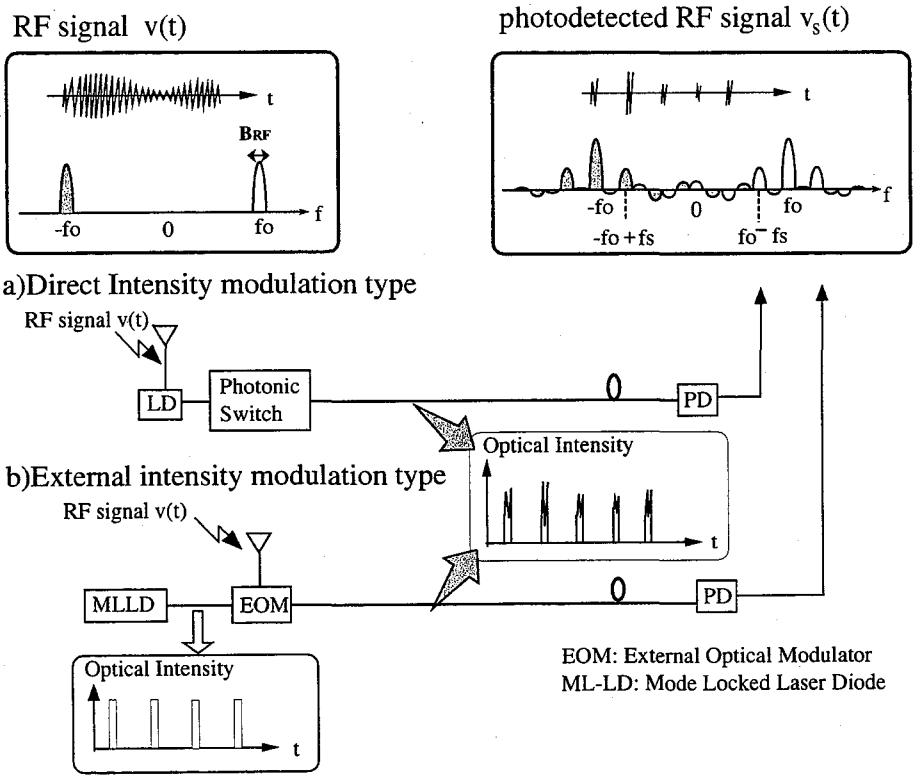

Figure 2.3: Principle of photonic natural bandpass sampling.

Another important concept is photonic natural sampling. Photonic sampling means that the sampling process is executed in optical stage. Figure 2.3 shows fundamental architectures of photonic natural sampling system in two ways. One way is that a photonic switch samples the optical carrier whose intensity was directly modulated by radio signals (Fig.2.3(a)). Another way is that optical pulses generated by a mode-locked laser diode (MLLD)[38][39] are modulated in intensity by the use of external optical modulator (EOM)[40](Fig22.3(b)). The optical pulses obtained by such operations are referred to as Pulse Amplitude Modulated / Intensity Modulated (PAM/IM) optical pulses. In the viewpoint of cost-efficiency, the former is superior to the latter because a MLLD is still comparatively expensive. However the latter scheme has the possibility of very high-speed sampling operation and broadband modulation due to the EOM utilization[41][42].

Let $v(t)$ be a radio signal which is bandlimited to B_{RF} and has the center frequency

of f_0. The PAM/IM optical pulses obtained by the photonic sampling is written by

$$P_r(t) = P_s(1 + mv(t)) \sum_{n=-\infty}^{\infty} p(t - nT_s) \tag{2.2}$$

where $P_r(t)$, P_s, m, and $p(t)$ are optical intensity, average transmitting optical power, modulation index, and sampling pulse waveform, respectively. n is an integer. The output current after photodetection of this PAM/IM optical pulses, $i_s(t)$, is given by,

$$i_s(t) = \alpha_o P_s m v(t) \sum_{n=-\infty}^{\infty} p(t - nT_s) \tag{2.3}$$

where α_o is the responsivity of photodetector. The spectrum of $i_s(t)$ is given by Fourier transforming of $i_s(t)$.

$$I_s(f) = \frac{\alpha_o P_s m}{T_s} \sum_{n=-\infty}^{\infty} P(nf_s)V(f - nf_s) \tag{2.4}$$

where $P(f)$ and $V(f)$ are Fourier transforms of $p(t)$ and $v(t)$, respectively. The waveform $i_s(t)$ and the spectrum $I_s(f)$ have the appearance as illustrated in Fig.2.3 for the case that $p(t)$ is a rectangular pulse waveform and $T_s = 1/2B_{RF}$. Figure 2.3 shows that photodetected PAM signals contains the original radio spectrum, and its replicas at intervals of f_s. The overall spectrum is symmetrical about the frequency f_0. Therefore the original radio signal can be obtained by the use of bandpass filter with the center frequency of f_0 and the bandwidth of B_{RF}. In this example case, $P(f)$ has a Sinc function characteristic and infinite bandwidth. So you can understand from the figure that the condition of Eq.(2.1) is required in order to avoid the interference due to image frequency component.

Now we further extend our discussions for the special case that bandlimited sampling pulse waveform is used instead of a rectangular pulse. Such a case seems to be often encountered in the actual systems. If the highest frequency component of the pulse waveform is limited to f_u and the condition of $f_u < 2f_0 - B_{RF}$ is satisfied, the image spectrum component does not appear in the radio frequency band. This result means that the required condition about sampling frequency can be further reduced to $f_s > B_{RF}$. However we must not forget that bandlimited pulse waveform has wider pulse width than the rectangular one, and it affects the capacity of the TDM systems, because the allowable number of multiplexing signals are determined by the sampling interval T_s divided by the pulse width.

2.4 Photonic TDM Bus Link Systems

Figure 2.4 shows the basic architecture of photonic TDM Bus Link system using photonic natural bandpass sampling technique. Several RBSs are connected to one fiber-optic bus link by use of photonic switch. The photonic switch performs two important functions of photonic sampling and multiplexing of several signals at the same time. Such a multiplexing scheme using photonic switch can much reduce the transmission loss of signal in comparison with the multiplexing scheme using directional coupler because the use of photonic switch can avoid 3 [dB] coupling loss, which is unavoidable in the case using directional coupler[25].

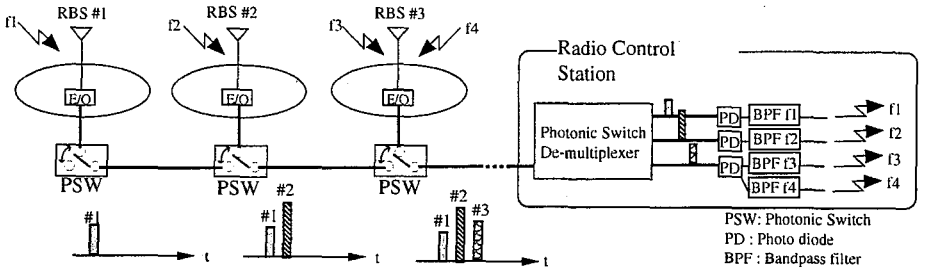

Figure 2.4: Configuration of photonic TDM bus link system.

The theoretical maximum number of multiplexed RBSs is given by,

$$N = T_s/T \tag{2.5}$$

where T_s and T are sampling interval and pulse width, respectively. However, to attain this number of multiplexed RBSs implies the difficulty of time synchronization control among RBSs because each RBS must drive the photonic switch strictly in given time slots. The required accuracy of the time synchronization increases in proportion to the bandwidth of radio signals or the number of connected RBSs, and the required order of accuracy becomes nano second order when the bandwidth of radio signals is mega hertz order. Then the schemes to solve the difficulty of the time synchronization have to be investigated. The solutions of this subject is dealt with in the following chapters 3 and 4 in detail.

As described in Sect.2.2, there exist several multiplexing schemes to construct photonic bus link systems. However here we introduce the SCM bus link systems in detail as the conventional systems competed with the TDM bus link systems. The fundamental system architecture of the SCM bus link is shown in Fig.2.5. The principle of the SCM bus link is based on the fact that frequency division multiplexed signals are obtained after photodetection if several optical carriers modulated by different frequency radio signals are mixed in optical stage. The SCM bus link system has excellence in its much simple configuration. However the optical beat noise between signals severely deteriorates the carrier-to-noise power ratio (CNR) performance of signals detected at the RCS unless the wavelength of optical sources are precisely controlled[19]-[21]. The optical beat noises are caused by photodetecting more than two optical carriers with the frequency difference less than the detection bandwidth. Therefore the TDM bus link systems can be kept from the performance degradation due to optical beat noise and the signal performance is much improved[25].

Another important advantage of the TDM bus link system is the fact the system allows all the connected RBSs to use the same radio frequency because the TDM system gives the independent optical time channel to each RBS. It means that the TDM system can be applied to the single frequency network (SFN) such as CDMA radio systems to be introduced as the radio access format for the IMT2000[34]. In addition, it becomes easier to execute macro-diversity[8] because radio signals of all RBSs are concentrated at the RCS.

Finally in this section, we discuss the capabilities of the photonic routing of radio signals. Suppose that the jth RBS and the kth RBS receive different types of radio service

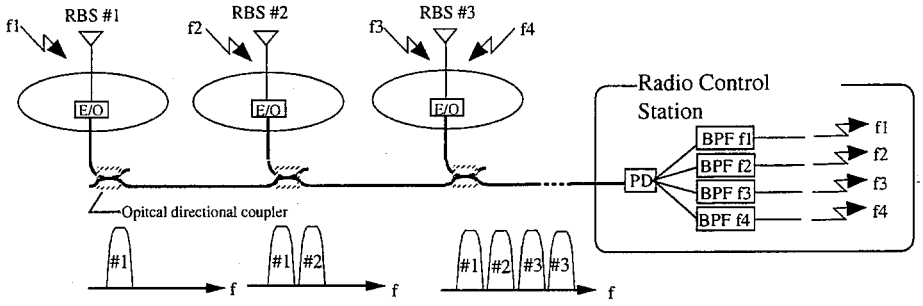

Figure 2.5: Configuration of SCM bus link system.

signals respectively, which have to be transfered to different RCSs in separated locations. Because the signals are multiplexed with TDM format in the fiber-optic bus link, the separation and routing of two radio services can be easily performed by the use of photonic switch. This capability of photonic routing is also an another advantage of the photonic TDM bus link system. However the above supposition means to construct the networks by the manner of one RBS per radio service and it reduces the possibility of universal use of RBSs among several radio services. In general situations, the different radio service is operated under different frequency band. Therefore if an RBS is shared among several radio services, received radio services are the signals with frequency division multiplexing (FDM) format unless any conversion is performed. Consequently, it is impossible to separate and route them in optical stage, once they are converted into optical intensity signals, because such multiple radio services are transfered with SCM format. This subject and the solution are treated in chapter 5 in detail.

2.5 Concluding Remarks

This chapter introduced the concept of fiber-optic radio access networks and several candidates for network configuration and photonic multiplexing scheme applicable to the networks. The suitability of each network configuration and multiplexing scheme was discussed from the viewpoints of simplicity of network configuration and easy realization of demultiplexing of signals in optical stage. As a result, the following advantages of photonic TDM bus link system was confirmed.

1. Photonic TDM bus link system allows a cost-effective construction of radio access networks by the use of IM/DD fiber-optic link.

2. Photonic TDM bus link system offers higher CNR performance of received radio signals than the conventional SCM bus link system because it can be kept from the performance deterioration due to optical beat noises.

3. Photonic TDM bus link system is available for single radio frequency networks.

4. The photonic routing of signals is easily executed by the use of photonic switch because of the time division multiplexing format.

Furthermore it was concluded that the following problems have to be studied and solved in order to realize photonic TDM bus link system and advance the functions of it.

1. The time synchronization control for TDM of signals is difficult, and the required accuracy of the synchronization increases in proportion to the bandwidth of radio signals and the number of connected RBSs.

2. The photonic routing of radio service is impossible when an RBS is universally used among different radio services.

Chapter 3

Photonic Self-synchronous Time Division Multiplexing Bus Link System

3.1 Introduction

Photonic TDM bus link system requires strict time synchronization control among all RBSs in order to realize time division multiplexing of signals. The difficulty of such synchronization control increases as the bandwidth of radio signal or the number of connected RBSs increases, because the required pulse width of TDM signals is inversely proportional to both of them.

In order to solve the difficulty of time synchronization control in TDM bus link system, this chapter newly proposes self-synchronous TDM bus link system. The proposed system needs no synchronization control to assign time slots to RBSs, and allows all RBSs to commonly use the identical optical source provided from the end of bus link. However the system severely degrades the signal power received at an RCS due to the splitting of optical source power and the insertions of many optical devices. Therefore, this chapter investigates the system performance by theoretical analysis of the CNR performance of radio signals detected at an RCS. Furthermore, this chapter proposes the application of an optical pre-amplifier in order to improve the CNR performance, and the improvement is theoretically investigated.

On the other hand, the proposed system needs two independent optical channels. One is the channel to transfer non-modulated optical pulses and the other is that to transfer modulated pulses. Such independent optical channels can be prepared by the use of various optical multiplexing schemes. However this chapter picks up two multiplexing schemes, fiber-space multiplexing utilization and polarization multiplexing utilization, from the viewpoint of the feasibility.

3.2 Self-synchronous TDM Bus Link System

Figure 3.1(a) illustrates the configuration on up link of the proposed self-synchronous TDM bus link system using fiber-space multiplexing scheme. N RBSs and one RCS are connected with two independent fiber-optic bus links. One of the link is used to

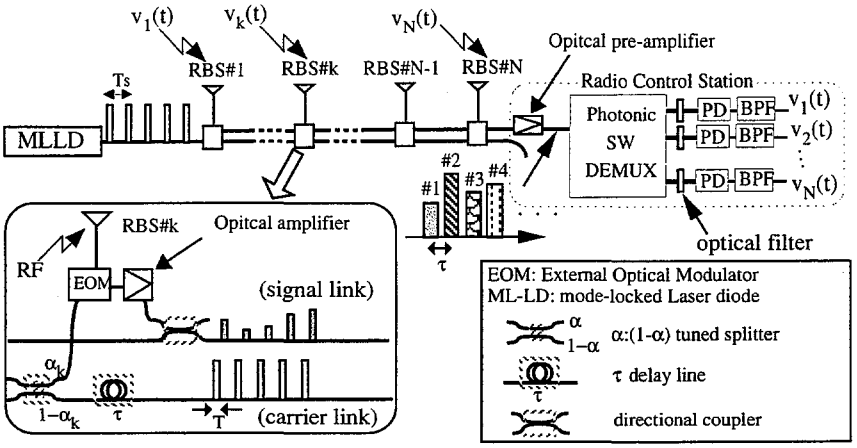

(a) fiber-space multiplexing utilization

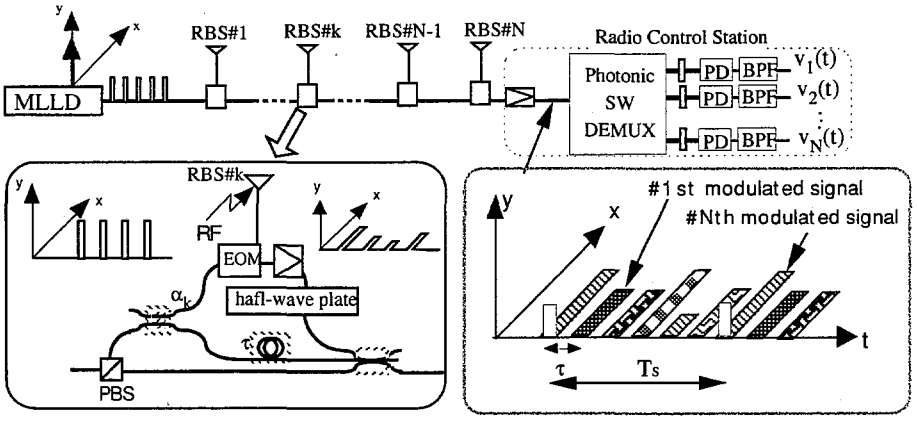

(b) polarization multiplexing utilization

Figure 3.1: System configuration of self-synchronous TDM bus link.

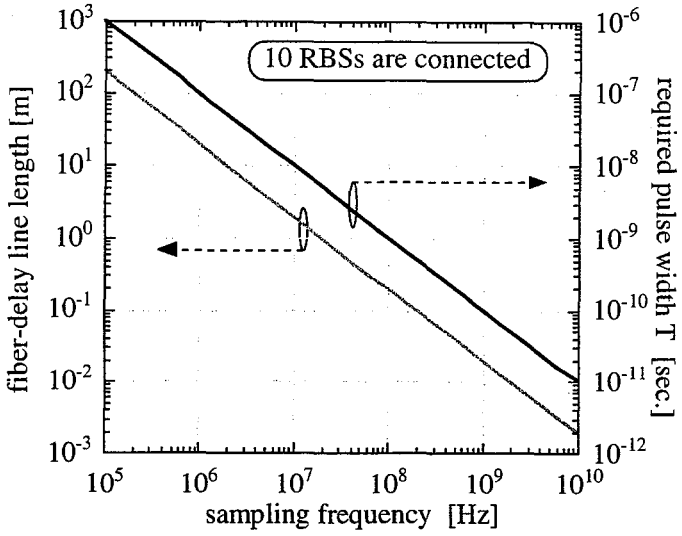

Figure 3.2: Required fiber delay length versus sampling frequency.

transfer non-modulated optical pulses (carrier link) and the other is used to transfer the pulses modulated at each RBS (signal link). Non-modulated optical pulse trains are provided from the end of bus link using a mode-locked pulsed laser diode (MLLD) or the combination of a Laser Diode (LD) and a photonic switch. The optical pulse trains are used to sample and transfer the radio signal, and their repetition rate has to be more than the double of bandwidth of radio signal in order to regenerate it at an RCS, as described in Chapter 3.

k-th RBS splits the power of received non-modulated optical pulses with the ratio of $\alpha_k : (1 - \alpha_k)$ and intensity-modulates them by radio signals using an external optical modulator (EOM) as shown in Fig.3.1(a). A fiber-optic delay line equipped in carrier link generates the appropriate time difference, τ, between the non-modulated pulses to be relayed to the next RBS and the pulses which was already modulated. The purpose of such delay processing is to prevent their overlaps on time axis at the time when they reach the next RBS. Therefore the generated time difference must be more than the pulse width at least. If such processing is executed at all the RBSs in series, time division multiplexing of the signals of all RBSs can be automatically realized and any other synchronization control signaling is not required. The pulse width and the delay time must satisfy the following condition in order to obtain successful TDM signals of all RBSs.

$$T \leq \tau = \frac{T_s}{N} \tag{3.1}$$

where T, T_s, and N are the pulse width, the pulse repetition interval, and the number of connected RBSs, respectively.

Figure 3.2 shows the required pulse width and that translated to the fiber delay length versus sampling frequency, where 10 RBS connection is assumed. For example, if we assume that the bandwidth of radio signal is 200 [MHz], which is the service bandwidth of Japanese PHS, the required repetition interval of pulses becomes T_s=2.5 [ns] (sampling frequency $1/T_s$ = 400[MHz]) and the required delay time becomes 0.25 [ns] which cor-

responds to 50 [mm] fiber-optic delay line. However this condition is valid in the ideal system where there is no time difference error between the signal link and the carrier link. In the real system where there is any time difference error between the two links due to the insertion of EOM, optical amplifier, and the fibers connecting such devices, we have to compensate the time difference error by adjusting the delay time τ, otherwise we have to use narrower pulse width than the delay time in order to avoid the overlaps between pulses in the obtained TDM signals.

At the optical receiver in the RCS, received optical signals are amplified by the use of optical pre-amplifier. The optical pre-amplification can much improve the signal performance as described in the following sections. Then, the TDM pulses are demultiplexed by the use of photonic switch after an optical bandpass filter which removes the excess optical noise. Finally, photodetection and bandpass filtering centered at radio frequency can regenerate the original radio signal of each RBS.

The self-synchronous TDM bus link needs two independent optical links to transfer non-modulated pulses and modulated pulses as already introduced. It can be realized not only by fiber-space multiplexing, but also by other optical multiplexing schemes such as polarization multiplexing. Figure 3.1(b) illustrates the self-synchronous TDM bus link system using polarization multiplexing. The difference from the system using fiber-space multiplexing is that modulated and non-modulated pulses are multiplexed into a single fiber-optic bus link with orthogonal polarization states. Therefore each RBS needs a polarization beam splitter to extract non-modulated pulses, a half-wave plate to rotate the polarization state by $\pi/2$, and a 3×1 directional coupler. Furthermore it is necessary to use polarization maintaining fiber such as PANDA fiber in order to keep the polarization state in the signal transmission. Thus, though the system using polarization multiplexing has an advantage that it needs only one fiber-optic link, it is obvious that the signal loss and the system complexity increases in comparison with the system using fiber-space multiplexing scheme.

3.3 Theoretical analysis of Received CNR

The optical peak power fed into k-th RBS's EOM is given by,

$$P_{in}(k) = P_s L_{bef}(k) \tag{3.2}$$

where P_s and $L_{bef}(k)$ are the transmitting optical peak power of the MLLD and the total loss from which the optical carrier suffers until it reaches the k-th EOM. According to multiplexing scheme used, it is differently given by,

$$L_{bef}(k) = \begin{cases} \Pi_{i=1}^{k-1}(1-\alpha_i)\alpha_k L_s^k & \text{:fiber-space multiplexing} \\ \Pi_{i=1}^{k-1}\left[\frac{1}{3}(1-\alpha_i)\right]\alpha_k (L_d L_s)^k L_c^{k-1} & \text{:polarization multiplexing} \end{cases} \tag{3.3}$$

where α_i, L_d, L_s, and L_c are the power ratio of the tuned splitter in i-th RBS, and the fiber-to-fiber insertion losses of polarization splitter, tuned power splitter, and directional coupler. The output signal power from the EOM is given by,

$$P_o(k,t) = L_m \frac{P_{in}(k)}{2}(1 + m v_k(t)) \tag{3.4}$$

where L_m, m, and $v_k(t)$ are the fiber-to-fiber insertion loss of EOM, modulation index, and modulating signal of k-th RBS, respectively. When the optical signal of k-th RBS reaches the RCS, the received optical power is reduced to,

$$P_r(k,t) = L_m G_p \frac{P_{in}(k)}{2}(1+mv_k(t))L_{after}(k) \tag{3.5}$$

where G_p is the optical pre-amplifier gain, and $L_{after}(k)$ is the total loss from which the modulated optical signal of k-th RBS suffers until it reaches the RCS. $L_{after}(k)$ is given by,

$$L_{after}(k) = \begin{cases} (\frac{1}{2})^{N-k+1} L_c^{N-k+1} L_f & \text{:fiber multiplexing} \\ (\frac{1}{3})^{N-k+1} L_t L_c^{N-k+1} L_d^{N-k} L_f & \text{:polarization multiplexing} \end{cases} \tag{3.6}$$

where L_t and L_f are the fiber-to-fiber insertion losses of half-wave plate and optical filter set up before photodetector at the RCS.

The expression of actual received optical signal in the proposed system equals to the above $P_r(k,t)$ that are sampled with the pulse duty of T/T_s (T:pulse width, T_s:sampling interval). Such sampled signal causes the power penalty of $\left(\frac{T}{T_s}\right)^2$ to photodetected signal[25]. Consequently, the photodetected radio signal power is given by,

$$< i_s^2(k) > = \frac{1}{2}\left(\frac{e\eta}{h\nu}\right)^2 [mG_pL_m\frac{P_{in}(k)}{2}L_{after}(k)]^2 \left(\frac{T}{T_s}\right)^2 \tag{3.7}$$

where e, η, and $h\nu$ are the electron charge, the quantum efficiency of photodetector, and the photon energy.

As for noise factors treated in the analysis of the CNR performance, the amplified spontaneous emission (ASE) should be considered when an optical amplifier is used. Then, the following noise factors are considered; beat noise current among ASEs and signal; beat noise current among ASEs; shot noise current from ASEs; shot noise current from signal; the relative intensity noise (RIN) current; and the receiver thermal noise current. The noise power due to the ASE is studied precisely in [43] and it can be modeled as white Gaussian noise process. Considering the splitting and coupling loss of signal and ASE power, the power spectrum density (PSD) level of each noise current is given by,

$$n_{s-sp}(k) = 4\frac{(\eta e)^2}{h\nu}(G_p-1)\chi n_{sp}L_f \cdot [G_pL_m\frac{P_{in}(k)}{2}L_{after}(k)] \tag{3.8}$$

$$n_{sp-sp} = 2\left[\eta e(G_p-1)\chi n_{sp}L_f\right]^2 W \tag{3.9}$$

$$n_{sp_{shot}} = 2e^2\eta(G_p-1)\chi n_{sp}L_f W \tag{3.10}$$

$$n_{s_{shot}}(k) = 2e^2\left(\frac{\eta}{h\nu}\right)[G_pL_m\frac{P_{in}(k)}{2}L_{after}(k)] \tag{3.11}$$

$$n_{RIN}(k) = RIN\left(\frac{\eta e}{h\nu}\right)^2\left[G_pL_m\frac{P_{in}(k)}{2}L_{after}(k)\right]^2 \tag{3.12}$$

$$n_{th} = \frac{4k_bT_{th}}{R} \tag{3.13}$$

where, χn_{sp}, W, k_b, T_{th}, and R are the spontaneous emission factor, the bandwidth of optical filter, Boltzmann constant, noise temperature, and load resistance of receiver.

Note that each PSD level in case that an optical pre-amplifier is not used is given by substituting 0 for G_p. Considering that the white Gaussian noise current that is sampled with pulse duty T/T_s decades its PSD level by T/T_s[25], the CNR of detected radio signal is finally given by,

$$CNR_k = \frac{< i_s^2(k) >}{\left[(n_{s-sp} + n_{sp-sp} + n_{sp_{shot}} + n_{s_{shot}} + n_{RIN})\frac{T}{T_s} + n_{th}\right] B_{RF}} \tag{3.14}$$

where B_{RF} is the bandwidth of radio signal.

From equations (3.7), (3.8)-(3.13), and (3.14), you can see that the equalization of $P_{in}(k)L_{after}(k)$ for all value of k realizes the equal CNR performance for signals of all RBSs. There exists the set of the power ratio of splitter, α_k, that satisfies this condition. Solving the simultaneous equations, $P_{in}(1)L_{after}(1) = P_{in}(2)L_{after}(2) = \cdots = P_{in}(N)L_{after}(N)$, and the use of the condition, $\alpha_N = 1$, give each α_k in the case of fiber-space multiplexing as,

$$\alpha_k = \begin{cases} \frac{\left(\frac{2L_s}{L_c}\right)^{N-k}\left(\frac{2L_s}{L_c}-1\right)}{\left(\frac{2L_s}{L_c}\right)^{N-k+1}-1} & ; L_c \neq 2L_s \\ \frac{1}{N-k+1} & ; L_c = 2L_s \end{cases} \tag{3.15}$$

and in the case of polarization multiplexing as,

$$\alpha_k = \begin{cases} \frac{(3L_s)^{N-k}(3L_s-1)}{(3L_s)^{N-k+1}-1} & ; L_s \neq \frac{1}{3} \\ \frac{1}{N-k+1} & ; L_s = \frac{1}{3} \end{cases} \tag{3.16}$$

3.4 Numerical results of the CNR Performance

In the following calculations, we use the parameters shown in table 3.1 unless value is specified in the figure.

Table 3.1: Default parameters used in calculations.

RIN	-152[dB/Hz]	T_{th}	300[K]
α_o	0.8[A/W]	R	50Ω
P_s	20 [dBm]	χn_{sp}	2.0
m	0.5	B	300 [kHz]
T/τ	1.0	W	1 [THz]
L_m	3 [dB]	L_s, L_c	0.5 [dB]
L_d, L_t	0.5 [dB]	L_f	0.5 [dB]

Figure 3.3 shows the received CNR performance versus the number of connected RBSs in case that optical pre-amplifier is not used. It includes the performance in fiber-space multiplexing utilization (fiber-space MUX) and that in polarization multiplexing utilization (polarization MUX) for different values of transmitting optical peak power P_s. You can see that the CNR in both schemes decreases as the number of RBSs increases. However the degradation slope in polarization MUX is more rapid than that in fiber-space

MUX because of the additional optical power loss due to the insertions of PBSs, half-wave plates, and couplers. In the small number of RBSs, the increase of P_s cannot much improve the CNR performance because the relative intensity noise dominates the performance. On the other hand, in the large number of RBSs, 5[dBm] addition in P_s can improve the CNR performance by 10[dB] because the thermal noise dominates the performance. This figure shows that the system using fiber-space MUX allows only 7 RBSs connection at $P_s = 10$[dBm] if 40 [dB] of CNR is required.

In the region where thermal noise dominates the performance, optical pre-amplification before photodetection is effective to improve the CNR performance. Figure 3.4 shows the received CNR performance of fiber-space MUX system versus pre-amplifier gain. You can see that the pre-amplification can much improve the CNR performance especially in the condition that large number of RBSs are connected. For example, in the case of $N = 15$ and $P_s = 20$ [dBm], the pre-amplification improves the CNR by 28 [dB]. You can also find the saturation characteristic of the CNR performance at the large pre-amplifier gain because the optical beat noise between signal and ASE dominates the CNR performance.

Figure 3.5 shows the relationship between the connectable number of RBSs and pre-amplifier gain. The connectable number of RBSs is the maximum number of RBSs that can satisfy the threshold CNR, CNR_{th}. You can see that pre-amplification can increase the number of connectable RBSs. For example, the system using fiber-space MUX allows the connection of 12 RBSs at $G_p = 22$ [dB] under the requirement of $CNR_{th} = 40$ [dB].

As described in Sect.3.2, we may have to reduce the pulse width than the width required in the ideal system in order to avoid stringent requirement of accuracy in delay length adjustment. Therefore we should investigate the affection of pulse duty reduction on the CNR performance. Figure3.6 shows the relationship between received CNR versus pulse duty. The pulse duty is here defined as the ratio of the pulse width in the real system, T, and that in ideal system, τ, that is, T/τ. The figure shows that the CNR is degraded as the pulse duty decreases in spite of the value of G_p. You can see that in the case that G_p is small, the CNR degradation is proportional to the pulse duty to the second power because the thermal noise dominates the performance, while in the case that G_p is large, the CNR degradation is proportional to the pulse duty because the beat noise between ASE and signal dominates the CNR performance. Consequently, the use of optical pre-amplification is also effective to reduce the performance degradation due to the pulse width reduction.

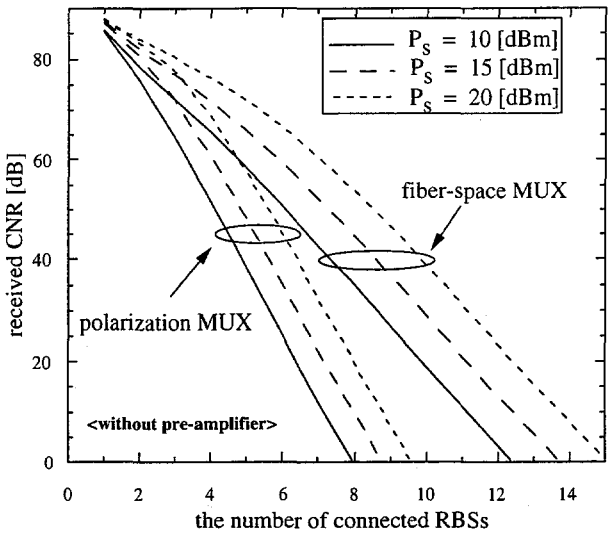

Figure 3.3: Received CNR versus the number of connected RBSs in case of no pre-amplification.

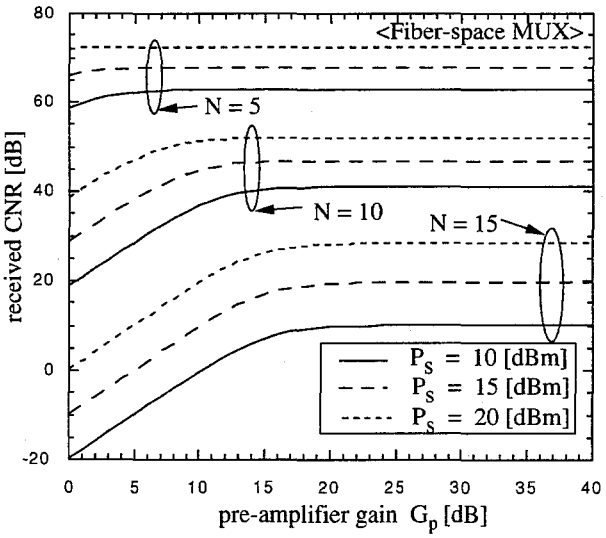

Figure 3.4: Received CNR versus pre-amplifier gain.

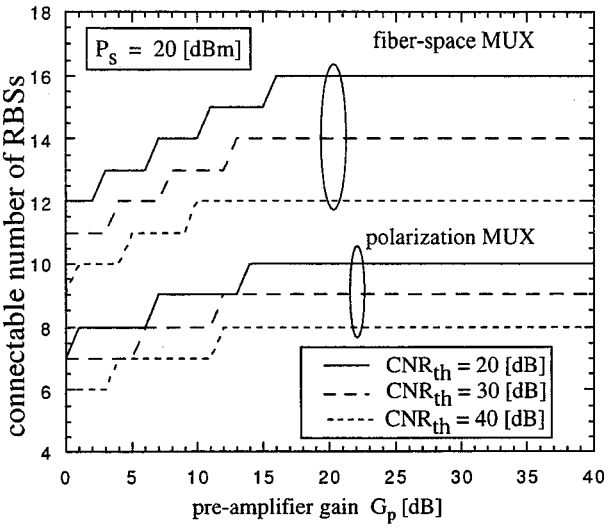

Figure 3.5: Connectable number of RBSs versus pre-amplifier gain.

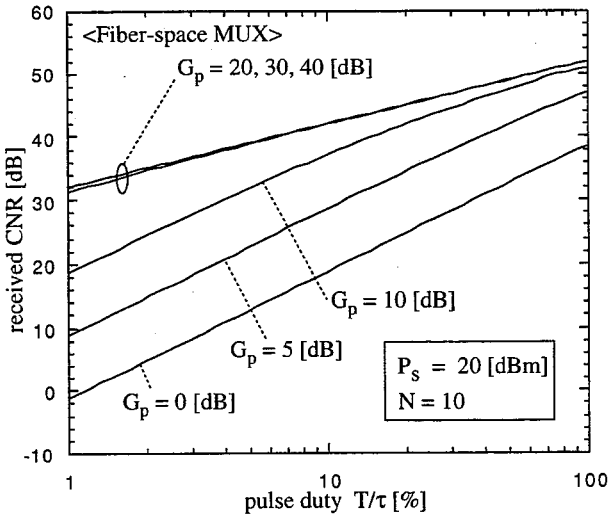

Figure 3.6: Received CNR versus pulse duty.

3.5 Concluding Remarks

This chapter proposed photonic self-synchronous TDM bus link system for fiber-optic radio access networks, which need no time synchronization control among RBSs connected to a fiber-optic bus link and can share a single laser source among RBSs. The configurations of the systems utilizing fiber-space multiplexing and polarization multiplexing were described, and the CNR performance of radio signal detected at an RCS was theoretically analyzed. The splitting power ratio used at each RBS was optimized to balance the CNR performance of all RBSs. The theoretical analysis clarifies the relationship among the CNR, number of connected RBSs, transmitting optical power, and pre-amplifier gain. It was shown that the use of optical pre-amplifier is effective to improve the received CNR performance, and the CNR of 40 [dB] can be attained when 12 RBSs is connected.

Chapter 4

Photonic Asynchronous Time Division Multiple Access Bus Link System

4.1 Introduction

In the previous chapter, the self-synchronous TDM bus link system was proposed, where the synchronization control for time division multiplexing of signals is automatically performed by the use of fiber-optic delay line equipped in each RBS.

Another approach to solve the difficulty of synchronization control among RBSs is the adoption of asynchronous access technique. The asynchronous access system does not require any synchronization control among RBSs, and allows much flexible construction of networks because the system can easily extend some RBSs connected to the fiber-optic bus link without any change of system.

On the other hand, in the perspective on the future pico-cellular radio environment for multimedia data transmissions, such as wireless ATM, it is expected that wide band radio packet communications becomes popular. It means that each RBS receives radio bursts occasionally, and the probability that all the RBSs are receiving any radio signal at the same time is not much high. In such environment, the TDM system where all RBSs are always keeping its own optical channel does not seem to be effective from the viewpoint of the efficient use of fiber-optic link.

This chapter therefore proposes Asynchronous Time Division Multiple Access (TDMA) bus link system and discusses its availability. The asynchronous TDMA system allows RBS to access the fiber-optic bus link only when it receives radio bursts. Such asynchronous access system however causes collision among radio bursts if several RBSs access the fiber-optic link at the same time, and the collision causes radio burst loss. Thus, the proposed asynchronous TDMA system uses natural bandpass sampling technique in order to convert received radio bursts into narrow pulsed optical bursts in order to reduce the probability of the collision. The converted signal is referred to as pulse amplitude modulated/optical intensity modulation (PAM/IM) bursts, and the probability that a radio burst is lost due to the collision is referred to as burst loss probability, in this chapter. The burst loss probability depends on the number of RBSs connected to the bus link and the traffic intensity generated at each radio zone. Then, this chapter theoretically

investigates the dependencies, and moreover, proposes access control methods to reduce the burst loss probability and investigates their effectiveness.

Section 2 describes the concept and the configuration of asynchronous TDMA bus link system, section 3 shows the analytical model for the burst loss probability. Sections 4 and 5 theoretically analyze the burst loss probability and the carrier-to-noise power ratio (CNR), respectively. Section 6 shows and discusses numerical results of the burst loss probability and the CNR.

4.2 Asynchronous TDMA Bus Link System

Figure 4.1 illustrates the configuration of the proposed asynchronous TDMA bus link system. Many RBSs and RCSs are connected with a fiber-optic bus link with intermediate

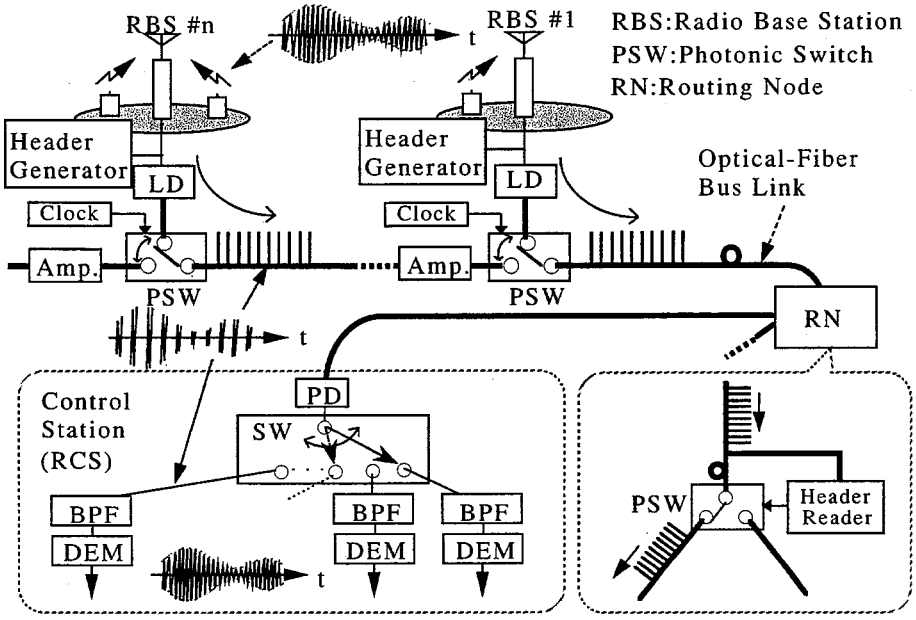

Figure 4.1: Configuration of Asynchronous TDMA bus link system.

routing node (RN). The function of the intermediate RN is to de-multiplex the transfered radio signals and switch them into the desired optical path if they have different destination RCSs.

Radio burst signals received at an RBS directly modulate a laser diode (LD) after a digital header signal is attached to recognize the start point of the burst frame, the base station number, and the destination RCS address. As a result, the intensity-modulated (IM) optical signal with a optical digital header signal is obtained. Then this IM optical signal is asynchronously fed into the fiber-optic bus link by the use of photonic switch. This photonic switch not only connects a RBS to the optic bus link but also performs the natural bandpass sampling of the optical IM signal at the same time. Consequently radio signals launched from many RBSs are asynchronously time-division multiplexed with pulse amplitude modulated radio (PAM)/ optical intensity modulation (IM) signal format.

The asynchronous TDMA bus link system has the additional advantages of much flexible construction of networks because the system can easily extend some RBSs connected to the fiber-optic bus link without any change of system. Furthermore, fast and broadband operations of RN can be expected because the RN is composed of a simple photonic switch. However the RN requires the sub-system to detect a digital header signal and recognize both of the destination address and the start point of PAM/IM burst, however it seems that the RN and the RCS are allowed to equip more complicated configurations than RBSs. On the other hand, the asynchronous TDMA system have the problem that burst signals may be lost due to the collision among asynchronously transmitted PAM/IM bursts. This problem is discussed in detail in the next section.

At the receiver in the RCS, radio signals can be reproduced by de-multiplexing after photodetection, and bandpass filtering, if we use the appropriate sampling frequencies described in Sect.2.3.

4.3 Radio Burst Collision

In the asynchronous TDMA bus link system, PAM/IM bursts generated by radio signals at RBSs are asynchronously multiplexed into the fiber-optic bus link, thus the radio bursts may be lost due to collisions if several RBSs transmit their radio bursts at the same time. Figure 4.2 illustrates the mechanism of collision among PAM/IM bursts. A PAM/IM

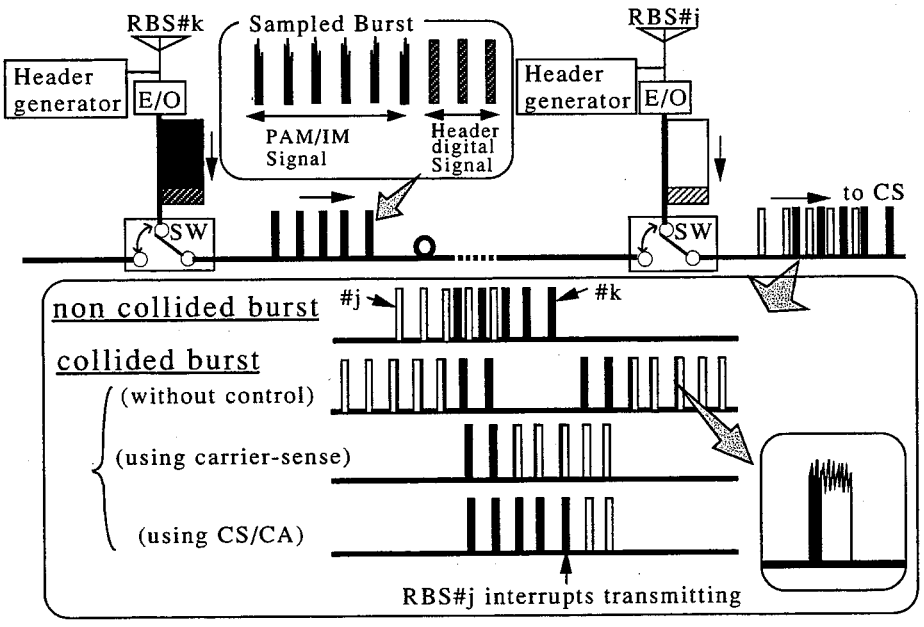

Figure 4.2: Mechanism of collision among PAM/IM bursts.

burst is lost when the transmission of it are accidentally terminated at the photonic switch of an intermediate RBS which are transmitting a radio burst at the same time. The occurrence of collision between two radio bursts drops the one transfered from the RBS which locates further from the RCS. In other words, the collision between the radio burst from jth RBS and that from kth RBS ($j < k$) causes the loss of the radio burst

from kth RBS. Consequently, the throughput of radio bursts decreases, and the quality of the received radio signal is deteriorated. One of the methods to reduce the burst loss probability is the reduction of the pulse width of PAM/IM signals because even if two RBSs transmit radio bursts at the same time, the burst loss does not occur unless their pulse transmitting time is just same. However the reduction of pulse width causes the decrease of signal power detected at the RCS under the condition of the fixed optical peak power. The relationship between the pulse width reduction and the degradation of carrier-to-noise power ratio performance are discussed in Sect.4.6. Here we consider the use of some access controls in order to reduce the burst loss probability without the reduction of received signal power: carrier sense (CS) control, and carrier sense / collision avoidance (CS/CA) control. In the theoretical analysis of burst loss probability, we consider the following three types of access control;

1) with no control
Each RBS transmits the PAM/IM bursts without any attention to other busts on the fiber-optic bus link. This type of system is the most fundamental and simplest one.

2) with carrier-sense (CS) control
Each RBS is always monitoring the existence and the timing of optical pulses that are already fed into the bus link from other RBSs. When an RBS tries to transmit its own signals, it can start its sampling and transmission at the different timing from the monitored pulses and can avoid the collision. However the optical pulses that RBS can monitor are limited to those transmitted from further located RBSs than that. In other words, further RBSs cannot recognize whether the nearer RBSs are transmitting signals or not, and of course the timing of the optical pulses. Therefore it is unable to avoid the collision perfectly even if the carrier sense control is applied. In the case that further RBSs starts the transmission of its optical pulses when a nearer RBS is already under the state of transmission, the pulses may be lost due to the collision.

3) with carrier-sense and collision avoidance (CS/CA) control
In the above, we mentioned that we can not avoid collisions perfectly even if the carrier-sense control is applied. However collisions can be detected at each RBS by the carrier-sense. Then in this type of control, each RBS not only monitors transfered optical pulses, but also interrupts its own transmission of signals when the collision is detected. Hence, the further RBS on the optic bus link has the higher priority of transmitting the signals than the nearer RBS, in contrast to the types of control **1)** and **2)**, where the signals transmitted from further RBSs are lost when a collision occurs.

Another technique to reduce the probability of burst collision is pulse width control of the PAM/IM bursts. The improvement due to the control is based on the fact that the narrower pulse width is sufficient for the nearer RBSs to attain the required received signal power. The improvement effect on the performance due to this techniques is discussed in Sect..4.6.

4.4 Theoretical Analysis of Burst Loss Probability

In this section, we theoretically analyze burst loss probability. RBSs are numbered from one which is nearest to the RCS. Concerning radio signal model, it is assumed that one radio carrier is used to multiplex all users with TDMA format in a radio zone. It is also assumed that the length of the TDMA radio burst is fixed value, H [sec.], and that the interval between two successive bursts has an exponential distribution with mean a. According to these assumptions, mean traffic per RBS is given by

$$A_{RBS} = \frac{H}{a+H} \quad \text{[erl/RBS]}. \tag{4.1}$$

Let A_{kj} denote the event that a PAM/IM burst from jth RBS is not lost due to the collision with bursts from kth RBS ($k \neq j$) when the jth RBS receives a radio burst at time t_0 and transmits it into the fiber-optic bus link. In this paper, "collision" means the case that two bursts overlap and the optical pulses included in them further overlap. Thus the probability of the event A_{kj}, $P(A_{kj})$, is given by

$$\begin{aligned} P(A_{kj}) &= 1 - P_{over} \cdot p_c \\ P_{over} &: \text{the probability that bursts overlap} \\ p_c &: \text{the probability that the included optical pulses overlap.} \end{aligned} \tag{4.2}$$

In the following analysis, $P(A_{kj})$ will be first derived, and next will be derived the throughput , $P_{through_j}$, which is the probability that a certain burst from jth RBS successfully reaches the RCS without any collision with other bursts. Since traffic controls in all radio zones are mutually independent, $P(A_{kj})$ $(k = 1, 2, \ldots, M)$ is mutually independent of the value of k. Therefore $P_{through_j}$ is given by

$$P_{through_j} = \prod_{k=1}^{M} P(A_{kj}), \tag{4.3}$$

where M is the total number of RBSs connected to a bus link. By the use of $P_{through_j}$, the burst loss probability of the jth RBS's burst, P_{loss_j}, is written by

$$P_{loss_j} = 1 - P_{through_j}. \tag{4.4}$$

Now, to derive $P(A_{kj})$ we consider two cases (a) and (b) as shown in Fig.4.3: one is the case that the jth RBS starts the transmission just during the transmission of the other kth RBS (Fig.4.3a). For example of $k < j$, the kth RBS is just transmitting a burst when the burst from jth RBS reaches the kth RBS's photonic switch, and for $k > j$, the jth RBS starts to transmit a burst while the burst from kth RBS is passing through the jth RBS's photonic switch. Another is the case that the jth RBS starts the transmission in the presence of no other burst on the bus link (Fig.4.3b).

For the case (a), let z_i denote the time interval between the start point of the burst from the jth RBS, t_0, and that of ith burst from the kth RBS. Here z_1 is composed of two portion, x_0 and y_0 as shown Fig.4.3. For the case (b), z_i' is defined by the similar manner to z_i in the case (a). The probability that a state is the case (a) and the probability that one is the case (b), those are p_a and p_b, are derived from the probability that a certain RBS is transmitting a burst at an arbitrary time. Since this probability is given by mean traffic per RBS, A_{RBS} [erl], p_a and p_b are given by $H/(a+H)$ and $a/(a+H)$, respectively.

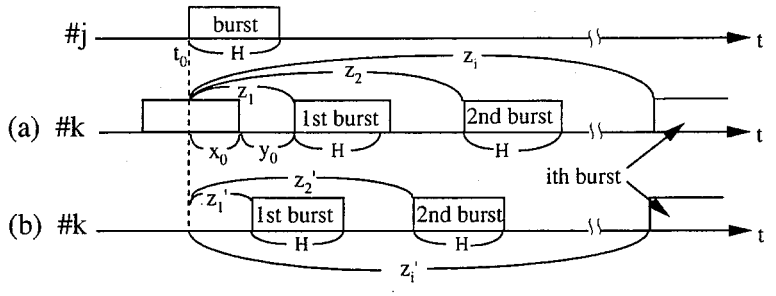

Figure 4.3: Collision among bursts.

4.4.1 Analysis in case of no control

Let $P_{over}(i)$ denote the probability that a burst from the jth RBS overlaps with i bursts from kth RBS. Taking into account that burst length is fixed value H, $P_{over}(i)$ is given by

$$P_{over}(0) = p_b \int_H^\infty p_{z_1'}(z_1')dz_1', \tag{4.5}$$

$$P_{over}(1) = p_a \int_H^\infty p_{z_1}(z_1)dz_1 + p_b \int_0^H p_{z_1'}(z_1')dz_1', \tag{4.6}$$

$$P_{over}(2) = p_a \int_0^H p_{z_1}(z_1)dz_1, \tag{4.7}$$

$$P_{over}(i) = 0 \quad ; i \geq 3, \tag{4.8}$$

where $p_{z_i}(z_i)$ and $p_{z_i'}(z_i')$ are the pdf (probability density function) of z_i and z_i' , respectively. x_0 is an uniform distributed variable in the interval $0 \leq x_0 \leq H$, and y_0 is an exponential distributed variable with mean a. Since x_0 and y_0 are mutually independent, the pdf of $z_1 = x_0 + y_0$, $p_{z_1}(z_1)$, is derived from the convolution of $p_{x_0}(x_0)$ and $p_{y_0}(y_0)$ as

$$p_{z_1}(z_1) = \begin{cases} \frac{1}{H}(1 - e^{-\frac{z_1}{a}}) & ; 0 \leq z_i \leq H \\ \frac{1}{H}e^{-\frac{z_1}{a}}(e^{\frac{H}{a}} - 1) & ; z_i > H \\ 0 & ; z_i < 0. \end{cases} \tag{4.9}$$

On the other hand, z_1' is also an exponential distributed variable with mean a, and its pdf is given by

$$p_{z_1'}(z_1') = \begin{cases} \frac{1}{a}e^{-\frac{z_1'}{a}} & ; z_1' \geq 0 \\ 0 & \text{otherwise.} \end{cases} \tag{4.10}$$

Substitution of Eq.(4.9) and (4.10) into Eq.(4.5)-(4.7) gives,

$$P_{over}(0) = \frac{1}{1 + \frac{H}{a}}e^{-\frac{H}{a}}, \tag{4.11}$$

$$P_{over}(1) = \frac{2}{1 + \frac{H}{a}}(1 - e^{-\frac{H}{a}}), \tag{4.12}$$

$$P_{over}(2) = \frac{\frac{H}{a}}{1 + \frac{H}{a}}\left\{1 + \frac{a}{H}(e^{-\frac{H}{a}} - 1)\right\}. \tag{4.13}$$

Now, a burst is composed of optical PAM/IM pulses with sampling interval T_s and pulse width τ_j. Then, two bursts doesn't collide unless their optical pulses overlap with each other. Since the sampling time can be modeled as an uniform distributed random variable in the interval $[-\frac{T_s}{2}, \frac{T_s}{2}]$, the probability that a pulse in the burst from kth RBS overlaps with one from jth RBS, $p_{c_{jk}}$, is given by

$$p_{c_{jk}} = \begin{cases} \frac{\tau_j+\tau_k}{T_s} & ;\tau_j + \tau_k \leq T_s \\ 1 & ;\tau_j + \tau_k > T_s. \end{cases} \tag{4.14}$$

Therefore, when i bursts from kth RBS overlap with a burst from jth RBS, the probability that no optical pulse overlaps between the jth and kth RBS's bursts is given by $(1-p_{c_{jk}})^i$. By averaging it with respect to i, $P(A_{kj})$ is obtained as

$$P(A_{kj}) = \begin{cases} \sum_{i=0}^{\infty} \left(1 - p_{c_{jk}}\right)^i P_{over}(i) & ;k < j \\ 1 & ;k \geq j. \end{cases} \tag{4.15}$$

Finally substituting Eq.(4.15) into Eq.(4.3) gives

$$P_{through_j} = \prod_{k=1}^{M} \sum_{i=0}^{\infty} \left(1 - p_{c_{jk}}\right)^i P_{over}(i). \tag{4.16}$$

4.4.2 Analysis in case of carrier sense control

As a result of carrier sense control use, a burst from jth RBS is lost only when it reaches the photonic switch of the kth RBS which is nearer to the RCS ($k < j$) and the RBS is just transmitting its own burst (see Fig.4.3a). Hence, $P(A_{kj})$ is given by

$$P(A_{kj}) = \begin{cases} \left(1 - p_{c_{jk}}\right) p_a + p_b & ;k < j \\ 1 & ;k \geq j, \end{cases} \tag{4.17}$$

and substituting Eq.(4.17) into Eq.(4.3) gives

$$P_{through_j} = \prod_{k=1}^{j-1} \left[\left(1 - p_{c_{jk}}\right) p_a + p_b\right]. \tag{4.18}$$

4.4.3 Analysis in case of carrier-sense / collision avoidance control

In case of CS/CA use, the burst from jth RBS is lost when it collides with bursts from the further kth RBS's ($k = j+1, \ldots, M$), unlike the case of only carrier sense control use. The jth RBS interrupts to transmit its own burst in order to avoid the collision with bursts from the further RBSs if detecting the occurrence of collision. Therefore, the burst signal of jth RBS is lost when it collides with the 1st burst signal of the further kth RBS in the cases of Fig.4.3(a) and 4.3(b). Then $P(A_{kj})$ is given by

$P(A_{kj})$

$$= \begin{cases} p_b \int_H^\infty p_{z_1'}(z_1')dz_1' + p_a \int_H^\infty p_{z_1}(z_1)dz_1 \\ \quad + \left(1 - p_{c_{jk}}\right)\left[p_a \int_0^H p_{z_1}(z_1)dz_1 + p_b \int_0^H p_{z_1'}(z_1')dz_1'\right] & ; k > j \\ 1 & ; k \leq j, \end{cases} \tag{4.19}$$

and substituting Eq.(4.19) into Eq.(4.3) gives

$$P_{through_j} = \prod_{k=j+1}^{M} P(A_{kj}). \tag{4.20}$$

4.5 Theoretical Analysis of Received CNR

In this section, we theoretically analyze carrier-to-noise ratio (CNR) of radio burst received at the RCS. In this chapter, we assume that an optical amplifier is equipped just before every photonic switch and before the RCS in order to compensate fiber transmission loss and switch insertion losses. The power spectral density (psd) of the amplified spontaneous emission (ASE), N_{sp}, is given by[46]

$$N_{sp} = \frac{n_{sp}}{\eta_a}\frac{G_a - 1}{G_a} h\nu \tag{4.21}$$

where G_a, n_{sp}, η_a and $h\nu$ are the amplifier gain, the spontaneous emission factor, the quantum efficiency of the amplifier and the photon energy, respectively. In the following analysis, we ignore the nonlinearity of LD and the noise generated in radio link.

When the kth RBS receives a radio burst, $g_k(t)$, and the PAM/IM burst generated from it are transfered to the RCS without any collision with other bursts, the photo-detector output current, $i_{out}(t)$, at the RCS is written by

$$i_{out}(t) = \sum_k \sum_{l=-\infty}^{\infty} \alpha_o P_r (1 + g_k(t)) p(t - lT_s + t_k) + n(t), \tag{4.22}$$

where $p(t)$, t_k, P_r and α_o are a rectangular pulse with the unit amplitude and the pulse width of τ_k, the start time of sampling, the average received optical power and the responsivity of PD, respectively. In this paper, G_a[dB] is assumed to equal to the transmission loss between two neighboring RBSs, L[dB], which including the fiber loss and the insertion loss of photonic switch. Thus, the received optical power from all RBSs, P_r, is equal to the transmitting optical power, P_t. $1/T_s$ is the sampling frequency which is given by the double of the bandwidth of radio signal, B_{RF},

$$\frac{1}{T_s} = 2B_{RF}. \tag{4.23}$$

The white noise photocurrent $n(t)$ is given by

$$n(t) = i_{RIN}(t) + i_{shot}(t) + i_{th}(t) + i_{s-sp}(t) + i_{sp-sp}(t), \tag{4.24}$$

where $i_{RIN}(t)$, $i_{shot}(t)$, $i_{th}(t)$, $i_{s-sp}(t)$ and $i_{sp-sp}(t)$ are the relative intensity noise (RIN) current, the shot noise current, the receiver thermal noise current, the beat noise current

among ASEs and optical signal and the beat noise current among ASEs, respectively. These noise powers in the bandwidth of radio signal, B_{RF}, are given by

$$\begin{aligned} < i_{RIN}^2 > &= RIN\,(\alpha_o P_r)^2\, B_{RF}, && (4.25)\\ < i_{shot}^2 > &= 2e\alpha_o(P_r + m_k N_{sp} W) B_{RF}, && (4.26)\\ < i_{th}^2 > &= \frac{4kT_{th}}{R} B_{RF}, && (4.27)\\ < i_{s-sp}^2 > &= 4\alpha_o^2 m_k N_{sp} P_r B_{RF}, && (4.28)\\ < i_{sp-sp}^2 > &= 2\alpha_o^2 (m_k N_{sp})^2 (W - f_0) B_{RF}, && (4.29) \end{aligned}$$

where RIN, m_k, W, k, T_{th}, and R are the psd of the relative intensity noise of LD, the number of optical amplifiers between the kth RBS and the RCS, the bandwidth of optical filter at the RCS, Boltzmann constant, the noise temperature and the load resistance, respectively.

After demultiplexing of PAM signals from the output current $i_{out}(t)$ by the distributor, and filtering by the ideal bandpass filter with the center-frequency of f_0 and the bandwidth of B_{RF}, we can reproduce an original radio burst, $\hat{g}_k(t)$, which is given by

$$\hat{g}_k(t) = \frac{\tau_k}{T_s} \alpha_o P_r g_k(t). \quad (4.30)$$

Therefore the carrier power of $\hat{g}_k(t)$ is given by

$$< i_k^2 > = \frac{1}{2}\left(\frac{\tau_k}{T_s}\right)^2 (\alpha_o P_r)^2. \quad (4.31)$$

On the other hand, after the demultiplexing and the filtering, the noise power $n_{PAM}(t)$ is equal to $\frac{\tau_k}{T_s}$ times the power of $n(t)$[24]. From Eq.(4.25)-(4.29) and (4.31), consequently, the received CNR of the reproduced radio signal at the RCS is given by

$$\begin{aligned} \left(\frac{C}{N}\right)_{RCS} &= \frac{< i_k{}^2 >}{\frac{\tau_k}{T_s}\left[< i_{RIN}^2 > + < i_{shot}^2 > + < i_{th}^2 > + < i_{s-sp}^2 > + < i_{sp-sp}^2 >\right]} \\ &= \frac{\frac{1}{2}\frac{\tau_k}{T_s}(\alpha_o P_r)^2}{\left[RIN\,(\alpha_o P_r)^2 + 2e\alpha_o\{P_r + m_k N_{sp} W\} + \frac{4kT_{th}}{R}\right.} \\ &\qquad \left. + 4\alpha_o^2 m_k N_{sp} P_r + 2\alpha_o^2 (m_k N_{sp})^2 (W - f_0)\right] \frac{1}{2T_s}. \end{aligned} \quad (4.32)$$

4.6 Performance Evaluations

In this section, the burst loss probability and the CNR are calculated and compared among three types of transmission control (with no control, using CS, and using CS/CA). Parameters used for the calculations are shown in Table 4.1.

4.6.1 Performance in case of no control

Figure 4.4 shows burst loss probabilities versus pulse width of PAM/IM bursts for different values of average traffic A_{RBS}. The abscissa is the pulse width normalized by the sampling

Table 4.1: Parameters used in calculations

RIN	-152dB/Hz	f_0	1GHz
α_o	0.8[A/W]	R	50Ω
n_{sp}	2.0	T_{th}	300[K]
η_a	0.5	L	5dB
W	1THz	P_t	10dBm

interval T_s, that is, the pulse duty. In this figure, numerical results of P_{loss} of 10th RBS's bursts are shown assuming that 10 RBSs are connected on the fiber-optic bus link. It is seen that burst loss probability is much improved as pulse width is reduced for any values of A_{RBS}.

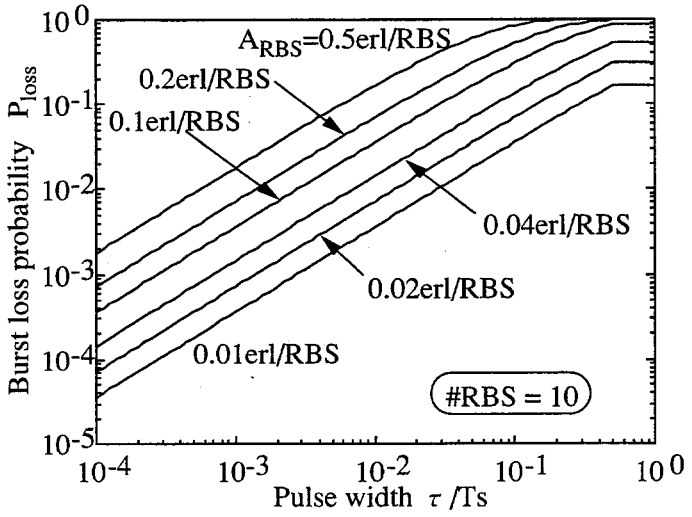

Figure 4.4: Burst loss probability versus pulse width.

Figure 4.5 indicates required pulse width for 10th RBS's bursts to satisfy $P_{loss} = 10^{-3}$ as a function of average traffic per RBS, and also shows the received CNR when the value of required pulse width is used. The required pulse width and the received CNR in synchronous TDMA (STDMA) method are also shown as the system performance to be compared. It is seen that the received CNR in the proposed system deteriorates in comparison with STDMA because we must reduce the pulse width into one divided hundreds or thousand in comparison with that in the STDMA system in order to satisfy the quality of $P_{loss} = 10^{-3}$. However, even under the condition of $\tau/T_s = 10^{-4}$ and $A_{RBS} = 0.4$[erl/RBS], the received CNR of more than 40[dB] is obtained at the RCS.

Figure 4.6 shows burst loss probability and received CNR versus the RBS number which is numbered from the RCS for the case of $\tau/T_s = 10^{-3}$. In case of no control, P_{loss} and CNR deteriorate as the RBS becomes farther from the RCS (as the RBS number increases), because of the use of photonic switch to multiplex PAM/IM bursts. However, we can easily add some RBSs without any troublesome change of the whole system only

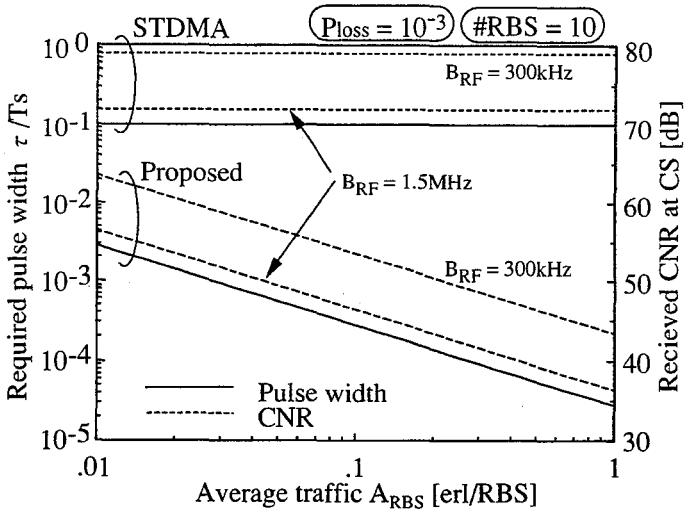

Figure 4.5: Required pulse width and received CNR as a function of average traffic per RBS.

if we can put up with a little deterioration of burst loss probability and received CNR.

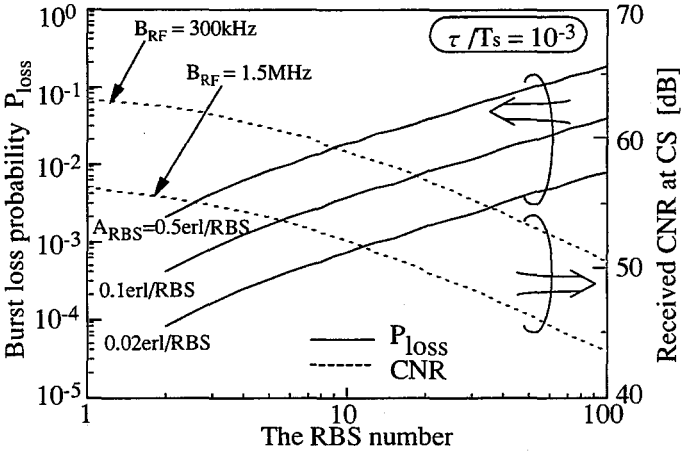

Figure 4.6: Burst loss probability and received CNR versus the RBS number.

4.6.2 Performance improvement due to CS, CS/CA, and variable pulse width controls

Figure 4.7 shows the relationship between burst loss probability and RBS number for three types of transmission control (with no control, CS, and CS/CA) when 10 RBSs are connected to bus link. In this figure, the solid lines shows P_{loss} for the case that all RBSs use the same pulse width by which the CNR of the farthest RBS, that is, the most deteriorated CNR obtained in the system, can attain the required CNR of 40 [dB]. As

shown in Fig.4.6, the burst from the RBS nearer to the RCS has a better received CNR at the RCS, in other words, the narrower pulse width is sufficient for the nearer RBS to obtain the required CNR. Thus, it is expected to reduce the burst loss probability due to such pulse width reduction. Then, with the dashed lines this figure also shows the burst loss probability for the case that each RBS uses the independent pulse width by which each RBS can attain the required CNR (variable pulse width). It is also seen from Fig.4.7

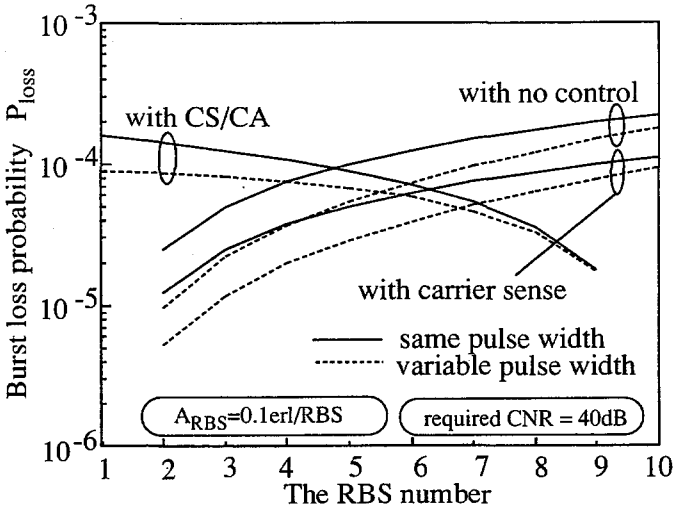

Figure 4.7: Burst loss probability and received CNR versus the RBS number with variable pulse width and control.

that using variable pulse width is more effective to improve P_{loss} for the nearer RBS in any types of control.

It is seen from the figure that we can reduce burst loss probability to the half of that with no control by the use of carrier sense. On the other hand, the characteristic of P_{loss} in the system with CS/CA is reverse to those of the systems with no control or with CS because the further RBS has the higher priority to transmit bursts.

Comparing among all control types of control method, it is found that the CS method with variable pulse width is the best choice in order to minimize the worst P_{loss}. And from another viewpoint of system's simplicity, the method without any carrier sense and only with variable pulse width is effective.

Figure 4.8 shows the connectable number of RBSs versus pulse width in case of no control or carrier-sense. The connectable number of RBSs is defined as the maximum number of RBSs that can satisfy required burst loss probability of 10^{-3} when all RBSs use the same pulse width. It is seen that the system with carrier sense control can connect double number of RBSs in comparison with the system with no control for any values of pulse width. On the other hand, the received CNR decreases as the total number of RBSs increases. But even when 50 RBSs are connected to bus link using pulse duty of 10^{-4}, the CNR of more than 36[dB] can be obtained by calculations under the condition of $B_{RF} = 1.5$MHz.

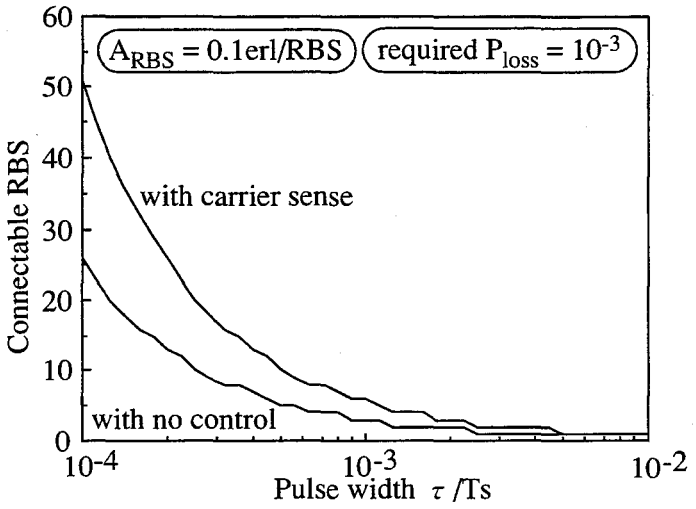

Figure 4.8: Maximum number of connectable RBSs versus pulse width in the network with CS or with no control.

4.7 Concluding Remarks

This chapter proposed asynchronous time division multiple access bus link system for fiber-optic radio access networks, which can remove the difficulty of time synchronization control for time division multiplexing of signals and can provide the capability of easy extension of networks. It was shown that the performance degradation due to collision among signals occurs. Then the carrier sense control and the variable pulse width technique were also proposed to improve the system performance.

We have theoretically analyzed the burst loss probability and the CNR performance of the proposed system. Following results were obtained:

1. We can multiplex and transfer radio signals without any time synchronization among RBSs with burst loss probability of 10^{-3} and received CNR of more than 40[dB] by the use of photonic natural bandpass sampling technique.

2. The use of carrier-sense control reduces the burst loss probability to half of that in case of no control.

3. Variable pulse width technique can improve the burst loss probability and it is more effective for the performance improvement of the nearer RBS.

Chapter 5

Chirp Multiplexing Transform Fiber-Optic Radio Access System

5.1 Introduction

The fiber-optic radio access networks have the potential to be universally used among different kinds of radio service or different providers. The realization of such universal radio access networks can reduce time and cost for infrastructures, keeping the advantages of microcellular systems. Different kinds of radio service are ordinarily operated under different frequency bands, and their RCSs probably locate at different locations. In order to handle such multiple radio services universally, the fiber-optic radio access networks need a routing node (RN) in the networks, which distinguishes kind of radio service and switches each service signal into its desired RCS.

The conventional fiber-optic link to transfer radio signals is subcarrier multiplexing / optical intensity modulation / direct detection (SCM/IM/DD) link, which has advantages in simplicity and cost-efficiency of RBS configuration[9]. However from the viewpoint of the feasibility of the RN, the SCM/IM/DD link has a primary disadvantage that it is impossible to distinguish kind of radio service unless the optical signals are photodetected because optical intensity includes the multiple radio services with subcarrier multiplexing format.

In order to realize seamless routing of radio service, this chapter newly proposes the new application of Chirp Fourier Transformer (CFT)[47] to the fiber-optic radio access networks. We refer to the system as Chirp Multiplexing Transform (CMT)/IM/DD system, where CMT equipped at RBS converts multiple service radio signals operated under the different frequency bands into ones operated with TDM format before E/O conversion. Therefore the RN composed of simple photonic switch can distinguish and switch radio service in the optical stage. The Chirp Multiplexing Transformed signals (CMT signals) can be demodulated with correlation demodulator or Inverse CMT.

As for the photonic time switching, there are progressing techniques such as self-routing photonic switching[31] and we can expect the fast switch operation, the high cost-efficiency and the large capacity. As the alternative to CFT, you may think of the FDM-to-TDM conversion scheme using digital signal processing[48]. However it isn't suitable for our purpose because it spoils the flexibility of RBSs due to the requirement of digital processing and can not handle broadband radio signals. On the other hand, the

CFT realized by SAW (surface acoustic wave) devices is suitable for our purpose because of its broadband characteristics and its function as a real-time analog Fourier transformer.

The CFT has been studied in many applications such as spectrum analyzer[47], time compression of signal[49], and multiplexer and demultiplexer in satellite communications[50]. Especially group demodulator using the CFT has been proposed in [51][52], where the CFT transforms FDM radio signals into TDM signal, and digital processing can demodulate the transformed TDM signal. The bit error rate performance has been clarified by using simulation analysis. However there has been no study of signal performance applied for the CMT fiber-optic radio access system where CMT signals are transfered via fiber-optic link. Therefore this chapter proposes a new type of the configuration of CMT/IM/DD fiber-optic radio access system and theoretically analyzes the signal-to-noise power ratio (SNR) performance on uplink considering the nonlinearity of LD, the receiver noises in optical IM/DD link, and inter-channel interferences (ICI) and inter-symbol interferences (ISI) caused by the CMT. Furthermore this paper shows that the parallel use of CFT proposed in [52] is also effective to improve the SNR performance of the CMT/IM/DD systems.

This chapter is organized as follows. Section 5.2 describes the principle of CMT. Section 5.3 clarifies the characteristic of the CMT signal. Section 5.4 describes the direct demodulation scheme for the CMT signal and theoretically analyzes signal to inter-channel interference power ratio (S/ICI) and signal to inter-symbol interference power ratio (S/ISI). Next, Sect.5.5 proposes the parallel use of two CMTs to reduce ICI and ISI. Finally Sect.5.6 theoretically analyzes SNR performance taking into account the LD nonlinearity and overall performance including SNR, S/ICI and S/ISI. From the results of analysis, the performance of the proposed system is compared to the conventional SCM system.

5.2 Principle of Chirp Multiplexing Transform

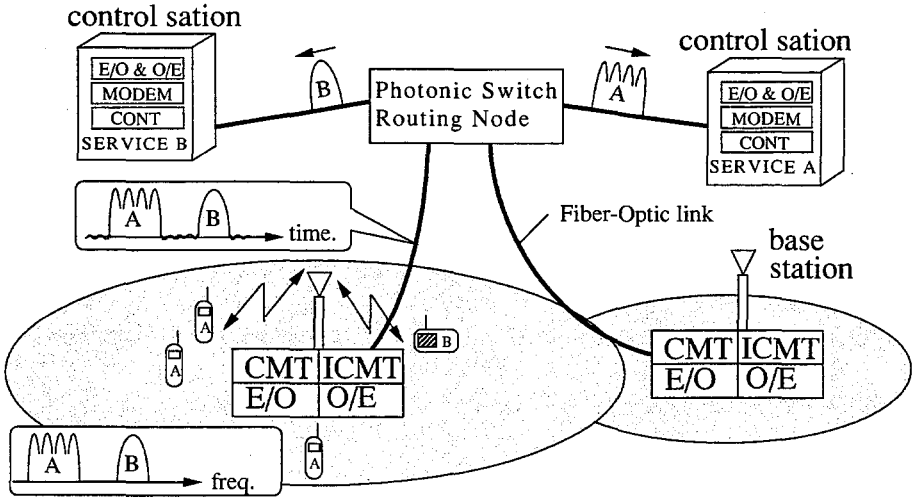

Figure 5.1: Network configuration of CMT fiber-optic radio access system.

Figure 5.1 illustrates the network configuration of CMT fiber-optic radio access system

and the principle of its operation for multiple radio services. The networks consist of RBSs for the universal use among multiple radio services, RCSs prepared for each radio service, an RN, and fiber-optic links to connect them. The main functions of RBS are CMT and E/O conversion. The figure is illustrating the example case that RBS receives two service frequency bands, A and B. The CMT converts such multiple radio services with FDM format into ones with TDM format in electric stage. Afterward, the converted signals are transmitted into a fiber-optic link with E/O conversion toward an RN. The RN distinguishes the kind of radio service by its transmitted time and switches each service signal into the desired RCS by the use of simple photonic switch.

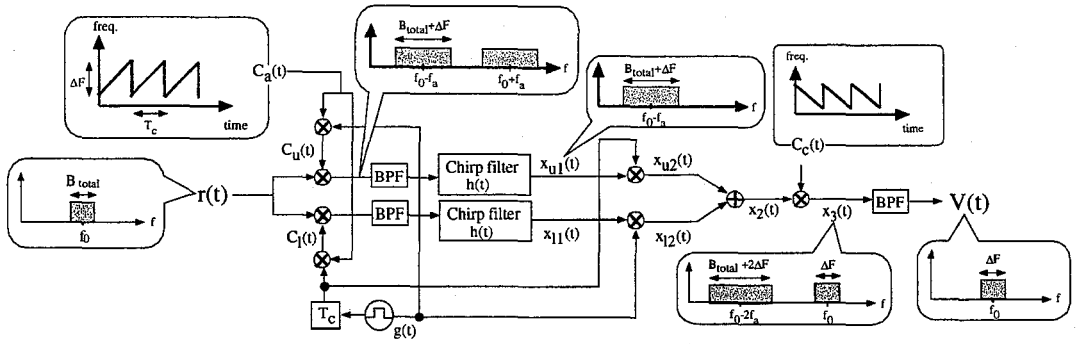

Figure 5.2: Configuration of CMT.

To investigate the operation of CMT, we assume the bandlimited signal $r(t)$.

$$r(t) = Re[u(t)e^{j2\pi f_0 t}] \tag{5.1}$$

where $u(t)$ is the complex envelope whose spectrum is bandlimited into $|f| \leq \frac{B_{total}}{2}$. f_0 is the center frequency of radio. The configuration of CMT is shown in Fig.5.2. The fundamental process of CMT consists of two multiplications with a chirp signal and a filtering with a chirp filter. However one process can converts only a T_c time duration signals at intervals of two times T_c. Therefore two identical processes (upper and lower processes in Fig.5.2) have to be operated in parallel in order to convert continuous signals that are longer than T_c without any omission of signal.

The first process in CMT is the pre-multiplication of $r(t)$ with an upchirp signal, $C_a(t)$. The term "upchirp" means that its frequency increases as time passes, while "downchirp" means that its frequency decreases. An upchirp signal can be obtained as an impulse response of an upchirp filter in which the higher frequency component is delayed longer. Introducing a complex low-pass upchirp signal $c(t)$, the upchirp signal with its center frequency f_a, $C_a(t)$, is given by[49]

$$C_a(t) = Re[\sqrt{2}c(t)e^{j2\pi f_a t}] \tag{5.2}$$

$$c(t) = \begin{cases} \exp(j2\pi\beta t^2/2) & ; -\frac{T_c}{2} \leq t \leq \frac{T_c}{2} \\ 0 & ; \text{otherwise} \end{cases} \tag{5.3}$$

where β is the chirp slope in [Hz/s] and T_c is the chirping dispersion time. Then we can define the frequency range of sweep, ΔF, as

$$\Delta F = \beta T_c \tag{5.4}$$

For the upper and the lower processes, we need two upchirp signals that are alternately gated at the intervals of $2T_c$, $C_u(t)$ and $C_l(t)$. They are obtained by multiplying an upchirp signal with its period T_c, $\sum_{k=-\infty}^{\infty} C_a(t-kT_c)$, by two alternate gating functions, $G(t)$ and $G(t-T_c)$, with their period $2T_c$ and duration T_c:

$$G(t) = \sum_{k=-\infty}^{\infty} g(t-2kT_c) \tag{5.5}$$

$$g(t) = \begin{cases} 1 & ;-\frac{T_c}{2} \le t \le \frac{T_c}{2} \\ 0 & ;\text{otherwise} \end{cases} \tag{5.6}$$

Then $C_u(t)$ and $C_l(t)$ are respectively written by

$$C_u(t) = \sum_{m=-\infty}^{\infty} C_a(t-2mT_c) \tag{5.7}$$

$$C_l(t) = \sum_{m=-\infty}^{\infty} C_a(t-(2m+1)T_c) \tag{5.8}$$

The radio signal $r(t)$ is multiplied by the gated upchirp signals, $C_u(t)$ and $C_l(t)$, respectively on the upper path and the lower path as shown in Fig.5.2. The multiplication generates two components of (f_0-f_a) frequency band signals and (f_0+f_a) frequency band signals. Any image frequency component and any overlap of the two frequency band signals are not generated in the case of $|f_0-f_a| \gg (\Delta F+B_{total})/2$ and $f_a \gg (\Delta F+B_{total})/2$. Therefore we can use either of frequency band signals for the next filtering process with a downchirp filter. However since the carrier frequency of radio signal f_0 is microwave or millimeter wave band in recent trend, it seems comparatively difficult to realize a chirp filter with such high center frequency, (f_0+f_a). Consequently it is reasonable to use the upchirp filter for the lower frequency band (f_0-f_a) in the filtering process. Hence,

$$r(t)\cdot C_u(t) = Re[\sum_{m=-\infty}^{\infty} \frac{\sqrt{2}}{2} u(t)c^*(t-2mT_c)e^{j2\pi(f_0-f_a)t}] \tag{5.9}$$

$$r(t)\cdot C_l(t) = Re[\sum_{m=-\infty}^{\infty} \frac{\sqrt{2}}{2} u(t)c^*(t-(2m+1)T_c)e^{j2\pi(f_0-f_a)t}] \tag{5.10}$$

and the impulse response of the upchirp filter, $h(t)$, is given by

$$h(t) = \begin{cases} Re\left[\sqrt{\beta}e^{j2\pi(\frac{\beta}{2}t^2-\Delta Ft)}\cdot e^{j2\pi(f_0-f_a)t}\right] & ;0 \le t \le 2T_c \\ 0 & ;\text{otherwise)} \end{cases} \tag{5.11}$$

Therefore, the outputs after the filtering process on each path, $x_{u1}(t)$ and $x_{u2}(t)$ are respectively written by

$$\begin{aligned} x_{u1}(t) &= \{r(t)C_u(t)\}\otimes h(t) \\ &= Re\left[\sum_{m=-\infty}^{\infty} U^{(2m)}(t)C_{if}^{(2m)}(t)\right] \end{aligned} \tag{5.12}$$

$$\begin{aligned} x_{l1}(t) &= \{r(t)C_l(t)\}\otimes h(t) \\ &= Re\left[\sum_{m=-\infty}^{\infty} U^{(2m+1)}(t)C_{if}^{(2m+1)}(t)\right] \end{aligned} \tag{5.13}$$

where $\otimes$ denotes convolution, and $U^{(k)}(t)$ and $C_{if}^{(k)}(t)$ are given by

$$U^{(k)}(t) = \begin{cases} \int_{-\frac{T_c}{2}}^{t} u(\tau + kT_c)e^{-j2\pi\beta[t-(k+1)T_c]\tau}d\tau & ; -\frac{T_c}{2} \le t - kT_c < \frac{T_c}{2} \\ \int_{-\frac{T_c}{2}}^{\frac{T_c}{2}} u(\tau + kT_c)e^{-j2\pi\beta[t-(k+1)T_c]\tau}d\tau & ; \frac{T_c}{2} \le t - kT_c \le \frac{3T_c}{2} \\ \int_{t-2T_c}^{\frac{T_c}{2}} u(\tau)e^{-j2\pi\beta[t-T_c]\tau}d\tau & ; \frac{3T_c}{2} < t - kT_c \le \frac{5T_c}{2} \\ 0 & ; \text{otherwise} \end{cases} \quad (5.14)$$

$$C_{if}^{(k)}(t) = \frac{\sqrt{2\beta}}{4} e^{j2\pi\beta\frac{[t-(k+1)T_c]^2}{2}} \cdot e^{j2\pi(f_0-f_a)t} \quad (5.15)$$

Figure 5.3 illustrates the relationship between the input and the output signals of the chirp filter in the time domain. The part of the output in the range of $\frac{T_c}{2} \le t - kT_c \le \frac{3T_c}{2}$ in Eq.(5.14), that is, $U^{(k)}(t)g(t-(k+1)T_c)$ is illustrated as the shadowed parts in Fig.5.3. The part corresponds to the Fourier transform of $u(t)$ gated in the time range T_c, and is necessary for our purpose. Then, the necessary parts from each path, $x_{u2}(t)$ and $x_{l2}(t)$ are extracted by gating functions, and summed. The result is written by $x_2(t)$.

$$x_2(t) = Re\left[\sum_{k=\infty}^{\infty} U^{(k)}(t)C_{if}^{(k)}(t)g(t-(k+1)T_c)\right] \quad (5.16)$$

It is found from Eq.(5.16) that the center frequency of $x_2(t)$ increases periodically due to $C_{if}^{(k)}(t)$. $x_3(t)$ in which the effect of $C_{if}^{(k)}(t)$ is eliminated can be obtained by multiplying $x_2(t)$ by a downchirp signal $C_c(t)$ which is given by

$$C_c(t) = Re[\sqrt{2}c^*(t)e^{j2\pi f_a t}] \quad (5.17)$$

After band-pass filtering $x_3(t)$ $(= x_2(t) \cdot C_c(t))$ by the use of bandpass filter with its center frequency f_0, we finally obtain the desired Chirp Multiplexing Transformed signal (CMT signal), $V(t)$.

$$V_(t) = Re[v(t)e^{j2\pi f_0 t}] \quad (5.18)$$

$$v(t) = \sum_{k=-\infty}^{\infty} U^{(k)}(t) \cdot g(t-(k+1)T_c) \quad (5.19)$$

where the amplitude constant $\sqrt{2\beta}/8$ and the phase constant are dropped. $U^{(k)}(t) \cdot g(t-(k+1)T_c)$ is referred to as Time Limited Fourier Transform (TLFT) signal in this chapter because it is the Fourier transform output of $u(t+kT_c) \cdot g(t)$ where the conversion of the frequency axis to the time axis, that is, f axis to βt axis is executed. The time waveform of the TLFT signal represents the spectrum information of $u(t+kT_c) \cdot g(t)$, but it is further limited in the time range of T_c. Consequently it is necessary that βT_c covers the spectrum range of radio signals, B_{total}.

$$\Delta F = \beta T_c \ge B_{total} \quad (5.20)$$

Under this condition, the CMT can successfully perform FDM-to-TDM conversion of radio signals. On the other hand, we supplement that the spectrum shape of the TLFT signal represents the time waveform of $u(t+kT_c) \cdot g(t)$, and also bandlimited in the range of $\beta T_c = \Delta F$.

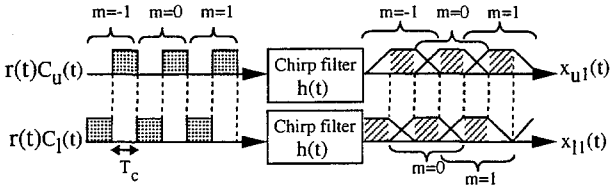

Figure 5.3: Input and output signals of the chirp filter.

5.3 CMT/IM/DD System for FDM-PSK Radio Signals

In this section,we discuss the characteristics of the CMT signal by assuming FDM-PSK radio signals are applied to the CMT/IM/DD systems. The figure 5.4 shows the analysis models of CMT/IM/DD system and SCM/IM/DD system for a compared system. In the CMT/IM/DD system, the CMT signal whose low-pass equivalent is represented by Eq.(5.19) directly modulates Laser Diode (LD) and is transfered via fiber-optic link. The receiver at the RCS detects the optical signal and directly demodulates the information using the proposed demodulator described in Sect.5.4. On the other hand, in the SCM/IM/DD system, the FDM-PSK signal directly modulates LD and is similarly transfered via optic-link and their informations are demodulated by the optimum demodulation using matched filter at the RCS.

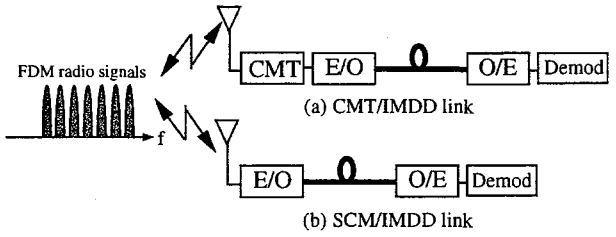

Figure 5.4: Performance analysis models of CMT/IM/DD system and SCM system.

The low-pass equivalent of FDM-PSK radio signals is written by

$$u(t) = \sum_{l=-M}^{M} \sum_{n=-\infty}^{\infty} f(t-nT)e^{j[2\pi l\Delta f t+\theta_{ln}]} \tag{5.21}$$

where θ_{ln} is the n-th modulation phase of the l-th FDM channel and $(2M+1)$ is the number of FDM channels . T, Δf, and $f(t)$ are the symbol duration, the channel separation, and the pulse waveform bandlimited into B, respectively. Then the total bandwidth, B_{total}, is written by

$$B_{total} = (2M+1)\Delta f \tag{5.22}$$

We investigate the $k = 0$th TLFT signal in $v(t)$ when Eq.(5.21) is substituted into Eq.(5.19). We represent it as $v_0(t)$.

$$v_0(t) = \int_{-\frac{T_c}{2}}^{\frac{T_c}{2}} u(\tau) e^{-j2\pi\beta(t-T_c)\tau} d\tau \quad ; \quad \frac{T_c}{2} \le t \le \frac{3}{2}T_c \tag{5.23}$$

Assuming the perfect synchronization between the symbol timing of $u(t)$ and the chirping dispersion time T_c, $v_0(t)$ becomes

$$v_0(t) = \sum_{l=-M}^{M} \sum_{n=-\infty}^{\infty} S_{ln}(t) \cdot e^{j\theta_{ln}} \quad ; \quad \frac{T_c}{2} \le t \le \frac{3}{2}T_c \tag{5.24}$$

$$S_{ln}(t) = \beta G(\beta t) \otimes \left[F[\beta(t-T_c) - l\Delta f] e^{-j2\pi[\beta(t-T_c)-l\Delta f]nT} \right] \tag{5.25}$$

where $G(f)$ and $F(f)$ are the Fourier transforms of $g(t)$ and $f(t)$, respectively. $S_{ln}(t)$ corresponds to the pulse waveform of the n-th symbol of the l-th channel. Note that the words "channel" and "symbol number" described in this chapter consistently indicate those in the original FDM-PSK radio signals defined in Eq.(5.21).

Equations (5.24) and (5.25) can be generally applied to any kind of pulse waveform, $f(t)$, and any value of Δf. However we focus our discussion on the case that $f(t)$ is pulse-shaped by the root Nyquist filter. Then $F(f)$ is given by[53]

$$F(f) = \begin{cases} 1 & ; 0 \le |f| \le \frac{1-\alpha}{2T} \\ \cos[\frac{\pi T}{2\alpha}(|f| - \frac{1-\alpha}{2T})] & ; \frac{1-\alpha}{2T} < |f| \le \frac{1+\alpha}{2T} \\ 0 & ; \text{otherwise} \end{cases} \tag{5.26}$$

where α is the roll-off factor. Figure 5.5 illustrates the relationship between the original radio signal $u(t)$ and its spectrum $U(f)$ and the resultant CMT signal $v_0(t)$ and its spectrum $V_0(f)$. It is seen from Eq.(5.25) and Fig.5.5 that the CMT signal consists of multicarrier PSK signals with carrier spacing βT, and pulse duration $\Delta f/\beta$. The different symbol in a certain channel is converted to the different carrier frequency in the same time slot, while the different channel's symbol is converted to the different time slot. Furthermore, the CMT signal is rectangularly bandlimited into the frequency range of ΔF, and its time waveform is limited into the time range of T_c, as described in Sect.5.2.

If the chirping dispersion time, T_c, is infinite ($T_c \to \infty$), we can ignore the convolution with $G(\beta t)$ in Eq.(5.25), thereby the set of $S_{ln}(t)(l = -M, \cdots, M; n = -\infty, \cdots, \infty)$ becomes orthogonal set and no ICI and no ISI occur(see Appendix A). However it can be seen from Eq.(5.25) and Fig.5.5 that in the resultant time domain, each pulse waveform corresponding to a channel, $F(\beta t - l\Delta f) \otimes G(\beta t)$, has a spreading sidelobe even if $F(f)$ is perfectly bandlimited. This spread causes interchannel interference (ICI). On the other hand, in the resultant frequency domain, each spectrum shape corresponding to a symbol, $f(f/\beta - nT) \cdot g(f/\beta)$, is partially truncated. This truncation causes intersymbol interferences (ISI) because of the imperfection of the orthogonality between different symbols even if the set of $f(t - nT)(n = -\infty, \cdots, \infty)$ is orthogonal set.

Here in order to estimate the number of carriers to be considered in the following analysis, we examine the symbol energy of $S_{ln}(t)$. Figure 5.6 shows the symbol energy of S_{0n} versus the symbol number n in the case of $T_c/T = 5.0$. Each symbol energy is normalized by the center symbol energy, S_{00}. It is seen that the energy of the symbols

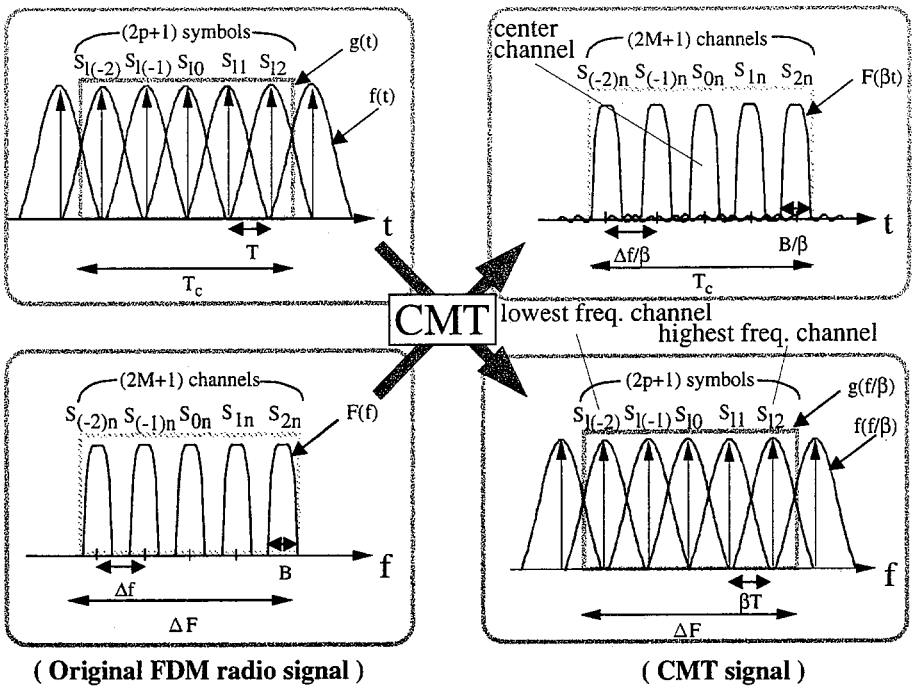

Figure 5.5: Radio signal and CMT signal.

out of center T_c/T symbols, that is, the energy of S_{0-3} and S_{03} in this example, suddenly decreases, and it is less than -36 [dB] of the energy of S_{00} in case of $\alpha = 1.0$. Consequently, we approximate the number of carriers to be considered in the following discussion as T_c/T. Then when T_c/T is represented by $(2p+1$;p is a positive integer), $v_0(t)$ can be rewritten as

$$v_0(t) \approx \sum_{l=-M}^{M} \sum_{n=-p}^{p} S_{ln}(t) e^{j\theta_{ln}} \tag{5.27}$$

5.4 Theoretical ICI and ISI Performance Analyses

Fig.5.7 shows the configuration of the proposed suboptimal correlation receiver. The term "suboptimal" indicates that the waveform correlated with the received CMT signal at the receiver is the waveform omitting the convolution term, $G(\beta t)$, in Eq.(5.25). The demodulator performs the multiplications of the received CMT signal with $F(\beta t - l\Delta f)$ and $e^{j2\pi[\beta nT]t}$ which are followed by an integrator and a decision circuit. In the demodulation, the perfect synchronization of frequency and phase, and the condition of "ΔfT = integer" are assumed. The latter condition is desirable to make the configuration of the receiver simple. Under the condition of "$\Delta fT \neq$ integer", the carrier phase in $S_{ln}(t)$ (Eq.(5.25)) changes according to the channel number l, therefore the receiver needs to control the phase of multiplying carriers according to the value of l.

Furthermore, when the proposed receiver is applied to the case of asynchronous symbol timing between channels, both of the phase and the frequency of the multiplying carriers have to be changed according to the channel number l.

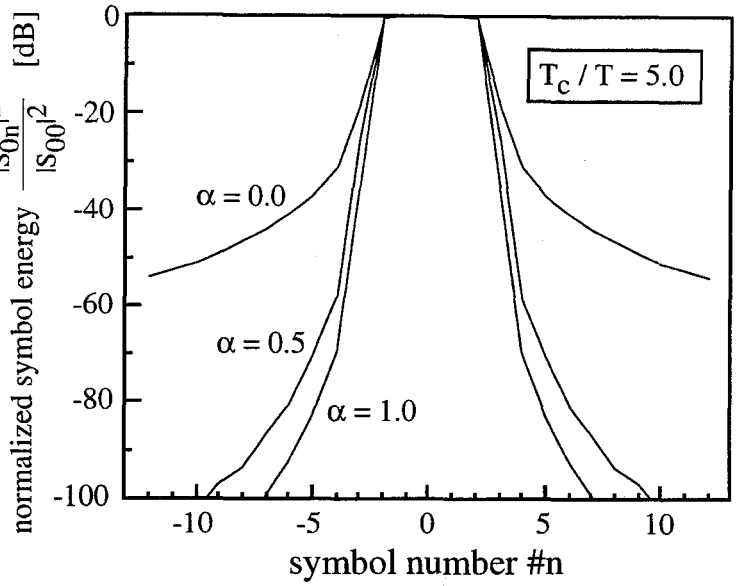

Figure 5.6: Normalized symbol energy versus symbol number.

The decision sample of the demodulated n-th symbol of the l-th channel, Q_{ln}, is written by

$$\begin{aligned} Q_{ln} &= \int_{t_{la}}^{t_{lb}} v_0(t) S'_{ln}(t) dt \\ &= \int_{t_{la}}^{t_{lb}} \left[S_{ln}(t) e^{j\theta_{ln}} \right] S'_{ln}(t) dt + \sum_{\substack{k=-M \\ k\neq n}}^{M} \sum_{\substack{s=-p \\ s\neq n}}^{p} \int_{t_{la}}^{t_{lb}} \left[S_{ks}(t) e^{j\theta_{ks}} \right] S'_{ln}(t) dt \end{aligned} \quad (5.28)$$

$$S'_{ln}(t) = F[\beta(t - T_c) - l\Delta f] e^{j2\pi[\beta(t-T_c)]nT} \quad (5.29)$$

$$t_{la} = T_c + \frac{1}{\beta}(l\Delta f - \frac{B}{2}) \quad (5.30)$$

$$t_{lb} = T_c + \frac{1}{\beta}(l\Delta f + \frac{B}{2}) \quad (5.31)$$

The first term of Eq.(5.28) represents the desired signal and the second term represents ICI and ISI. Consequently when we demodulate the n-th symbol of the l-th channel, the signal-to-ICI power ratio (S/ICI) and signal-to-ISI power ratio (S/ISI) are derived as

$$\left(\frac{S}{ICI}\right)_{ln} = \frac{\left(Re\left[\int_{t_{la}}^{t_{lb}} S_{ln}(t) S'_{ln}(t) dt\right]\right)^2}{\left(\sum_{\substack{k=-M \\ k\neq l}}^{M} Re\left[\int_{t_{la}}^{t_{lb}} S_{kn}(t) S'_{ln}(t) dt\right]\right)^2} \quad (5.32)$$

$$\left(\frac{S}{ISI}\right)_{ln} = \frac{\left(Re\left[\int_{t_{la}}^{t_{lb}} S_{ln}(t) S'_{ln}(t) dt\right]\right)^2}{\left(\sum_{\substack{s=-p \\ s\neq n}}^{p} Re\left[\int_{t_{la}}^{t_{lb}} S_{ls}(t) S'_{ln}(t) dt\right]\right)^2} \quad (5.33)$$

Figures 5.8 and 5.9 show the S/ICI and the S/ISI performances of the center channel versus chirping dispersion time normalized by symbol duration (T_c/T). The total number

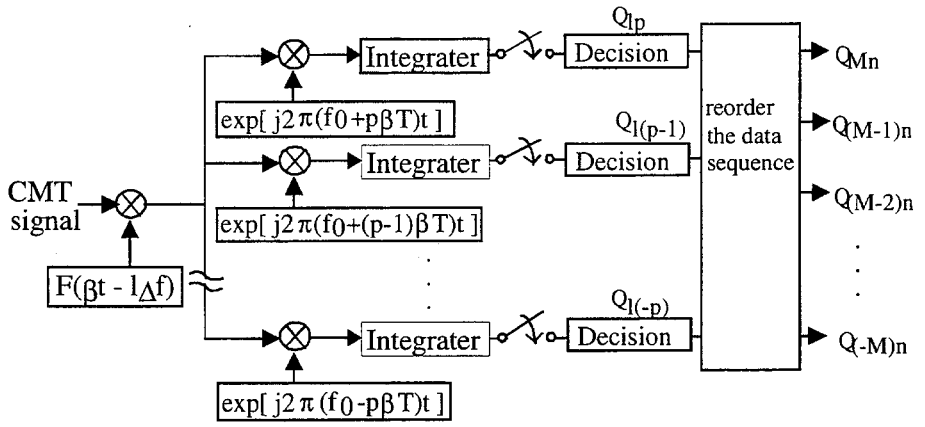

Figure 5.7: Configuration of suboptimal correlation receiver.

of channels, $2M+1$, is 3, and the roll-off factor α and the symbol number n are parameters. In the figures, $n = p$ indicates the highest frequency symbol in the CMT signal.

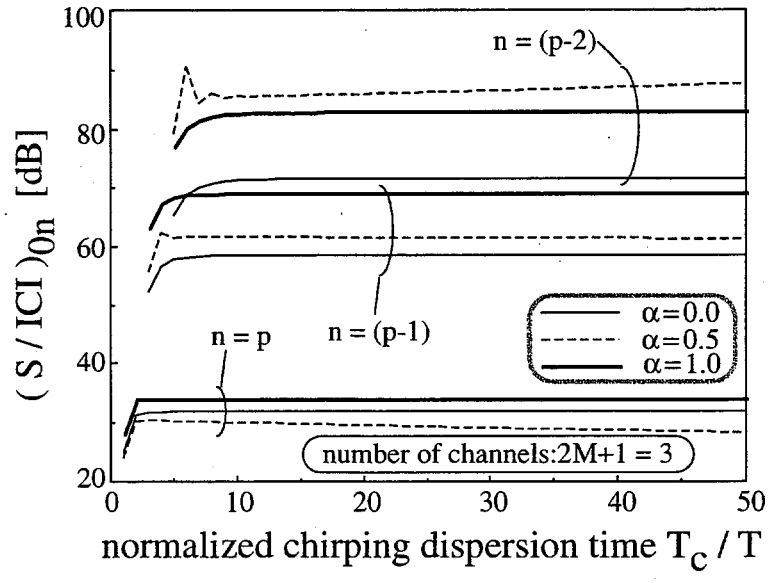

Figure 5.8: S/ICI versus chirping dispersion time.

As described in Sect.5.3, the convolution of $G(\beta t)$ with $F(\beta t)$ causes spreading sidelobes of each channel's pulse, therefore the ICI. Figure 5.8 shows the performance of the most highest frequency symbol is most deteriorated and its S/ICI doesn't change even if the T_c becomes large, though the S/ICI of the center frequency symbol or the identical frequency symbol is improved. The reason is that the larger spreading of sidelobe in the time domain is caused by the larger truncation of spreading sidelobe in the frequency domain, and the highest frequency symbol in the CMT signal suffers from the largest truncation (see CMT signal in Fig.5.5).

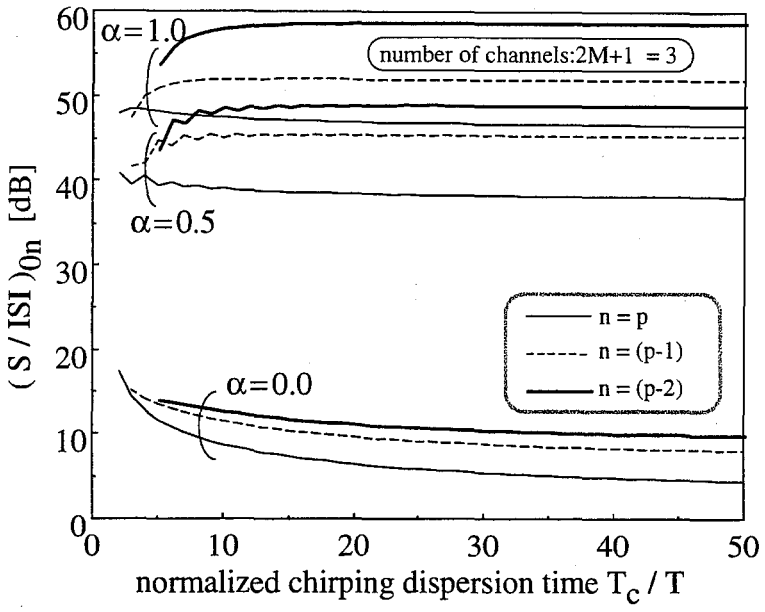

Figure 5.9: S/ISI versus chirping dispersion time.

On the other hand, it is seen from Fig.5.9 that the difference of the roll-off factor influences the S/ISI more than that of the symbol number, and $\alpha = 1$ gives the maximum S/ISI. The reason is that the spreading of each symbol's spectrum shape in the CMT signal becomes narrowest when $\alpha = 1$, and it results in the smallest truncated part and the smallest distortion.

5.5 Double CMT System

As shown in Sect.5.4, the S/ICI and the S/ISI performances of the highest and the lowest frequency symbols in the CMT signal are most deteriorated and dominate the total system performance. Figure 5.8 shows that there exists 34 [dB] difference between the S/ICI of $n = p$ and that of $n = p - 1$ when $T_c/T = 5.0$ and $\alpha = 1.0$.

Similar problem occurs in the Group Demodulation system using Chirp Fourier transform for FDM signals. To solve this problem, the dual-parallel use of Chirp Fourier transform has been proposed in [52]. In the system, the chirp sweep timings of the two transformers are offset by half of the chirping dispersion time from each other, and only the center $k/2$ symbols ($k = T_c/T$) from each transformer output is used for demodulation.

The parallel use of Chirp Fourier transformer is also effective for our systems, and we call the system "Double CMT systems". However we are faced with the problem that two fiber-optic links are required in order to transfer each output signals from two CMTs and it increases the complexity of network configuration. This problem is inherent to our applications where the CMTs and the demodulation functions are separately equipped in the networks. Therefore we propose to multiplex the two parallel CMT outputs into a single fiber-optic link with TDM format. Figures 5.10 illustrates the configuration of the double CMT systems. It consists of two CMTs whose chirp sweep timings are offset

from each other by half of the chirping dispersion time, $T_c/2$, in the case of "T_c/T = even integer", otherwise by $(T_c + T)/2$ in the case of "T_c/T = odd integer". Equation (5.19) shows that when we enlarge the frequency range of sweep, ΔF, into more than double of total radio bandwidth B_{total}, we can reduce the time width of the TLFT signal, $U^{(k)}(t) \cdot g(t-(k+1)T_c)$, to less than $T_c/2$. Consequently two CMT outputs can be time division multiplexed by simply adding the two outputs.

Figure 5.11 illustrates the configuration of the receiver for the double CMT system in the case of $T_c/T = 4.0$. At the receiver, we use only center $T_c/2T$ symbols in the frequency domain to demodulate and it is sufficient to prepare only $T_c/(2T)$ demodulation circuits in the case of "T_c/T = even integer". The sampling process is executed at the interval of the half of $\Delta f/\beta$ and the demultiplexing for two parallel CMT outputs is not required. In the case of "T_c/T = odd integer", we need $(T_c + T)/(2T)$ demodulation circuits.

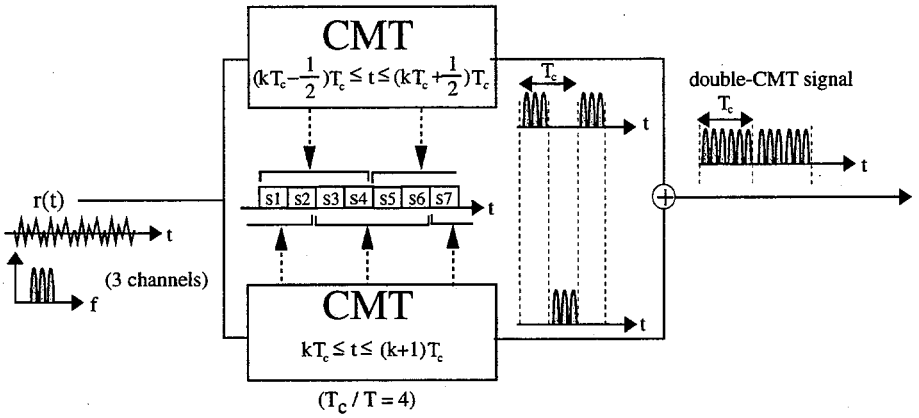

Figure 5.10: Configuration of double CMT.

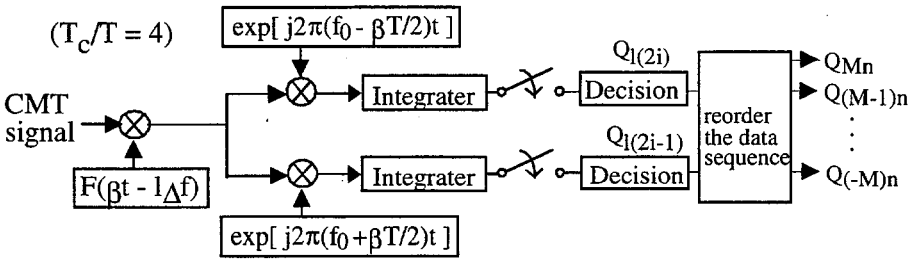

Figure 5.11: Configuration of the receiver for double CMT system.

Another important merit of the double CMT system is robustness against the imperfect synchronization between the chirping dispersion time period and the symbol duration assumed in Sect.5.4. The reasons are that the imperfection generates more truncated part and performance degradation mainly to the highest or the lowest frequency symbol in the CMT signal, and however the double CMT system doesn't use the damaged symbol for demodulation.

5.6 Theoretical Analyses of SNR and Overall Performances

In this section, we theoretically analyze the signal-to-noise power ratio (SNR) obtained by the suboptimal correlation detection in the CMT/IM/DD system. Here we assume that T_c is enough larger than T, and we neglect the effect of the convolution with $G(\beta t)$ in Eq.(5.24). Under this assumption, the suboptimal correlation detection is considered as the optimum detection scheme which maximizes the SNR because the signal for correlation at the receiver is matched to the waveform of received signal.

In the CMT/IM/DD systems, the LD is modulated by the CMT signals. The output optical intensity of the LD, $P(t)$ can be characterized by the use of polynomial equation when the non-linear characteristics of the LD is taken into consideration[54]. modulated by the CMT signal is given by

$$P(t) = P_0[1 + mV(t) + a_2\{mV(t)\}^2 + a_3\{mV(t)\}^3 + \cdots] \tag{5.34}$$

where P_0 is the average transmitting optical power and m is the modulation index. When this optical signal is received at the RCS, the output current of photo-diode (PD), $I_o(t)$, is given by

$$I_o(t) = \alpha_o P_r\,(1 + mV(t)) + I_{RIN}(t) + I_{shot}(t) + I_{th}(t) + I_{im3}(t) \tag{5.35}$$

where P_r and α_o are the average received optical power and the responsibity of PD, respectively. $I_{RIN}(t)$, $I_{shot}(t)$, and $I_{th}(t)$ are the relative intensity noise current, the shot noise current, and the thermal noise current, respectively. $I_{im3}(t)$ is the 3rd order intermodulation distortion current. Assuming that each noise current is white noise current, the power spectrum density (PSD) level of each noise current is given by

$$n_{RIN} = RIN\,(\alpha_o P_r)^2 \tag{5.36}$$

$$n_{shot} = 2e\alpha_o P_r \tag{5.37}$$

$$n_{th} = \frac{4k_B T_{th}}{R} \tag{5.38}$$

where RIN, k_B, T_{th} and R are the PSD of relative intensity noise of LD, Boltzmann constant, the noise temperature, and the load resistance, respectively. When N non-modulated carriers with equal amplitude and equal frequency spacing are applied as $V(t)$, the IM3 power in the k-th carrier band, $< I_{im3}^2 >_{(N,k)}$, is given by[9][55]

$$< I_{im3}^2 >_{(N,k)} = \begin{cases} \frac{1}{2}\left(\frac{3}{4}a_3 m^3 D_{(N,k)}^{(2)} + \frac{3}{2}a_3 m^3 D_{(N,k)}^{(3)}\right)^2 (\alpha_o P_r)^2 & ;N \geq 3 \\ 0 & ;N < 3 \end{cases} \tag{5.39}$$

$$D_{(N,k)}^{(2)} = \frac{1}{2}[N - 2 - \frac{1}{2}\left\{1 - (-1)^N\right\}(-1)^k] \tag{5.40}$$

$$D_{(N,k)}^{(3)} = \frac{k}{2}(N - k + 1) + \frac{1}{4}\left\{(N-3)^2 - 5\right\} - \frac{1}{8}\left\{1 - (-1)^N\right\}(-1)^{N+k} \tag{5.41}$$

The $< I_{im3}^2 >_{(N,k)}$ has the largest value at the center carrier frequency band. We take the IM3 currents into consideration for the SNR analysis by translating the IM3 current into

the bandlimited white noise current with its PSD level of n_{im3}.

$$n_{im3} = \begin{cases} \frac{(2p+1)\cdot<I_{im3}^2>_{(2p+1,p)}}{\Delta F} & ;2p+1 \geq 3 \\ 0 & ;2p+1 < 3 \end{cases} \tag{5.42}$$

where $2p+1$ is the number of carriers represented by $2p+1 = T_c/T$.

The symbol energy E_s is written by

$$\begin{aligned} E_s &= \frac{1}{2}(\alpha_o P_r)^2 m^2 \int_{-\infty}^{\infty} F^2(\beta t)dt \\ &= \frac{1}{2}(\alpha_o P_r)^2 m^2 \frac{T_c}{T\Delta F} \end{aligned} \tag{5.43}$$

where the modulation index m needs to satisfy the following condition in order not to cause the over modulation distortion at LD in Eq.(5.34).

$$m \leq \frac{1}{2p+1} = \frac{T}{T_c} \tag{5.44}$$

It is seen from Equations (5.43) and (5.44) that the symbol energy E_s decreases as ΔF increases because the pulse waveform of the CMT signal becomes narrower, and that E_s also decreases as T_c becomes large because the number of carriers, that is, T_c/T increases and m should be proportional to the inverse of it.

The SNR attained by the correlation detection, that is, the energy contrast, is given by,

$$\left(\frac{S}{N}\right)_{cmt} = \frac{E_s}{n_{RIN} + n_{shot} + n_{th} + n_{im3}} \tag{5.45}$$

There exists the optimum modulation index m_{opt} which gives the maximum SNR because n_{RIN}, n_{shot} and n_{th} are independent to the modulation index m, while E_s increases proportional to m^2, and n_{im3} increases proportional to m^6. The m_{opt} is given by

$$m_{opt} = \left(\frac{n_{RIN} + n_{shot} + n_{th}}{2n_{im3}|_{m=1}}\right)^{\frac{1}{6}} \tag{5.46}$$

where m_{opt} needs to satisfy the condition of Eq.(5.44) at the same time. Regarding the frequency range of sweep, ΔF, we can choose any value of ΔF more than B_{total} (see Eq.(5.20)), but since E_s is proportional to the inverse of ΔF, it should be the following value to attain the maximum SNR:

$$\Delta F = \begin{cases} B_{total} & ;\text{single CMT} \\ 2B_{total} & ;\text{double CMT} \end{cases} \tag{5.47}$$

Figure.5.12 shows the $(S/N)_{cmt}$ versus the number of FDM radio channels for both the single CMT scheme and the double CMT scheme, and for different values of the normalized chirping dispersion time, T_c/T. In the calculation, the optimum modulation index m_{opt} and parameters shown in Table 1 are used.

It is seen from the Fig.5.12 that the SNR decreases as the number of channels increases and that the SNR of the double CMT is deteriorated than that of the single CMT scheme

Table 5.1: Parameters used in calculations

RIN	-152[dB/Hz]	T_{th}	300[K]
α_o	0.8[A/W]	R	50Ω
a_3	0.01	P_r	-10[dBm]
$1/T$	192 symbol/s	Δf	2/T

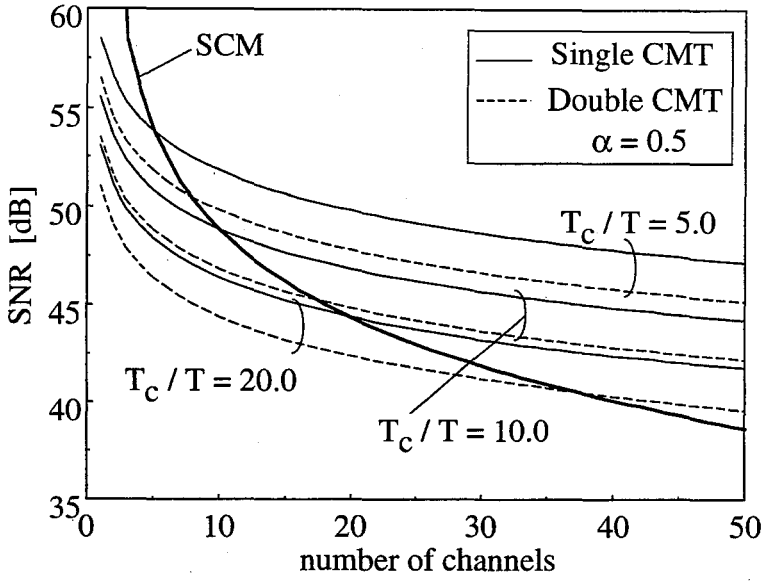

Figure 5.12: SNR versus the number of radio channels.

because the increase of the frequency range of sweep, ΔF, causes the decrease of the symbol energy. It is also seen that the SNR for large T_c/T is degraded because of the increase of the intermodulation distortion power, therefore it is desired to use small T_c/T. In the figure, the SNR performance of the conventional SCM scheme is also shown. It is seen that the SNR of the SCM system more rapidly decreases in comparison with the proposed system as the number of channels increases. The reason is that the IM3 power in the SCM system rapidly increases as the number of channels increases, while the IM3 power in the CMT/IM/DD system is independent of the number of channels, but dependent on the T_c/T. As a result, the SNR performance of the proposed system becomes superior to the SCM system in the condition of large number of channels in spite of the value T_c/T. In the case of $T_c/T = 5.0$, the SNR of the single CMT system is superior at the number of channels more than 6, and that of the double CMT system is superior at the number of channels more than 8.

Figure 5.13 shows overall SNR performance of the proposed system in which the S/ICI, the S/ISI and the SNR are taken into consideration. The overall SNR is given by

$$\left(\frac{S}{N+I}\right) = \left[\left(\frac{S}{ICI}\right)^{-1} + \left(\frac{S}{ISI}\right)^{-1} + \left(\frac{S}{N}\right)^{-1}\right]^{-1} \tag{5.48}$$

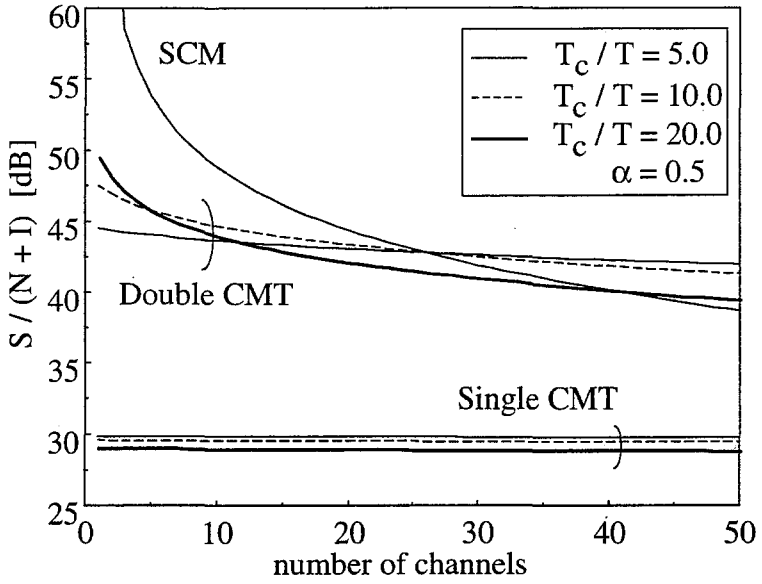

Figure 5.13: S/(N+I) versus the number of radio channels.

In the calculation of the (S/ICI) and the (S/ISI), $\alpha = 0.5$ is assumed, and we examine the performances of the most degraded symbol, that is, the highest frequency symbol in the CMT signal. It is seen from the figure that the overall performance of the single CMT system is always inferior to the SCM system in spite of value T_c/T because it is dominated by the low S/ICI performance. On the other hand, the double CMT system can much improve the overall performance because it is dominated by the SNR performance shown in Fig.5.12, and it is superior to the SCM system at $T_c/T = 5.0$ and the number of radio channels more than 26. In the figure, 3 [dB] improvement of the overall performance is obtained when the number of channels is 50 and $T_c/T = 5.0$. This superiority is caused by the fact the CMT system can decrease the number of carriers and is tolerable against the LD nonlinearity. Consequently, the performance of the CMT system is superior to the SCM system in the condition that the LD nonlinearity dominates the signal performance.

5.7 Concluding Remarks

This chapter proposed the CMT fiber-optic radio access system suitable for fiber-optic radio access networks in the point of seamless routing of radio services, and theoretically analyzed the SNR performance on uplink considering the ICI, the ISI, the LD nonlinearity, and the receiver noise inherent to IM/DD fiber-optic link. Furthermore in order to decrease the ICI and the ISI, the double CMT system was proposed. The theoretical analysis investigated the relationship between the SNR performance and the parameters inherent to the CMT systems compared the SNR performance to the conventional SCM radio access system. Following results were obtained:

1. The CMT can successfully transform multiple radio services with FDM format into ones with TDM format. Then the CMT radio access system can provide more simple and seamless radio access networks because an RN composed of photonic time switch can distinguish and switch radio service in the optical stage in the networks.

2. By the use of the suboptimal correlation demodulator, the CMT signal can be directly demodulated with high (S/ISI) and high (S/ICI) performances, however such performances are different according to the symbol number and the roll-off factor of pulse shaping. In particular, the S/ICI performance of the highest and the lowest frequency symbol in the CMT signal is most deteriorated, and the use of the largest value of roll-off factor gives the highest S/ISI performance.

3. The double CMT system can improve the S/ICI and the S/ISI performance though the SNR performance is deteriorated. The double CMT system obtains 32 [dB] improvement of the S/ICI in case of $T_c/T = 5.0$ and $\alpha = 1.0$.

4. The SNR performance of the CMT radio access system is superior to the conventional SCM system in spite of the value T_c/T when the number of radio channels becomes large.

5. The overall SNR performance of the CMT radio access system is superior to the conventional SCM system when the number of channels is large and the double CMT is used. In case that the number of channels is 50, $T_c/T = 5.0$, and $\alpha = 0.5$, the improvement of the overall SNR performance was 3 [dB].

Chapter 6

Asynchronous Time Division Multiple Access Bus Link System using Chirp Multiplexing Transform

6.1 Introduction

Asynchronous time devision multiple access (TDMA) bus link system was proposed in Chap.4. The chapter introduced that the employment of the asynchronous TDMA bus link for fiber-optic radio access networks can realize simple construction and easy extension of the networks because the difficulty of time synchronization among RBSs can be obviated, while the optical pulse loss occurs due to the asynchronous access of signals. In that chapter, the asynchronous TDMA was realized by transforming radio signals into narrow optical PAM/IM (pulse amplitude modulated / optical intensity modulated) pulses by the use of photonic natural bandpass sampling technique.

This chapter proposes the asynchronous TDMA bus link system using Chirp Multiplexing Transform (CMT), in which radio signals are also transformed into narrow optical PAM/IM pulses in order to allow the asynchronous access of radio signals with TDMA format, however such transformation is executed by the use of CMT proposed in Chap.5, not by the use of photonic natural sampling technique.

As described in Chap.5, the CMT can transform radio signals with FDMA format into ones with TDMA format. Therefore the fiber-optic radio access networks using CMT provide the possibility of universal use of the networks among different types of radio service because it is able to distinguish and switch radio service signals in the optical stage by the use of photonic switch at a RN in the network.

Besides such advantage of the use of CMT, if we can perform the time compression of output signals from the CMT, the configuration of asynchronous TDMA bus link combined with CMT system are allowed. Such combination of asynchronous TDMA system and CMT system provides much universal and flexible fiber-optic radio access networks because the advantage of each system are also combined. Fortunately, the CMT has the ability to compress the output at the same time if enlarging the chirp sweep bandwidth enough than the bandwidth of radio signal. Therefore in this chapter, the asynchronous TDMA bus link system using CMT are proposed and discussed.

Another topic dealt in this chapter is the affection of traffic distribution on the pulse

loss probability and the call blocking probability. The obtained results about them can be also applied to the performance of the asynchronous TDMA bus link systems using photonic natural sampling technique in Chap.4.

The remainder of this chapter is organized as follows. Section 6.2 describes the configuration of the Asynchronous TDMA bus link systems using CMT. Section 6.3 theoretically analyzes the pulse loss probability and the call blocking probability, considering traffic distribution in the area covered by a bus link. Section 6.4 discusses the affection of traffic distribution on the pulse loss probability and the call blocking probability, and the relationship between them by showing some numerical results. Final part of the section introduces one of manners to determine the area size covered by a bus link and the number of RBSs connected to the bus link.

6.2 Asynchronous TDMA Bus Link System using Chirp Multiplexing Transform

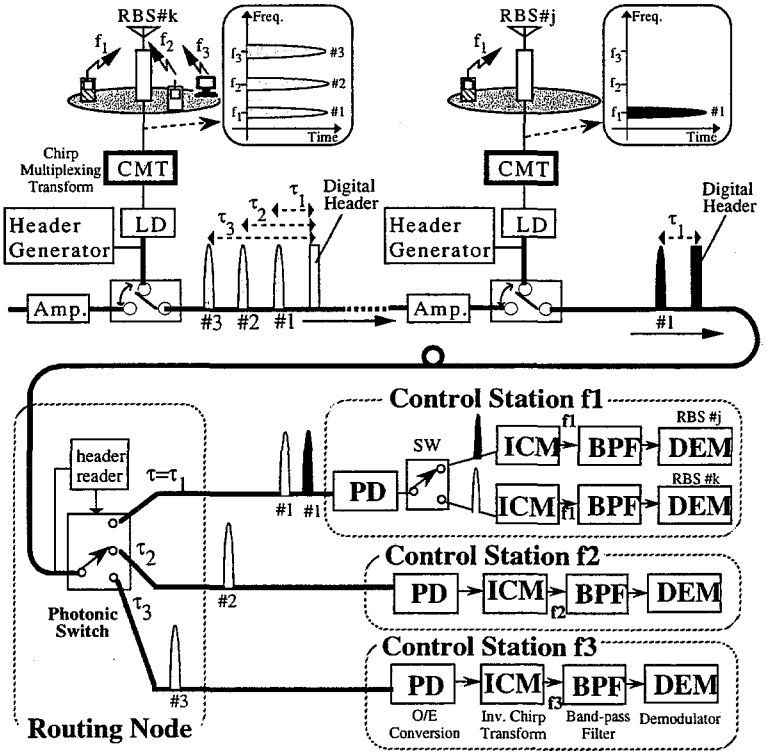

Figure 6.1: Asynchronous TDMA bus link systems using CMT.

Figure 6.1 illustrates the configuration of asynchronous TDMA bus link systems using chirp multiplexing transform (CMT). Many RBSs and several RCSs are connected with a fiber-optic bus link, and each RBS equips the Chirp Multiplexing Transformer (CMT) that was proposed in the previous Chap.5. The CMT can perform the conversion of received several radio service signals operated under different frequency bands into ones with TDM format as described in Chap.5. Therefore the routing node (RN) included in

the network can distinguish and switch radio service into the appropriate RCS by the use of simple photonic switch. Besides such utilization of the CMT as a FDM-TDM converter, the system proposed in this chapter utilizes the CMT as time compressor for radio signals into narrow pulse format. The time compression of radio signals allows asynchronous time division multiple access of radio signals into a fiber-optic bus link as introduced in Chap.4.

The RBS receives several radio services and feeds them into CMT. Figure 6.2 illustrates the configuration of CMT and the relationship between the received radio signals and resultant chirp multiplexing transformed signal (CMT signal). In the CMT, input radio signals, $r(t)$, are pre-multiplied with a periodical chirp signal, passed a chirp filter and post-multiplied with a chirp signal. The output of CMT, $V(t)$, is represented by the following as described in Chap.5.

$$V(t) = \mathrm{Re}[\sum_{l=-\infty}^{\infty} U^{(l)}(t)e^{j2\pi f_0 t}] \tag{6.1}$$

$$U^{(l)}(t) = \begin{cases} \int_{-\frac{T_c}{2}}^{\frac{T_c}{2}} u(\tau + lT_c)e^{-j2\pi\beta[t-lT_c]\tau}d\tau & ; -\frac{T_c}{2} \leq t - lT_c \leq \frac{T_c}{2} \\ 0 & ; \text{otherwise} \end{cases} \tag{6.2}$$

where $u(t)$ is the complex envelope of input radio signals. T_c and ΔF are the chirping dispersion time and the frequency sweep range of CMT, respectively. β is the chirping angle given by $\Delta F/T_c$. l in the equation is an integer and f_0 is a center frequency of the chirp filter. You can understand from Eq.(6.2) that the CMT executes the Fourier transformation of original radio signals with every time-width of T_c, and outputs the results as the function of time. Consequently, the one radio service with its bandwidth B_{RF} is transformed into periodical pulses with its pulse width B_{RF}/β and its interval T_c as illustrated in Fig.6.2. Therefore, if we enlarge the frequency sweep range, ΔF, than the bandwidth of radio signal B_{RF}, we can compress its pulse width at the same time. The relationship between the pulse duty of obtained pulse trains and the radio signal is given by,

$$\frac{\tau}{T_c} = \frac{B_{RF}}{\Delta F}. \tag{6.3}$$

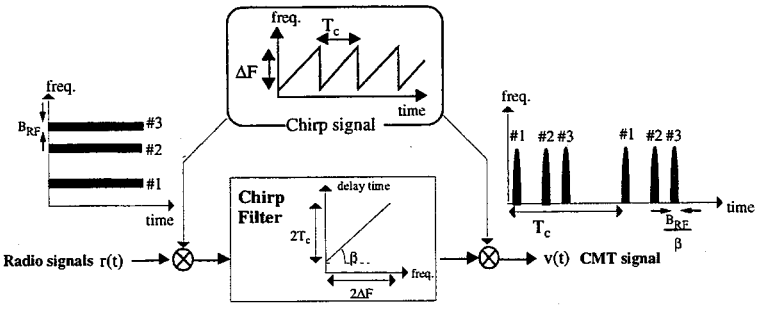

Figure 6.2: Configuration of CMT.

Figure 6.1 illustrates the example case in which kth RBS is receiving three radio carriers, f_1, f_2, and f_3, that respectively correspond to radio service 1, service 2, and

service 3. The CMT transforms them into TDM pulses whose time positions are different from each other (τ_1, τ_2, and τ_3 in the figure). Then the TDM pulses are transformed into optical PAM/IM (pulse amplitude modulated / intensity modulated) pulses by directly modulating Laser Diode (LD) and fed into fiber-optic bus link using photonic switch after attaching digital header to recognize the start point of the TDM frame and the destination address of included radio service signal. Then, each RBS transmits the generated optical PAM/IM pulse trains without any the synchronization control to the other RBSs. In other words, the PAM/IM pulses from many RBSs are asynchronously multiplexed in fiber-optic bus link with TDMA format.

Such asynchronous TDMA bus link system has the advantage in the flexibility and the simplicity of system because the network need no synchronization control among RBSs and the networks can be easily extended. Furthermore it allows the unified transmission of multiple radio services with TDMA format, therefore the switching of radio service in the optical stage can be executed. We consider that such capability of photonic routing of radio service provides the possibility of the universal use of fiber-optic networks among different types of radio service. However one of the problems inherent to the asynchronous TDMA bus link systems is that a PAM/IM pulse is lost if several RBSs transmit ones into a bus link at just the same time. Then the pulse loss probability will be discussed in Sect.6.3.

Another problem to be studied is the degradation of received signal power due to pulse width narrowing and many optical devices passed in the transmission. Therefore in the asynchronous TDMA bus link systems, it is required to compensate such the degradation of received signal power by the use of optical amplifier with inline type of insertion as illustrated in Fig.6.1, and that can also realize to balance the signal power received at the RCS among every RBSs. The topic about carrier-to-noise power ratio performance of asynchronous TDMA bus link and CMT systems have already dealt in the previous Chapters 4 and 5 in detail. Therefore this chapter does not refer to that topic anymore.

At the RCS, optical PAM/IM pulses received from several RBSs are detected by a photodetector (PD) and demultiplexed into the signal from each RBS by the use of switch. Inverse CMT (ICM) with the same configuration as transmitting CMT's regenerates the original radio signals or the information data conveyed on the radio signal can be directly demodulated by the use of correlation demodulator as described in chapter 5.

6.3 Theoretical Analyses of Pulse Loss and Call Blocking Probabilities

Since the PAM/IM pulses from many RBSs are multiplexed asynchronously in the fiber-optic bus link, some of the pulses may not be able to reach the RCS and lost when several RBSs transmit ones at just the same time. The pulse loss probability in asynchronous TDMA systems was studied in Chapter 4, however in which only the uniform traffic distribution model was considered in the analysis and the affection on it of the traffic partiality have never been clarified yet. Therefore in this chapter, we theoretically analyze the pulse loss probability and the call blocking probability considering the traffic partiality in the area covered by a fiber-optic bus link. As for the traffic distribution model, Gaussian model is the most simple and popular one[56] because the traffic partiality can

be simulated by only two parameters, its mean and variance, and it is also suitable for us to investigate the fundamental affection of the traffic partiality on the call blocking probability or on the pulse loss probability.

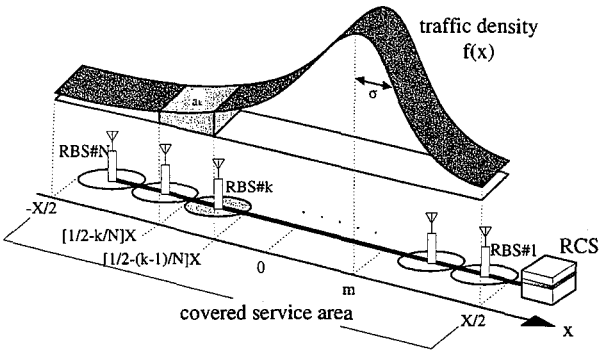

Figure 6.3: Traffic density distribution.

Figure 6.3 illustrates the one dimensional Gaussian traffic model used in the analysis. The fiber-optic bus link covers the service area with its size X, and it is equally divided into N radio zones. RBS is numbered from the nearest one to the RCS. The traffic density at the distance x from the center of the service area, $f(x)$, is given by,

$$f(x) = \frac{A}{\sigma\sqrt{2\pi}} \exp\left[-\frac{(x-m)^2}{2\sigma^2}\right] \tag{6.4}$$

where m is the position with the peak intensity and σ is the standard deviation. By modifying these values, the various state of traffic partiality can be simulated. Furthermore in order to fairly study the affection of the traffic partiality on the call blocking probability or the pulse loss probability, A is determined in the manner that the total traffic covered by the service area, $[-\frac{X}{2}, \frac{X}{2}]$, is fixed to a_t. Thus, by solving the equation of $\int_{-2/X}^{2/X} f(x)dx = a_t$, A is given by,

$$A = \frac{a_t}{\frac{1}{2}\left[\mathrm{erf}\left(\frac{X/2-m}{\sigma\sqrt{2}}\right) - \mathrm{erf}\left(\frac{-X/2-m}{\sigma\sqrt{2}}\right)\right]} \tag{6.5}$$

Consequently the traffic generated in the kth zone, a_k, is given by,

$$\begin{aligned} a_k &= \int_{[-\frac{1}{2}+\frac{k-1}{N}]X}^{[-\frac{1}{2}+\frac{k}{N}]X} f(x)dx \\ &= \frac{a_t\left[\mathrm{erf}\left(\frac{[-\frac{1}{2}+\frac{k}{N}]X-m}{\sigma\sqrt{2}}\right) - \mathrm{erf}\left(\frac{[-\frac{1}{2}+\frac{k-1}{N}]X-m}{\sigma\sqrt{2}}\right)\right]}{\left[\mathrm{erf}\left(\frac{X/2-m}{\sigma\sqrt{2}}\right) - \mathrm{erf}\left(\frac{-X/2-m}{\sigma\sqrt{2}}\right)\right]} \end{aligned} \tag{6.6}$$

Figure 6.4 shows some example states of traffic distribution in case that 10 RBSs are connected and $a_t = 3.0$. The parameters σ and m are normalized by the service area size X. For example, $\sigma/X = 0.15$ and $m/X = 0$ is the state that the center 30% area of the service zone includes 70% of the total traffic. However the difference of value of m

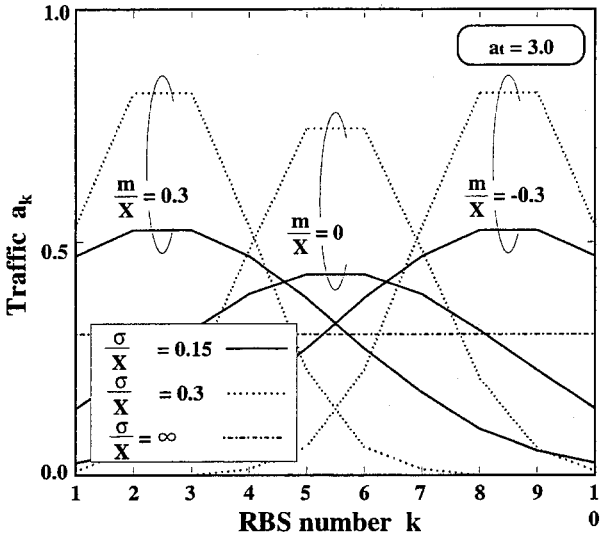

Figure 6.4: Traffic versus the RBS number.

causes the difference of peak intensity even if the same value of σ/X is used, because of the assumption of fixed total traffic in the service area.

We assume that the capacity of every RBS is fixed to n channels, and the radio channels available in each radio zone are multiplexed with FDMA format. The initial call blocking occurs if call connections over the channel capacity n are requested at the same time in the radio zone. The call blocking probability in k-th zone, R_k, is given by the use of Erlang B formula[37] as,

$$R_k = \frac{\frac{a_k^n}{n!}}{\sum_{i=0}^{n} \frac{a_k^i}{i!}} \tag{6.7}$$

Therefore, the average traffic virtually accepted by RBS can be estimated as $a_t(1 - R_k)$. We assume that the traffic accepted by RBS is equally assigned to each channel in average. Then, the average traffic per channel at kth RBS, a_{k_c}, is given by,

$$a_{k_c} = \frac{a_k(1 - R_k)}{n} \tag{6.8}$$

Figure 6.5 illustrates the mechanism of pulse loss. The pulse loss occurs at the stage of photonic switch multiplexing. If jth RBS transmits its PAM/IM pulse when the kth RBS's pulse are passing the photonic switch, the transmission of kth RBS's pulse are terminated and the pulse is lost. Therefore the RBS which is nearer to the RCS has the priority in the transmission of pulses, and the pulse loss probability performance of the further RBS is more deteriorated.

As described in Sect.6.2, the CMT at a RBS transforms one radio carrier into compressed pulse trains with its pulse duty $\frac{B_{RF}}{\Delta F}$ and its repetition interval T_c, while under the condition that RBS is receiving several carriers, such pulse trains are generated as much as the number of receiving carriers. Under the condition that jth RBS is receiving only one carrier when kth RBS' pulse is passing the photonic switch, the probability that the

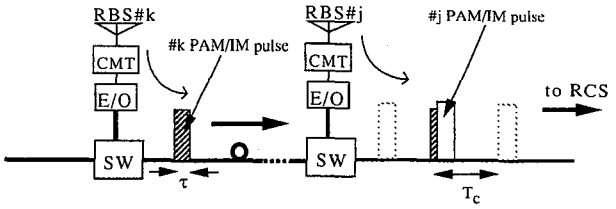

Figure 6.5: Mechanism of PAM/IM pulse loss.

pulse loss occurs is given by $2\tau/T_c$ because the occurrence time difference between the jth and the kth RBS's pulse can be modeled as an uniform distributed random variable in the interval $[-\frac{T_c}{2}, \frac{T_c}{2}]$ as described in Chapter 4. The probability that jth RBS is receiving carrier on a channel at arbitrary time is given by a_{j_c}. Let A_{kj} denote the event that one PAM/IM pulse transmitted from the kth RBS isn't lost at the stage of photonic switching of jth RBS ($j < k$). Considering n channels are independently operated in radio zone, the probability of the event A_{kj} is given by,

$$P(A_{kj}) = \left[1 - \frac{2\tau}{T_c} a_{k_c}\right]^n \quad (j < k) \tag{6.9}$$

Furthermore since the traffics in all radio zones are mutually independent, the probability, P_{th_k}, that the PAM/IM pulse from kth RBS successfully reach the RCS without any pulse loss is obtained as

$$\begin{aligned} P_{th_k} &= \prod_{j=1}^{k-1} P(A_{kj}) \\ &= \prod_{j=1}^{k-1} \left[1 - \frac{2\tau}{T_c} a_{k_c}\right]^n \end{aligned} \tag{6.10}$$

Therefore, the pulse loss probability in fiber-optic bus link for the kth RBS's radio signal, P_{loss_k}, is given by

$$P_{loss_k} = 1 - P_{th_k} \tag{6.11}$$

6.4 Numerical Results of Pulse Loss and Call Blocking Probabilities

This section shows some numerical results of the pulse loss probability and the call blocking probability. It is consistently assumed that radio bandwidth per carrier, B_{RF}, is 300 [KHz] and the maximum number of carrier received at an RBS, that is, the channel capacity n, is 4.

Figures 6.6 and 6.7 show the pulse loss probability versus the RBS number for different value of σ/X and m/X, respectively. An RBS transmits PAM/IM pulses using photonic switch, and the pulse loss occurs when a PAM/IM pulse from any another RBS further from the RCS tries to pass the switch of the RBS which is in its transmitting time.

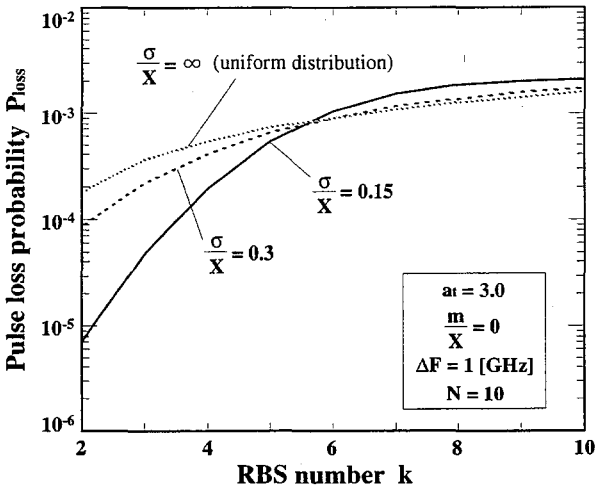

Figure 6.6: Pulse loss probability versus the RBS number.

Therefore the PAM/IM pulse of nearer RBS has the priority in the transmission and especially the PAM/IM pulses of the 1st RBS are never lost. Then it can be seen from the figures that the pulse loss probability is degraded as the RBS number increases. Its degradation curve is different according to the value of σ/X or m/X. The pulse loss probability of kth RBS depends only on the traffics covered by RBSs nearer to the RCS than that. Therefore in Fig.6.6, the pulse loss probability of RBS which is located nearer to the RCS than the position of the peak intensity ($m/X = 0$) is much improved as σ/X decreases. Also in Fig.6.7, the pulse loss probability of nearer RBS is improved as m/X decreases. However the performance of the RBS furthest from the RCS, that is, the worst performance in this system, have little dependence on the parameters σ/X and m/X.

Figure 6.8 shows the pulse loss probability and the call blocking probability versus the number of connected RBSs. The increase of RBSs means the radio zone size reduction and the decrease of traffic per RBS. Both of the performance depend on the RBS number. Thus, This figure is indicating the worst performances obtained in all RBSs. The total traffic in the service area, a_t, is the parameter. In the condition that more than 4 RBSs is connected, the pulse loss probability has little dependency on the number of RBSs. On the other hand, the call blocking probability is much improved by enlarging the number of RBSs. As a result, lines of the two characteristics cross at 14 number of connecter RBSs at $a_t = 3.0$, and 20 number of RBSs at $a_t = 5.0$. From our point of view, the pulse loss may cause the intercept of communications and it seems to be serious problem than the initial call blocking. Therefore the pulse loss probability has to be smaller or much smaller than the call blocking probability. In the case of Fig.6.8, the connection of more than 10 RBSs are allowed in case of $a_t = 5.0$.

Consequently, we should determine the network size covered by a bus link in the manner that the included total traffic satisfies a required pulse loss probability. On the other hand, we should determine the number of connected RBSs, that is, the number of radio zones, in the manner that a required call blocking probability is satisfied though it depends on the standard deviation of traffic distribution.

Figure 6.9 shows the total accommodated traffic versus required pulse loss probability

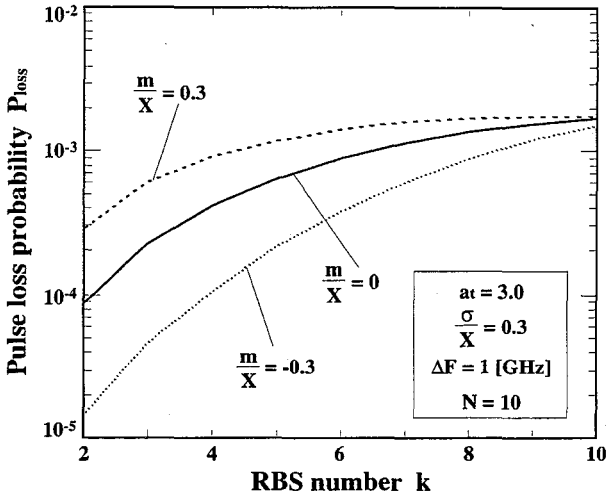

Figure 6.7: Pulse loss probability versus the RBS number.

for different values of frequency sweep range of CMT, ΔF. When required pulse loss probability is reduced, the total traffic which can be accommodated by a bus link decreases, however enlarging ΔF can improve the pulse loss probability or the accommodated total traffic, a_t. For example, if we assume 10^{-3} of pulse loss probability is required, the networks have to be constructed in the manner that a bus link includes 1.6 traffic when $\Delta F = 1$[GHz].

On the other hand, the reduction of pulse duty of PAM/IM signal, that is, the enlargement of ΔF, causes the degradation of carrier-to-noise power ratio (CNR) performance of signals detected at the RCS. The relationship between the pulse duty and the received CNR was theoretically analyzed in Chapter 4, and in the case of $\Delta F = 1$[GHz] and $B_{RF} = 300$ [KHz], the pulse duty is reduced to 3.0×10^{-4} from Eq.(6.3), but the CNR more than 50 [dB] is obtained at the pulse duty as shown in chapter 4.

Figure 6.10 shows the required number of RBSs to satisfy the call blocking probability of 10^{-2} versus the normalized standard deviation σ/X. It is seen from the figure that the required number of RBSs has much dependency not only on the total traffic but also on the standard deviation. For example, under the conditions of $\sigma/X = 0.15$ and $a_t = 3.0$, the connection of more than 10 RBSs is required.

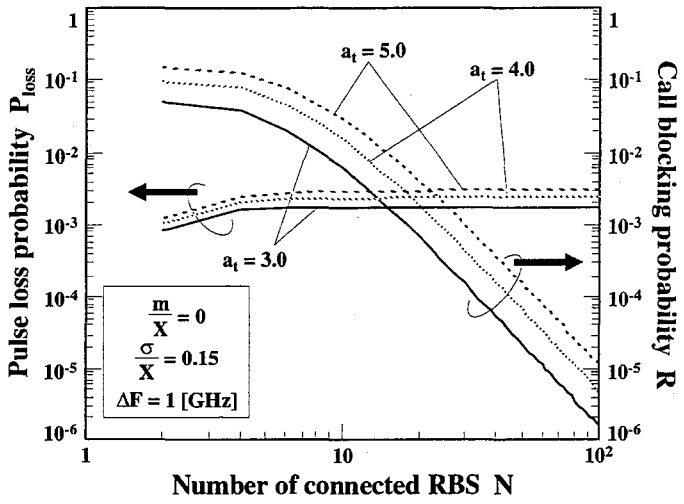

Figure 6.8: Pulse loss probability and call blocking probability versus the number of connected RBSs.

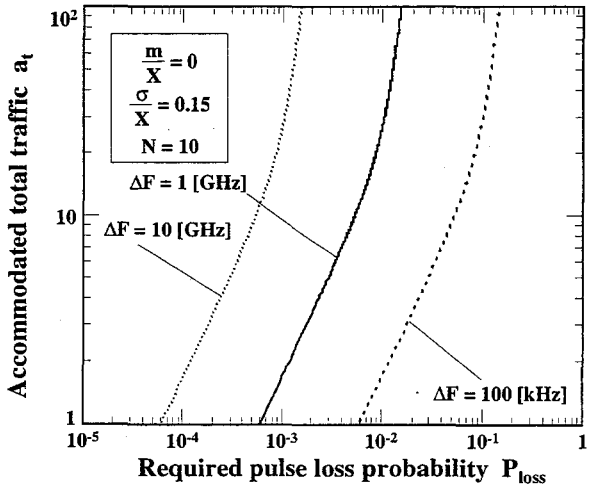

Figure 6.9: Accommodated total traffic versus required pulse loss probability.

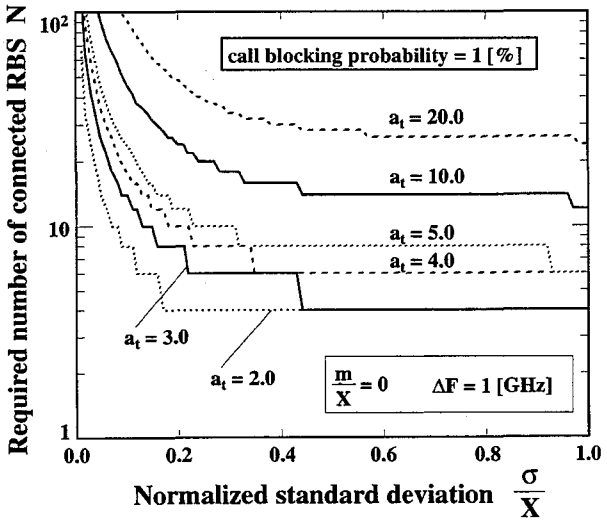

Figure 6.10: Required number of RBSs versus normalized standard deviation of traffic distribution.

6.5 Concluding Remarks

This chapter proposed asynchronous TDMA bus link system using chirp multiplexing transform (CMT). The performance of the proposed system was investigated by the theoretical analyses of the pulse loss probability and the call blocking probability considering the traffic partiality in the area covered by a fiber-optic bus link. This chapter investigates the relationship between the pulse loss probability and the call blocking probability, the affection of the traffic partiality on them, the the total allowable traffic covered by a bus link, and the required number of connect RBSs. Following results were obtained:

1. Asynchronous TDMA bus link system can be constructed by the use of CMT technique. Since kind of radio service can be distinguished by its transmitted time in the proposed system, the switching of radio signals according to its type of service can be performed in the optical stage by the use of photonic time switch.

2. The pulse loss probability performance depends only on the total traffic in the area covered by a bus link, but is independent of the traffic partiality, the position of peak traffic intensity, and the number of connected RBSs.

3. The call blocking probability performance is improved by increasing the number of connected RBSs, thus the number at which the call blocking probability becomes smaller than the the pulse loss probability exists. This systems should be operated under that number of RBSs.

4. The pulse loss probability can be improved by increasing the bandwidth of CMT or decreasing the total traffic in the area covered by a bus link.

5. One of the manners to determine the area size covered by a bus link and the number of connected RBSs was introduced. The area size covered by one bus link should be designed in the manner that the covered traffic satisfies the required pulse loss probability performance. On the other hand, the number of connected RBSs should be determined in the manner that it satisfies the required call blocking probability considering the traffic partiality.

Chapter 7

Fundamental Experiments on Fiber-Optic Radio Transmission System using Photonic Natural Bandpass Sampling

7.1 Introduction

This chapter reports and discusses the results of fundamental experiments on fiber-optic radio transmission system using photonic natural bandpass sampling. The principle of photonic natural bandpass sampling transmission is experimentally confirmed and its performances of carrier-to-noise power ratio (CNR), spurious free dynamic range (SFDR), and carrier-to-distortion power ratio (CDR) are investigated. Each performance is compared to that of the conventional IM/DD transmission system, and the penalty of each performance due to sampling transmission is discussed from experimental results and theoretical viewpoint. Section 7.2 describes experimental setups, Section 7.3 shows and discusses the experimental results, and Section 7.4 derives system parameters from the experimental results and estimates the system capacity.

7.2 Experimental Setup

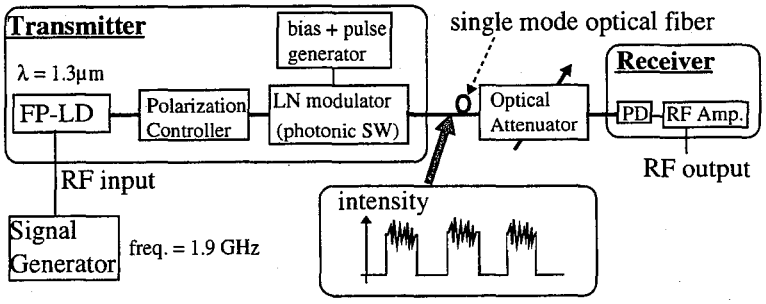

Figure 7.1: Experimental setup.

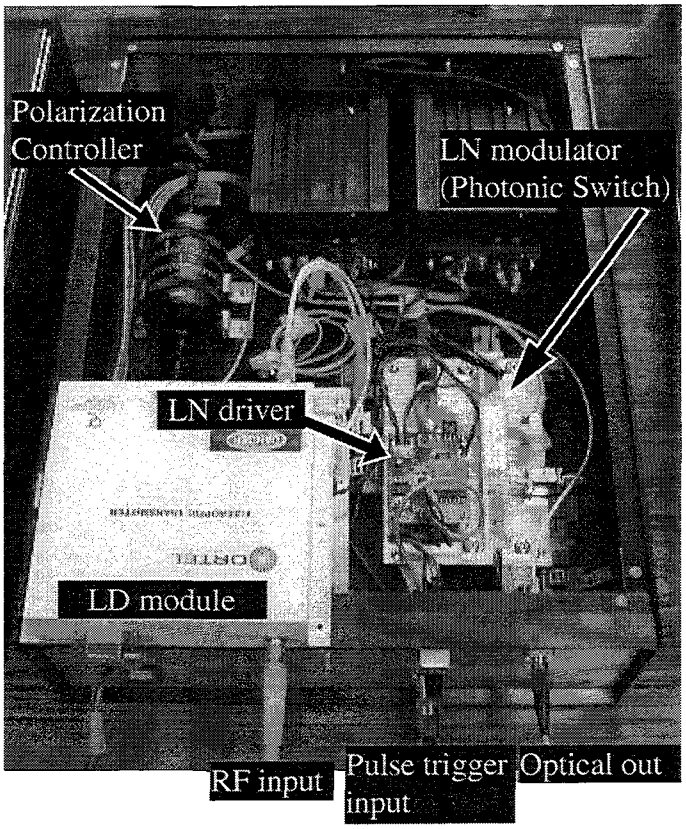

Figure 7.2: Inside view of transmitter.

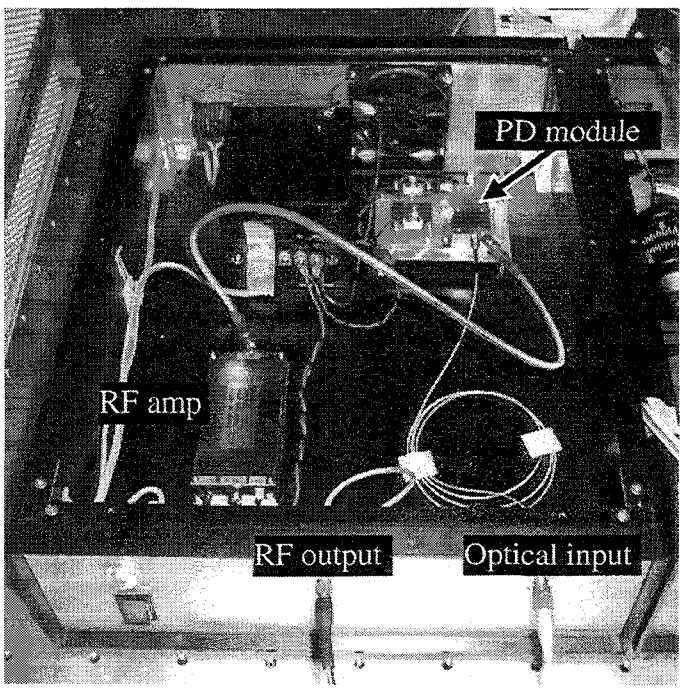

Figure 7.3: Inside view of receiver.

Table 7.1: Specifications of devices used in experiment.

Laser Diode Module (ORTEL 5515B)	Fabry-Perot multimode Laser wavelength λ : 1.3μm output power P_o: 0.7 [dBm] RIN $\leq$ -151 [dBm/Hz] (1-2 [GHz]) input impedance : 50 [Ω]
LN modulator (Sumitomo TMZ1.3-2.5)	insertion loss $\leq$ 5 [dB] on-off power ratio $\geq$ 20 [dB] 3[dB] bandwidth $\geq$ 3 [GHz] half-wave voltage $\leq$ 3.5 [V]
PD (NEC NDL5481P2C)	sensitivity α_o : 0.83 [A/W]
total insertion loss of LN modulator and polarization cont. : L_o	5.1 [dB]
sensitivity of LD module : r	1.26×10^{-2}[W/A]
total sensitivity of receiver : α_t	75 [A/W]
total link gain in 50% pulse duty (transmission loss = 0 [dB])	-20 [dB]
load impedance of receiver : R	50 [Ω]
bandwidth for noise power expression : B	300 [kHz]

Figure 7.1 illustrates the experimental setup, and Fig.7.2 and Fig.7.3 shows the photos of its external appearance. Table 7.1 are summarizing the specifications of devises used. The Fabry-Perot Laser Diode with 1.3 μm wavelength was directly modulated by RF signals generated from a Standard Signal Generator. The RF signal with the frequency of 1.9 [GHz] is used in the experiment to estimate the performance in case that the Japanese PHS radio service is applied to the photonic natural bandpass sampling transmission system. The obtained optical intensity modulated signal was sampled by the use of a $LiNbO_3$ (LN) intensity modulator. The modulation depth of LN modulator has dependency on the input optical polarization state, thus a polarization controller was inserted between the Laser Diode module and the LN modulator to obtain the maximum on-off power ratio of output optical signal.

Figure 7.4 shows the relationship between driving DC voltage on the LN modulator and obtained output optical power. The half-wave voltage was 1.95 [v] and the peak-to-peak (on-off) power ratio was 28 [dB]. From these data, we drove the LN modulator by rectangular bipolar pulses of 1.95 [v] peak-to-peak voltage with 2.8 [v] DC bias voltage in order to execute on-off optical switching.

Figure 7.5 illustrates the states of transmitted optical intensity in two transmission schemes. One is the conventional IM/DD transmission without sampling (in no use of LN modulator), and the other is the sampling transmission with 50% pulse duty. The average intensity in the IM/DD transmission always fixed on P_o = 0.7 [dBm], while that in the sampling transmission is on-off switched into rectangular pulses. Furthermore the peak intensity in the sampling transmission suffers from L_o = 5.1 [dB] power loss

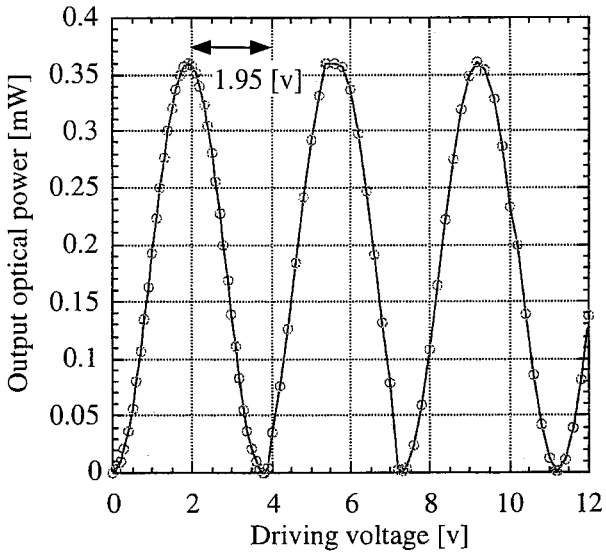

Figure 7.4: Output optical power versus driving voltage on LN modulator.

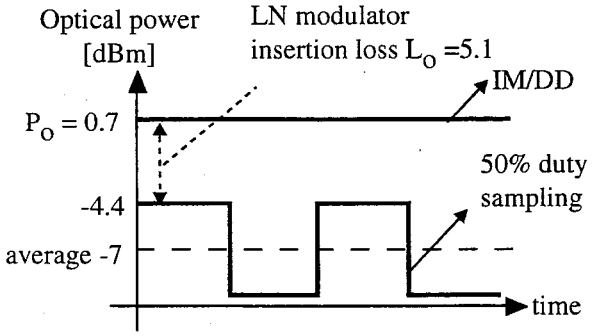

Figure 7.5: Output optical power of transmitter.

in comparison to that in the IM/DD transmission due to the insertion of polarization controller and LN modulator. Therefore the average power of the sampling transmission was typically around -7 [dBm] in case of 50% pulse duty.

At the receiver, received optical pulses were simply photodetected by the use of photodiode and amplified with wideband RF amplifier. The sensitivity of LD module, and receiver, and the total link gain at 1.9 [GHz] frequency band were measured by the use of lightwave component analyzer (HP8565E), and the Table 7.1 also includes the results.

Figure 7.6 shows the waveform of receiver output in the case of sampling frequency of 600 [kHz], which was measured by a digitizing oscilloscope. You can see that the radio signal sampled with 30 [%] pulse duty was obtained. Figure 7.7 shows the spectrum of receiver output when sampling frequency was 10 [MHz]. As proved in theoretical analysis, the spectrum is symmetric about the radio frequency and the carrier appears at intervals of sampling frequency.

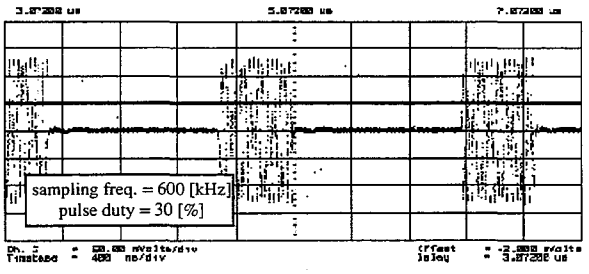

Figure 7.6: Waveform of a receiver output signal.

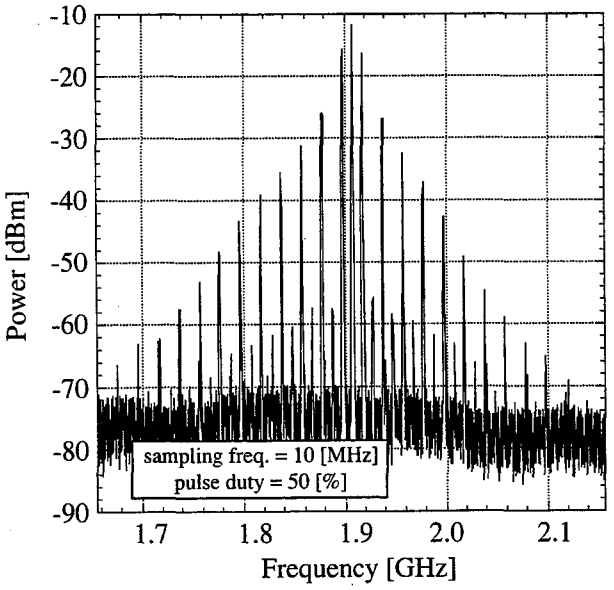

Figure 7.7: Spectrum of a receiver output signal.

7.3 Measured Received CNR and CDR Performances

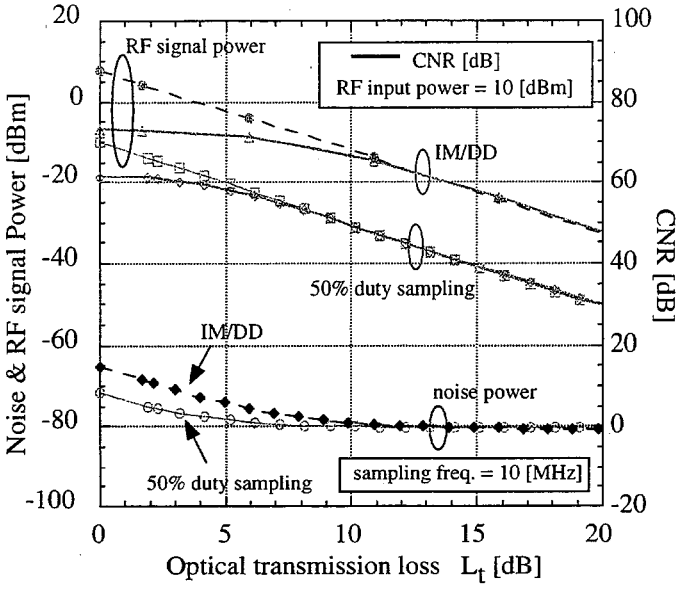

Figure 7.8: CNR performance versus optical transmission loss.

Figure 7.8 shows the experimental results of the CNR performance versus optical transmission loss L_t. In the figure, the CNR performance of the photonic natural band-pass sampling transmission is compared to that of the conventional IM/DD transmission. The various transmission loss, L_t, was simulated by the use of optical attenuator in the measurement. The average received optical power in case of $L_t = 0$[dB] was -6.3 [dBm] in the 50[%] pulse duty transmission, and 0.7 [dBm] in the IM/DD transmission. It was observed that the received RF signal power is degraded in proportion to the optical loss L_t to the 2nd power. It is seen in the Fig.7.8 that the received RF signal in the sampling transmission suffers from the power penalty of 16 [dB] in total, in comparison to the conventional IM/DD transmission. Therefore the CNR performance of the sampling transmission suffers from penalty of 16 [dB] in the region where the transmission loss is large, that is, where the thermal noise limits the CNR performance. On the other hand, in the region of low transmission loss, the CNR performance is limited by the relative intensity noise (RIN) and the saturation of the CNR performance was observed because the power of the RIN also increases in proportion to the received optical power to the 2nd power. In case that optical transmission loss, L_t, equals 0 [dB], it was observed that the penalty of the CNR performance was about 12 [dB].

Received power of RF signal (P_{sig}), thermal noise (P_{th}), RIN (P_{ring}), and shot noise (P_{shot}) are respectively written as follows from theoretical viewpoint.

$$P_{sig} = \frac{1}{2}\left(\frac{m\alpha_o P_o}{L_o L_t}\right)^2 \left(\frac{T}{T_s}\right)^2 \left(\frac{RG}{4}\right) \tag{7.1}$$

$$P_{th} = k_b T_{th} FGB \tag{7.2}$$

$$P_{rin} = RIN\left(\frac{\alpha_o P_o}{L_o L_t}\right)^2 \left(\frac{T}{T_s}\right)\left(\frac{RGB}{4}\right) \tag{7.3}$$

$$P_{shot} = 2e\left(\frac{\alpha_o P_o}{L_o L_t}\right)\left(\frac{T}{T_s}\right)\left(\frac{RGB}{4}\right) \tag{7.4}$$

where P_o, L_o, α_o, R, and B are the average transmitted optical power of LD, the insertion loss of LN modulator, sensitivity of PD, load impedance of receiver, and bandwidth for noise power expression respectively, and their specifications in the experiment are described in Table 7.1. $\frac{T}{T_s}$ and m are the pulse duty, and modulation index, and k_b, T_{th}, and F are the Boltzmann constant, noise temperature, and noise figure of receiver. G is the total electrical amplification gain after photodetection.

From the theoretical comparison of the sampling transmission to the conventional IM/DD transmission, the loss of $L_o = 5.1$[dB] and the pulse duty of $T/T_s = 1/2$ results in 16.2 [dB] penalty of RF signal power, and this result matches to the experimental result. As for the noise power, the power of RIN in the sampling transmission should have been degraded by 13 [dB] than that in the IM/DD transmission due to the L_o and 50% pulse duty. However in the measurement, the noise power degradation observed at $L_t = 0$ [dB] was 6 [dB]. Even if we consider the effect of thermal noise power, the noise power degradation seems to be small. The reason of that can be explained by assuming the RIN in the sampling transmission increases by 4 [dB] due to the insertion of polarization controller and LN modulator as calculated in the following Sect.7.4.

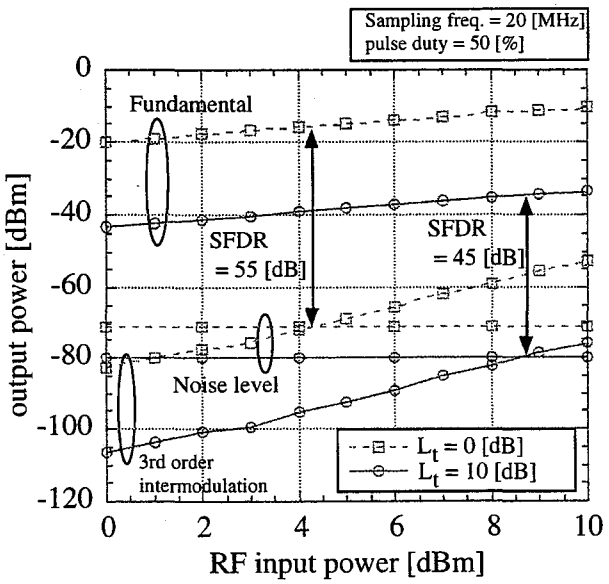

Figure 7.9: SFDR degradation due to received optical power degradation.

Figures 7.9 shows the the power of fundamental RF carrier, 3rd order inter-modulation (IM3), and noise versus driving RF power to LD. The figure shows the performances in two cases of $L_t = 0$ [dB], and $L_t = 10$ [dB]. The sampling frequency is 20 [MHz]. The 3rd order inter-modulation power was measured by modulating a Laser Diode with two RF tones. An example spectrum of received signals in the two-tone measurement is shown in Fig.7.10, where center two tones are fundamental carriers and the other two tones outside of them are IM3 components.

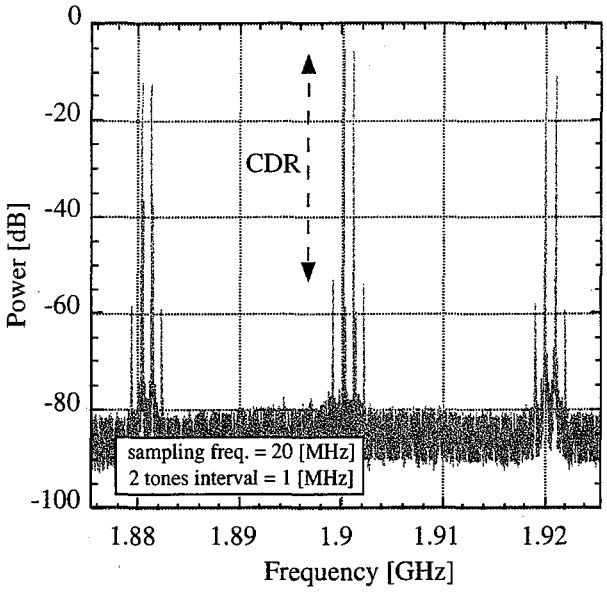

Figure 7.10: Spectrum of a receiver output in the CDR measurement.

Spurious free dynamic range (SFDR) is one of the important factors to determine the dynamic range performance of fiber-optic radio transmission systems. The SFDR is the range of RF input powers for which a two-tone RF input signal can be cleanly distinguished from noise and nonlinearities at the link output. The minimum RF input power is defined as the power which results in the received signal just reaching the noise floor generated by receiver noise and laser relative intensity noise (RIN). The maximum RF input power is defined as the power at which the in-band 3rd order intermodulation power generated by laser nonlinearities just reaches the noise floor. The theoretical expression of SFDR for a direct-detection analog optical link is derived in [10].

You can see from this figure that 55 [dB] of the SFDR, that is, 91 [dB·Hz$^{2/3}$] of the SFDR, was obtained in case of $L_t = 0$ [dB] and 45 [dB] of the SFDR, that is, 81 [dB·Hz$^{2/3}$] of the SFDR, was obtained in case of $L_t = 10$ [dB]. Consequently, it was observed that 10 [dB] degradation of received optical power causes 10 [dB] degradation of SFDR.

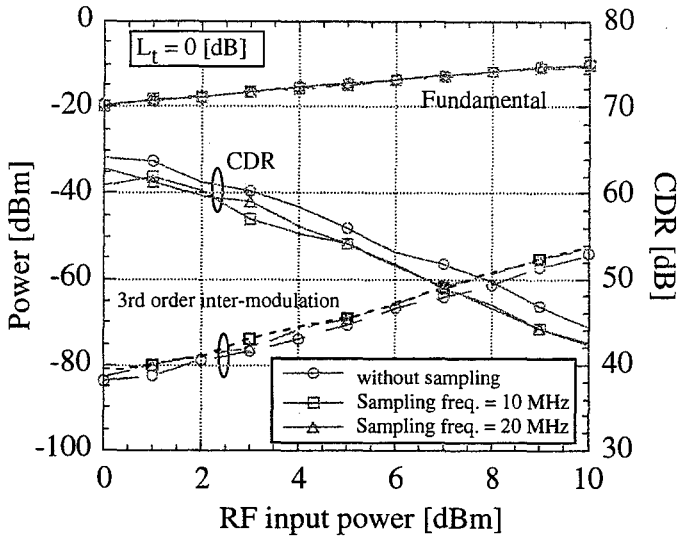

Figure 7.11: CDR performance versus RF input power.

Figure 7.11 shows the experimental results of the carrier-to-distortion power ratio (CDR) performance versus RF input power in cases that sampling frequency is 10 [MHz] or 20 [MHz] (DC bias plus bipolar pulse drives LN modulator), and in case that no sampling is applied (only DC bias drives the LN modulator). The driving DC bias voltage to the LN modulator was fixed among all the cases, therefore the average received optical power was same among all cases.

The CDR is defined as the power ratio of the fundamental carrier and the IM3. Each measured power of them is also shown in the figure. From the Fig.7.11, you can see that the obtained CDR performance does not depends on the sampling frequency, but the use of sampling transmission causes the increase of IM3 power by 2[dB]. It is guessed that this increase is due to nonlinearity of LN modulator (photonic switch). The exact reason of this phenomena should be further studied.

Figure 7.12 shows the experimental results of the carrier-to-noise plus distortion power ratio (CNDR) performance versus RF input power when the sampling frequency was 20 [MHz]. The power of received signal carrier increases in proportion to the inputted RF signal power, while the IM3 power increases in proportion to the power of inputted RF signal to the 3rd power. As a result, it was measured that the lines of the CDR and the CNR cross, and the existence of the optimum optical modulation index was observed. In the case of $L_t = 0$ [dB], 53 [dB] of the CNDR performance was obtained when the RF input power equals to 3 [dBm].

Figure 7.13 shows the experimental results of the CNR versus sampling pulse duty. The power of received optical power, RF power, and noise power are also shown in the figure. It was observed that the received RF power is proportional to the pulse duty to the 2nd power. From the theoretical viewpoint, the reduction of pulse duty into a half deteriorates the CNR performance by 3 [dB] in the condition of the RIN limitation or by 6 [dB] in the condition of the thermal noise limitation. However it was observed that reducing 80 [%] pulse duty into 40 [%] deteriorates the CNR performance by 4 [dB] because the thermal noise power level was close to the RIN power level in the measurement

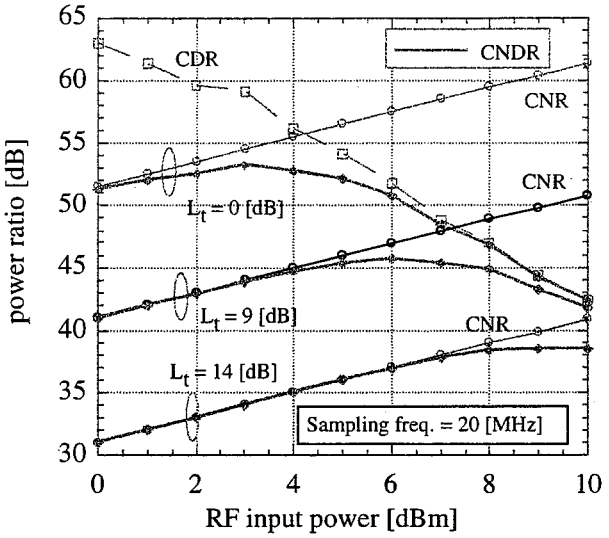

Figure 7.12: CNDR performance versus RF input power.

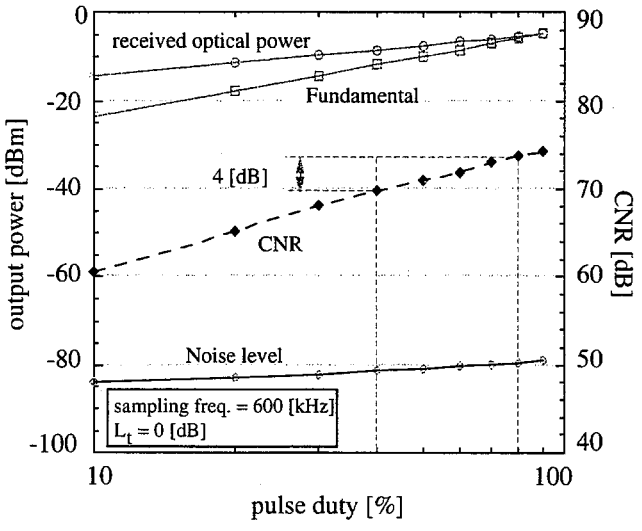

Figure 7.13: CNR performance versus pulse duty.

condition.

7.4 System Parameters Estimation from Measured Data

In this section, RIN, modulation index m, sensitivity of LD module, and 3rd order nonlinearity coefficient of LD's input-output characteristic are derived using the experimental results. The electrical receiver gain, G, is derived by the measured receiver sensitivity of α_t=75 [W/A] divided by the sensitivity of PD of α_o=0.83 [A/W].

$$G = 39[\text{dB}] \tag{7.5}$$

Then, using the experimental results of received noise power in case of $L_t = 0$ [dB], and the above gain G, we derive the equation,

$$\begin{aligned} P_{th} + P_{rin} &= k_b T_{th} FGB + RIN \left(\frac{\alpha_o P_o}{L_o}\right)^2 \left(\frac{T}{T_s}\right) \left(\frac{RGB}{4}\right) \\ &= -71[\text{dBm}] \end{aligned} \tag{7.6}$$

where, P_{th}=-80.2 [dBm] from the experimental results, $\frac{T}{T_s} = \frac{1}{2}$, $R = 50\Omega$, and $B = 300$ [kHz], and we are neglecting the contribution of the shot noise current because the power of it is enough small than that of others. Solving this equation, we get the value of RIN in the sampling transmission, RIN_s.

$$RIN_s = -133[\text{dB}] \tag{7.7}$$

In the similar manner, the RIN in case of the conventional IM/DD transmission, RIN_i, can be also derived by using the parameter of $\frac{T}{T_s} = 1$ and $L_o = 0$ [dB], and the equation, $P_{th} + P_{rin} = -65.4$ [dBm]. The value of RIN_i is derived as,

$$RIN_i = -137[\text{dB}] \tag{7.8}$$

Consequently, the increase of the RIN due to the insertion of LN modulator is 4 [dB].

The measured sensitivity of the LD module is $r = 1.26 \times 10^{-2}$[W/A]. Thus, the modulation index m in case that the RF input power equals 10 [dBm] is derived as,

$$\begin{aligned} m &= \frac{ri}{P_o} \\ &= \frac{1.26 \times 10^{-2}[\text{W/A}] \times 0.02[\text{A}]}{1.17 \times 10^{-3}[\text{W}]} \\ &= 0.215 \end{aligned} \tag{7.9}$$

On the other hand, the theoretical expression of the CDR is given by[9][55],

$$CDR = \frac{\frac{1}{2}m^2}{\frac{1}{2}\left(\frac{3}{4}a_3 m^3\right)^2} \tag{7.10}$$

Thus, using the above modulation index and the experimental results that CDR is 42.3 [dB] when RF input power is 10 [dBm], a_3 can be derived as,

$$a_3 = 0.221 \tag{7.11}$$

In the similar manner, the a_3 in the transmission without sampling is derived as,

$$a_3 = 0.176 \tag{7.12}$$

7.5 Estimation of the system capacity

Using Equations.(7.1)-(7.4), the CNDR is theoretically given by,

$$\left(\frac{C}{N+D}\right) = \frac{\frac{1}{2}m^2\left(\frac{\alpha_o P_o}{L_o L_t}\right)^2\left(\frac{T}{T_s}\right)^2}{\left[RIN\left(\frac{\alpha_o P_o}{L_o L_t}\right)^2 + 2e\left(\frac{\alpha_o P_o}{L_o L_t}\right) + \frac{4k_b T_{th} F}{R}\right]\left(\frac{T}{T_s}\right)B + < i^2_{im3} >_{(N,k)}\left(\frac{T}{T_s}\right)^2} \tag{7.13}$$

where, $< i^2_{im3} >_{(N,k)}$ is IM3 power in the k-th carrier band when N carriers modulate LD with equal amplitude and, and it is given by[9][55],

$$< I^2_{im3} >_{(N,k)} = \begin{cases} \frac{1}{2}\left(\frac{3}{4}a_3 m^3 D^{(2)}_{(N,k)} + \frac{3}{2}a_3 m^3 D^{(3)}_{(N,k)}\right)^2\left(\frac{\alpha_o P_o}{L_o L_t}\right)^2 & ; N \geq 3 \\ 0 & ; N < 3 \end{cases} \tag{7.14}$$

$$D^{(2)}_{(N,k)} = \frac{1}{2}[N - 2 - \frac{1}{2}\left\{1 - (-1)^N\right\}(-1)^k] \tag{7.15}$$

$$D^{(3)}_{(N,k)} = \frac{k}{2}(N - k + 1) + \frac{1}{4}\left\{(N-3)^2 - 5\right\} - \frac{1}{8}\left\{1 - (-1)^N\right\}(-1)^{N+k} \tag{7.16}$$

The optimum modulation index that maximize the CNDR performance is obtained by solving the equation, $d(CNDR)/dm = 0$ about m.

$$m_{opt} = \left(\frac{\left[RIN\left(\frac{\alpha_o P_o}{L_o L_t}\right)^2 + 2e\left(\frac{\alpha_o P_o}{L_o L_t}\right) + \frac{4k_b T_{th} F}{R}\right]B}{\left(\frac{3}{4}a_3 m^3 D^{(2)}_{(N,k)} + \frac{3}{2}a_3 m^3 D^{(3)}_{(N,k)}\right)^2\left(\frac{\alpha_o P_o}{L_o L_t}\right)^2\left(\frac{T}{T_s}\right)}\right)^{\frac{1}{6}} \tag{7.17}$$

Figure 7.14 shows the results of calculations about the CNDR performance versus the number of radio carriers in case of $L_t = 0$ [dB], where $a_3 = 0.221$ and $RIN_s = -133$ [dB] derived in the previous section are used, while figure 7.15 shows the results of calculations about the CNDR performance versus the optical transmission loss in cases that the number of carriers is 5, 10, or 15. In the calculations, the optimum modulation index in Eq.(7.17) is used and that transformed into input power per carrier is also shown. From Fig.7.14, you can see that the system used in this experiment can accommodate 7 radio carriers under the condition that $\frac{T}{T_s} = \frac{1}{10}$ and $CNDR = 30$ [dB] is required. You can also see from Fig. 7.15 that 10 [dB] transmission loss is allowed under the condition that 5 carriers are transmitted and $CNDR = 30$ [dB] is required. The allowance of 10 [dB] transmission loss roughly corresponds to the allowance of about 50 [km] fiber transmission.

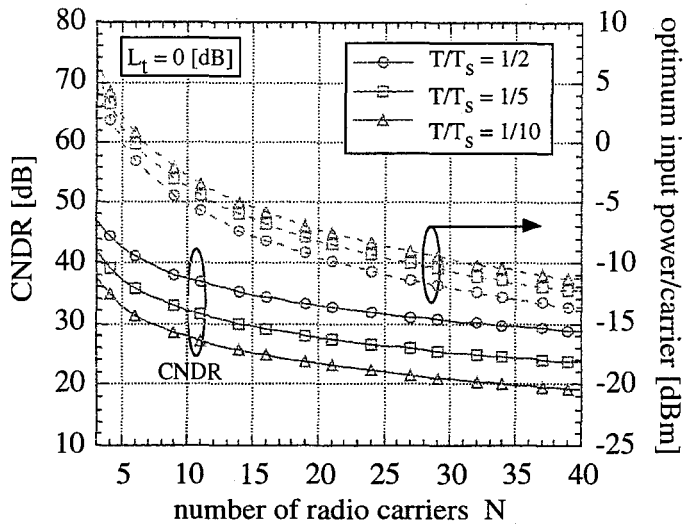

Figure 7.14: CNDR performance versus number of radio carriers.

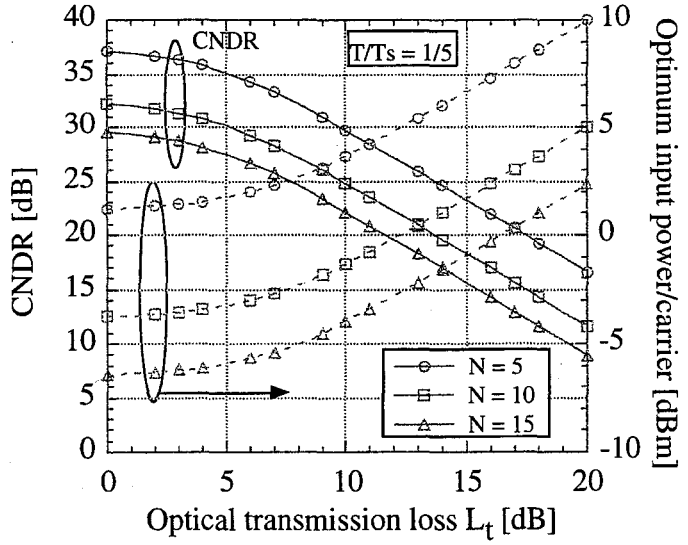

Figure 7.15: CNDR performance versus optical transmission loss.

7.6 Concluding Remarks

This chapter have reported and discussed the results of fundamental experiments about photonic natural bandpass sampling transmission of radio signals. The CNR performance in the photonic transmission system was experimentally compared with that in the conventional IM/DD transmission system. The penalty of the CNR in the photonic transmission system was 17 [dB] in the thermal noise limited conditions, and 12 [dB] in the RIN limited conditions. Next the CDR performance was measured by using 2 RF tones into transmitter. We measured that the the photonic sampling transmission causes the penalty of the CDR by 2 [dB]. Furthermore the existence of optimum optical modulation index that maximize total CNDR performance was experimentally confirmed. The degradation of CNR performance due to pulse duty reduction was experimentally measured and we measured that the reducing pulse width into a half degrades the CNR performance by 4 [dB]. Finally the system parameters of RIN, modulation index, and the 3rd nonlinearity coefficient, were derived from the experimental results, and system capacity of number of carriers accommodated and transmission loss allowed were calculated using the derived parameters. We concluded that the system used in the experiment allows 50 [km] transmission of 5 carriers when pulse duty is 20 [%] with more then the CNDR of 30 [dB].

Chapter 8

Conclusions

This thesis proposed and studied several types of photonic time division multiple access systems for fiber-optic radio access network. The self-synchronous TDM bus link system and the asynchronous TDMA bus link system were proposed in order to solve the difficulty of time synchronization control for photonic TDM signals among many base stations, and their performances were investigated by the theoretical analysis of the CNR performance or the burst loss probability performance. The chirp multiplexing transform (CMT) fiber-optic radio access system was proposed in order to provide the possibility of the universal use of radio base station and fiber-optic radio access networks among different radio services, and the overall SNR performance of detected radio signals was theoretically investigated. Furthermore the asynchronous TDMA bus link system that combined with the CMT system was proposed and discussed. Finally fiber-optic radio transmission system using photonic natural bandpass sampling was experimentally demonstrated, and its CNR and CDR performance were investigated on experiment.

Through our analysis, following results are obtained:

- The proposed photonic self-synchronous TDM bus link system needs no synchronization control to assign time slots to RBSs connected with a fiber-optic bus link and can realize the sharing of a single laser source among RBSs. The two system configurations of fiber-space multiplexing utilization and polarization multiplexing utilization were investigated. The splitting optical power ratio used at each RBS was optimized to balance the CNR performance of all RBSs, and the relationship among the CNR, number of connected RBSs, transmitting optical power, and pre-amplifier gain were theoretically clarified. The numerical results of the theoretical analysis concluded that the fiber-space multiplexing utilization can attain the higher CNR performance, and that the use of optical pre-amplifier is effective to improve the received CNR performance. The CNR performance of 40 [dB] can be attained when 12 RBSs are connected.

- The proposed photonic asynchronous time division multiple access bus link system can remove the difficulty of time synchronization control for photonic TDM. The performance degradation due to the radio bust loss was theoretically investigated. It was concluded that radio signals were multiplexed and transmitted with burst loss probability of 10^{-3} and received CNR of more than 40[dB] by photonic natural bandpass sampling transmission.

- The carrier sense control and the variable pulse width technique were also proposed to reduce the burst loss. Theoretical analysis of the burst loss probability clarified that the use of carrier-sense control reduces the burst loss probability to half of that in the case of no control. It was also clarified that the variable pulse width technique can improve the burst loss probability.

- The proposed CMT fiber-optic radio access system allows the transmission of FDM multiple radio services with photonic TDM format. Different radio services can universally use radio base stations and fiber-optic networks because radio service can be distinguished and switched in the optical stage by the use of photonic time switch.

  Considering the ICI, the ISI, the LD nonlinearity, and the receiver noise, SNR performance of detected radio signals was theoretically analyzed. Furthermore the double CMT system was proposed in order to decrease the ICI and the ISI. It was concluded that the double CMT system combined with the proposed suboptimal correlation demodulator can improve the SNR of detected radio signals in comparison to the conventional SCM system when the number of radio channels is large. 3 [dB] improvement of the SNR performance was obtained in case that the number of channels is 50.

- The proposed asynchronous TDMA bus link system using CMT can provide the combination of advantages of the asynchronous TDMA bus link system and the CMT system. The pulse loss probability and the call blocking probability were theoretically analyzed considering the traffic partiality in the covered area. It was concluded that the pulse loss probability performance was independent of the traffic partiality, the position of peak traffic intensity, and the number of connected RBSs, while the call blocking probability performance is much improved by increasing the number of connected RBSs. It was found that the number of connected RBSs when the call blocking probability becomes smaller than the pulse loss probability is independent of the total traffic, and this result means that the proposed asynchronous TDMA system should be operated under that number of RBSs.

- The fiber-optic radio transmission using photonic natural bandpass sampling technique was demonstrated. The CNR performance and the CDR performance were experimentally measured and compared to those of the system without photonic natural bandpass sampling. The penalty on the CNR was 17 [dB] in the thermal noise limited condition, and 12 [dB] in the RIN limited condition, and 2 [dB] of the penalty on the CDR was confirmed. The existence of optimum optical modulation index to maximize total CNDR performance was found. The degradation of CNR caused by the reduction of pulse duty was experimentally investigated. It was observed that reducing pulse duty into a half degrades the CNR performance by 4 [dB]. Finally the system capacity of the number of carriers accommodated and the transmission loss allowed were estimated from the experimental results. It was concluded that the system used in the experiment allows 50 [km] transmission of 5 radio carriers when pulse duty is 20 [%] with the CNDR of more than 30 [dB].

The fiber-optic radio access networks will become more and more important key technology in the infrastructure for future radio communication systems in which the univer-

sality and the flexibility to various kinds of multimedia radio services are important. The photonic time division multiple access systems treated in this thesis will become one of the candidates for the systems applied to such universal and flexible radio access networks. The author sincerely wishes that the present research contributes to the future fiber-optic radio access networks, and hopes for further progress of the research and the development aiming at the universality and the flexibility of fiber-optic radio access networks.

Appendix A

Proof of the orthogonality of Equation (5.25)

In this section, we prove the orthogonality of $S'_{ln}(t) = F[\beta t - l\Delta f]e^{-j2\pi[\beta t - l\Delta f]nT}$ where $G(\beta t)$ is removed from $S_{ln}(t)$ in Eq.(5.25). Generally for the two waveforms, $\psi_i(t)$ and $\psi_k(t)$, to be orthogonal, they must fulfill the orthogonality constraint of the Equation,

$$\int_{-\frac{T_s}{2}}^{\frac{T_s}{2}} \psi_i(t)\psi_k^*(t)dt = K_i\delta_{ik} \quad (i,\ k : \text{integer}) \tag{A.1}$$

$$\delta_{ik} = \begin{cases} 1 & (i = k) \\ 0 & (\text{otherwise}) \end{cases} \tag{A.2}$$

where T_s and K_i are the symbol duration and constants respectively. The orthogonality of $S'_{ln}(t)$ among different l is obviously satisfied because $F(f)$ is bandlimited. Then, we investigate the following complex correlation function R_{ik} to investigate the orthogonality among different n.

$$\begin{aligned} R_{ik} &= \int_{-\frac{B}{2\beta}}^{\frac{B}{2\beta}} S'_{0i}(t)\{S'_{0k}(t)\}^* dt \\ &= \int_{-\frac{B}{2\beta}}^{\frac{B}{2\beta}} |F[\beta t]|^2 e^{-j(2\pi d_{ik}\beta t + \theta_{ik})} dt \end{aligned} \tag{A.3}$$

where, $d_{ik} = i - k$ and $\theta_{ik} = \theta_i - \theta_k$. The real part of R_{ik} is given by

$$\begin{aligned} Re[R_{ik}] &= \int_{-\frac{B}{2\beta}}^{\frac{B}{2\beta}} |F[\beta t]|^2 \cos[2\pi d_{ik}\beta t]dt \cdot \cos[\theta_{ik}] \\ &\quad + \int_{-\frac{B}{2\beta}}^{\frac{B}{2\beta}} |F[\beta t]|^2 \sin[2\pi d_{ik}\beta t]dt \cdot \sin[\theta_{ik}] \end{aligned} \tag{A.4}$$

Because of the integration of the odd function $F[f]$ given by Eq.(5.26), the second term in Eq.(A.4) comes to be zero. Then $Re[R_{ik}]$ can be calculated as

$$\begin{aligned} Re[R_{ik}] &= 2\int_0^{\frac{1-\alpha}{2T}} \cos(2\pi T d_{ik} f)df \\ &\quad +2\int_{\frac{1-\alpha}{2T}}^{\frac{1+\alpha}{2T}} \cos(2\pi T d_{ik} f)\cos^2[\frac{\pi T}{2\alpha}(t - \frac{1-\alpha}{2T})]dt \\ &= \begin{cases} \frac{1}{T} & (d_{ik} = 0) \\ 0 & (\text{otherwise}) \end{cases} \end{aligned} \tag{A.5}$$

Consequently, we have proved that $S'_{ln}(t)$ is an orthogonal signal set.

References

[1] W. I. Way , "Subcarrier Multiplexed Lightwave System Design Considerations for Subcarrier Loop Applications", *IEEE J.Lightwave Tech.,* Vol.7, No.11, pp.1806-1818, November 1989.

[2] S. Komaki, K. Tsukamoto, S. Hara, and N. Morinaga, "Proposal Fiber and Radio Extension Link for Future Personal Communications", *Microwave and Optical Technology Letters*, Vol.6, No.1, pp.55-60, January 1993.

[3] J. Namiki, M. Shibutani, W. Domon, T. Kanai and K. Emura, "Optical Feeder Basic System Design for Microcellular Mobile Radio", *IEICE Trans. Commun.*, Vol.E76-B, No.9, pp.1069-1077, September 1993.

[4] H. Ogawa, "Microwave and Millimeter-wave Fiber Optic Technologies for Subcarrier Transmission Systems", *IEICE Trans. Commun.*, Vol.E76-B, No.9, pp.1078-1090, September 1993.

[5] W. I. Way, "Optical Fiber-Based Microcellular Systems: An overview", *IEICE Trans. Commun.*, Vol.E76-B, No.9, pp.1091-1102, September 1993.

[6] S. Komaki, K. Tsukamoto, M. Okada, and H. Harada, "Proposal of Radio High-way Networks for Future Multimedia-personal Wireless Communications", *1994 IEEE International Conference on Personal Wireless Communications (ICPWC 94'), Bangalore India*, pp.204-208, August 1994.

[7] S. Komaki, and E. Ogawa, "Trends of Fiber-Optic Microcellular Radio Communication Networks," *IEICE Trans. Electron.*, Vol.E79-C, No.1, pp.98-104, January 1996.

[8] S. Miyamoto, Y. Park, S. Komaki, "Effect of Optical Fiber Link Noise on Performance of Fiber-Radio Microcellular System," *technology reports of the Osaka university*, Vol.45, No.2228, pp.187-190, October 1995.

[9] H. Mizuguti, T. Okuno, S. Komaki, and N. Morinaga, "Performance Analysis of Optical Fiber Link for Microcellular Mobil Communication Systems", *IEICE Trans. Electron.*, Vol.E76-C, No.2, pp.271-278, February 1993.

[10] J. C. Fan, C. L. Lu, and L. G. Kazovsky, "Dynamic Range Requirements for Microcellular Personal Communication Systems Using Analog Fiber-Optic Links," *IEEE Transactions On Microwave Theory And Techniques*, Vol.45, No.8, pp.1390-1397, August 1997.

[11] C. Cox III, and R. Helkey, "Techniques and Performance of Intensity-Modulation Direct-Detection Analog Optical Links," *IEEE Transactions On Microwave Theory And Techniques*, Vol.45, No.8, pp.1375-1380, August 1997.

[12] Platt W. K., "Laser Communication Systems," *John willey & Sons*, New York, 1962.

[13] T. K. Fong, D. J. M. Sabido IX, R. F. Kalman, M. Tabara, and G. L. Kazavsky, "Linewidth-Insensitive Coherent AM Optical Links:Design, Performance and Potential Applications," *IEEE J. Lightwave Technol.*, Vol.LT-12, No.13, pp.526-534, March 1994.

[14] Kalman F. R., Fan C. J., and Kazavsky G. L., "Dynamic Range of Coherent Analog Fiber-Optic Links," *IEEE J. Lightwave Technol.*, Vol.LT-12, No.11, pp.1263-1277, July 1994.

[15] Y. Ishii, K. Tsukamoto, S. Komaki, and N. Morinaga, "Coherent Fiber-Optic Microcellular Radio Communication System Using a Novel RF-to-Optic Conversion Scheme," *IEEE Trans. Microwave Theory and Techniques*, Vol.43, No.9, pp.2241-2248, September 1995.

[16] M. Izutsu, S. Shikama, and T. Sueta, "Integrated Optical SSB Modulator / Frequency Shifter," *IEEE Journal of Quantum Electronics*, Vol.QE-17, No.11, pp.2225-2227, November 1981.

[17] G. H. Smith, D. Novak, and Z. Ahmed, "Novel Technique For Generation of Optical SSB with Carrier using a Single MZI to Overcome Fiber Chromatic Dispersion," *Proceeding of IEICE Microwave Phtonics'96 (MWP'96)*,PDP-2, pp.5-8, December 1996.

[18] K. Kitayama, "Highly Spectral Efficient OFDM Wireless Networks by using Optical SSB Modulation," *Technical Digest of Microwave Photonics'97 (MWP'97)*, FR2-4, pp.231-243, September 1997.

[19] N. K. Shankaranarayanan, S. D. Elby, and K. Y. Lau, "WDMA/Subcarrier-FDMA Lightwave Networks : Limitations due to Optical Beat Interference," *IEEE J. lightwave Tech.*, Vol.9, No.7, pp.931-943, July 1991.

[20] Y. Tarusawa and T. Nojima, "C/N Improvement Analog Optic-Fiber Transmission by Wavelength offset Combining," *Proceeding of IEICE Fall Conf. '93*, B-336, September 1993.

[21] T. Fujii, K. Tsukamoto, and N. Morinaga, "Transmission Characteristics Analysis of Optical Fiber Bus Link with Optical Amplifier for Microcellular Communication Systems," *IEICE Technical Report*, RCS92-76, October 1987.

[22] S. Kajiya, H. Harada, K. Tsukamoto, and S. Komaki, "TDM Optical Fiber Bus Link for Microcellular Radio Communication System," *Proceeding of IEICE Spring Conf.'94*, B-325, March 1994.

[23] H. Harada, K. Tsukamoto, S. Komaki, and N. Morinaga, "Optical TDM Scheme for Fiber-Optic Millimeter-Wave Radio System," *IEICE Trans. Commun.*, Vol.J77-CI, No.11, pp1-10, November 1994.

[24] K. Tsukamoto, H. Harada, S. Kajiya, S. Komaki, and N. Morinaga, "TDM Intercell Connection Fiber-Optic Bus link for Personal Radio Communication Systems," *1994 Asia-Pacific Microwave Conference(APMC'94)* ,Tokyo, Japan, pp1039-1042, December 1994.

[25] H. Harada, S.Kajiya, K. Tsukamoto, S. Komaki, and N. Morinaga, "TDM Intercell Connection Fiber-optic Bus Link for Personal Radio Communication System," *IEICE Trans. Commun.*, Vol.E78-B, No.9, pp.1287-1294, September 1995.

[26] H. Toba, and K. Nosu, "Optical Frequency Division Multiplexing Systems – Review of Key Technologies and Applications –," *IEICE Trans. Commun.*, Vol.E75-B, No.4, pp.243-255, April 1992.

[27] S. Kajiya, K. Tsukamoto, and S. Komaki,"Proposal of Fiber-Optic Radio Highway Networks Using CDMA Method," *IEICE Trans. Electron.*, Vol.E79-C, No.1, pp.111-117, January 1996.

[28] S. Benedetto and G. Olmo, "Performance evaluation of coherent optical CDMA," *Electronics Letter*, Vol.27, No.22, pp.2000-2002, October 1991.

[29] P. R. Prucnal, M. A. Santoro, and T. R. Fan, "Spread spectrum fiber-optic local area network using optical processing," *IEEE J. of Lightwave Tech.*, Vol.LT-4, No.5, pp.547-554, May 1986.

[30] W. C. Kwong, P. A. Perrier, and P. R. Prucnal, "Performance comparison of asynchronous and synchronous CDMA techniques for fiber-optic local area networks," *IEEE Trans. Commun.*, Vol.39, No.11, pp.1625-1634, November 1991.

[31] H. Ishikawa, and K. Yukimatsu, "Photonic Switching Technology," *The Telecommunications Association, Ohm-sha, Japan*, 1993.

[32] W. L. Ha, R. M. Fortenberry, R. S. Tucker, "Demonstration of Photonic Fast Packet Switching at 700 Mbit/s data rate", *Electron. Lett.*, Vol.27, No.10, pp.789-790, May 1991.

[33] J. P. Sokoloff, P. R. Prucnal, I. Glesk, and M. Kane, "A Terahertz Optical Asymmetric Demultiplexer (TOAD)," *IEEE Photonics Technology Letters*, Vol.5, No.7, pp.787-790, July 1993.

[34] K. Buchanan, R. Fudge, D. Mcfarlane, T. Phillips, A. Sasaki, and H. Xia, "IMT2000: Service Provider's Perspective," *IEEE Personal Communications*, Vol.4, No.4, pp.8-13, August 1998.

[35] S. Wako, "ITS: R & D and perception as the Open Information and Telecommunications Infrastructure", *IEICE Trans. A*, Vol.J81-A, No.4, pp.467-474, April 1998.

[36] N. Moshe, B. Josef, J. L. Anthony, M. L. Israel, and K. Yishai, "Progress in Externally Modulated AM CATV Transmission Systems," *IEEE J. Lightwave Technol.*, Vol.11, No.1, pp82-105, January 1993.

[37] H. Taub and D. L. Schilling, "Principles of Communication Systems," *McGRAW-HILL INTERNATIONAL EDITIONS, Electrical and Electronic Engineering Series*, 1986.

[38] K. Lau, "Short-Pulse and High-frequency Signal Generation in Semiconductor Lasers, " *IEEE Journal of Lightwave Technology*, Vol.7, No.2, pp.400-419, February 1989.

[39] S. Arahira, Y. Matsui, T. Kunii, S. Oshiba, and Y. Ogawa, "Optical Short Pulse Generation at High Repetition Rate Over 80GHz from a Monolithic Passively Modelocked DBR laser Diode," *Eletron. Lett.*, Vol.29, No.11, pp.1013-1014, May 1993.

[40] H. Ogawa, "Application of Optical Techniques to Microwave Signal Processing (MSP) –Optical-Microwave Signal Processing–," *IEICE Trans. Electron.*, Vol.E79-C, No.1, pp.87-97, January 1996.

[41] K. Komatsu, R. Madabhushi, "Gb/s-Range Semiconductor and Ti:$LiNb_3$ Guided-Wave Optical Modulators," *IEICE Trans. Electron.*, Vol.E79-C, No.1, pp.3-13, January 1996.

[42] K. Kitayama, T. Kuri, and Y. Ogawa, "Error-free optical 156 Mb/s millimeter-wave wireless transport through 60GHz external modulation," *Proceeding of Optical Fiber Conference (OFC'98)*, TuC2, February 1998.

[43] H. Ishio, (Ed.) "Optical Amplifiers and Their Applications," Ohm-sha, Japan, 1993.

[44] A. Kohlenberg,"Exact Interpolation of Band-Limited Functions," *J.Appl.Phys.*, Vol.24, No.12, pp.1432-1436, December 1987.

[45] A. S. Andrawis and I. Jacobs, "A New Compound Modulation Technique for Multichannel Analog Video Transmission on Fiber," *IEEE Journal of Lightwave Technology*, Vol.LT-11, No.1, pp.49-54, January 1993.

[46] S.S. Wagner, "Optical Amplifier Applications in Fiber Optic Local Networks," *IEEE Trans. Commun.*, Vol.COM-35, No.4, pp.419-426, April 1987.

[47] Mervyn A.J., Peter M.Grand, Jeffrey H.Collins, "The Theory, Design, and Applications of Surface Acoustic Wave Fourier-Transform Processors", *Proceeding of the IEEE*, Vol.68, No.4, pp.450-468, April 1980.

[48] F. Takahata, M. Yasunaga, and Y. Hirata, "A PSK Group Modem Based on Digital Signal Processing: Algorithm, Hardware Design, Implementation and Performance," *International Journal of Satellite Communications*, Vol.6, pp.253-266, 1988.

[49] Kai Y. E. and O. Yue, "Time Compression Multiplexing of Multiple Television Signals in Satellite Channels Using Chirp Transform Processors," *IEE Trans. Commun.*, Vol.COM-29, No.12, pp.1832-1840, December 1981.

[50] T. Kohri, M. Morikura, S. Kato, "Non-regenerative Onboard FDM/TDM transmultiplexer", *IEICE Trans.*, Vol.J69-B, No.11, pp.1480-1487, November 1986.

[51] K. Kobayashi, T. Kumagai and S. Kato, "A Group Demodulator Employing Multi-Symbol Chirp Fourier Transform", *IEICE Trans. Commun.*, Vol.E77-B, No.7, pp.905-910, July 1994.

[52] T.Kumagai, K.Kobayashi, "A New Group Demodulator with Multi-Symbol Chirp Fourier Transform for Mobile Communication Systems", *Proceeding of IEEE ICUPC'95*, pp.397-401, November 1995.

[53] K. Ohno, F. Adachi, "Postdetection Diversity Reception of QDPSK Signals in Land Mobile Radio Channels", *Trans. of IEICE*, Vol.J73-B-II, No.11, pp.651-657, November 1990.

[54] C. J. Daly, "Fiber Optic Intermodulation Distortion", *IEEE Trans. Commun.*, Vol.COM38, No.8, pp.1954-1958, August 1982.

[55] Westcott R.J., "Investigation of multiple f.m./f.d.m. carriers through a satellite t.w.t. operating near to saturation", Proceeding of IEE, Vol.114, No.6 pp.726-740, June 1967.

[56] R. Ganesh, K. Joseph, "Effect of non-uniform traffic distributions on performance of a cellular system," *1996 IEEE 6th International Conference on Universal Personal Communications Record (ICUPC'97)*, Vol.2, pp.598-602, October 1996.

Related Publications

[A1] Y. Shoji, K. Tsukamoto, and S. Komaki, "Proposal of the Radio High-way Networks Using Asynchronous Time Division Multiple Access," *IEICE Trans. Commun.*, vol.E79-B, no.3, pp.308-315, March 1996.

[A2] Y. Shoji, K. Tsukamoto, and S. Komaki, "Proposal of Chirp Multiplexing Transform / Intensity Modulation / Direct Detection System for Radio Highway Networks," *IEICE Trans. Fundamentals*, vol.E81-A, no.7, pp.1396-1405, July 1998.

[A3] Y. Shoji, T. Hida, K. Tsukamoto, and S. Komaki, "Proposal of Asynchronous Time Division Multiple Access Radio Highway Networks using Chirp Multiplexing Transform," *Wireless Personal Communications, Kluwer academic publishers* (Conditionally accepted)

[A4] Y. Shoji, K. Tsukamoto, M. Okada, and S. Komaki, "Proposal of Radio Highway Networks using Chirp Multiplexing Transform," *International Topical Meeting on Microwave Photonics (MWP'96)*, Kyoto Japan, pp.37-40, September 1996.

[A5] Y. Shoji, K. Tsukamoto, M. Okada, and S. Komaki, "Fiber-Optic Virtual Radio Free Space Network using Chirp Multiplexing Transform for Multiband Operation of Multimedia Mobile Radio," *Eighth International Workshop on Optical/Hybrid Access Networks*, Atlanta Georgia, p16, March 1997.

[A6] Y. Shoji, K. Tsukamoto, and S. Komaki, "A Consideration on Radio Highway Networks using FDM-TDM Conversion Scheme," *International Topical Meeting on Microwave Photonics (MWP'97)*, Duisburg Germany, pp.219-222, September 1997.

[A7] Y. Shoji, K. Tsukamoto, M. OKADA, and S. Komaki, "Fiber-optic radio access networks using photonic self-synchronized TDM bus link," *Proceeding of The First International Symposium on Wireless Personal Multimedia Communications (WPM*, Yokosuka, Japan, pp.145-150, November 1998.

[A8] P. Suwonpanich, Y. Shoji, K. Tsukamoto, and S. Komaki, "Proposal of CaSC Radio-Optic Direct Conversion Radio Highway," *1997 Asia Pacific Microwave Conference*, Hong Kong, vol.I, pp.385-388, December 1997.

[A9] P. Suwonpanich, Y. Shoji, K. Tsukamoto, and S. Komaki, "Study on Ca Radio-Optic Direct Conversion Radio Highway Using Optical Amplifier," *Pr of 1998 Asia Pacific Microwave Conference*,Yokohama, Japan, December 1

[A10] Y. Shoji, S. Kajiya, K. Tsukamoto, and S. Komaki, "A Consideration on Asynchronous Multiple Access Scheme for Optical Fiber Radio-Highway Networks," *Technical Report of IEICE.*, RCS95-29, pp.19-24, May 1995.

[A11] Y. Shoji, S. Kajiya, K. Tsukamoto, and S. Komaki, "A Consideration on Radio High-way Networks using FDM-TDM Conversion Scheme," *Technical Report of IEICE.*, OMI96-21, pp.62-67, April 1997.

[A12] S. Obata, Y. Shoji, K. Tsukamoto, and S. Komaki, "Proposal of Radio Highway Using Optical Frequency Encoding," *Technical Report of IEICE.*, MWP97-21, pp.67-72, January 1998.

[A13] T. Hida, Y. Shoji, K. Tsukamoto, and S. Komaki, "A Study on TDMA Radio Highway using Dynamic Optical Time Channel Assignment," *Technical Report of IEICE.*, MWP97-22, pp.73-79, January 1998.

[A14] Y. Shoji, S. Kajiya, H. Harada, K. Tsukamoto, and S. Komaki, "A Consideration on Asynchronous Multiple Access Optic Fiber Radio High-way Network," *Proceeding of IEICE. General Conference*, B-549, p.549, March 1995.

[A15] Y. Shoji, K. Tsukamoto, and S. Komaki, "Proposal of Asynchronous Time Division Multiple Access Fiber-Optic Radio Highway," *Record of Kansai-section Joint Convention of Institute of Electrical Engineering,* Japan, S8-2, November 1995.

[A16] Y. Shoji, K. Tsukamoto, and S. Komaki, "Proposal of Radio ATM Highway transferring Radio Cells," *Proceeding of IEICE. Fall Conference*, B-409, p.500, September 1996.

[A17] I Ra, Y. Shoji, K. Tsukamoto, and S. Komaki, "A Proposal of M-ary Polarization Ellipticy Angle Frequency Shift Keying / Optical Heterodyne Detection,",*Proceeding of IEICE. Fall Conference*, B-1090, p.575, September 1996.

[A18] T. Hida, Y. Shoji, K. Tsukamoto, and S. Komaki, "Analysis of Frequency Utilization Efficiency in Asynchronous TDMA Bus Type Radio Highway Network," *Proceeding of IEICE. Spring Conference*, B-5-261, p.648, March 1997.

[A19] T. Kagimoto, Y. Shoji, K. Tsukamoto, and S. Komaki, "Proposal of Optical Spectrum Switching Scheme Using Optical FDM-TDM Conversion in Radio Highway Networks," *Proceeding of IEICE. Spring Conference*, B-5-261, p.625, March 1998.